Evaluation of loss generated by edge- burrs in electrical steel

By

Asheraf .S. Abdullah Eldieb

Thesis submitted in fulfilment of the requirement for the degree of

Doctor of Philosophy

Wolfson Centre for Magnetics
School of Engineering, Cardiff University

PAPERS PRODUCED FROM THIS THESIS

1- A. **Eldieb**, F. Anayi and A. Fahmy, "Investigation of short-circuit fault effects on non-oriented steel at different range of magnetisations," *2015 50th International Universities Power Engineering Conference (UPEC)*, Stoke on Trent, 2015, pp. 1-6.

2- A. **Eldieb**, F. Anayi and A. Fahmy, "Experimental investigation on effect of edge burrs fault on toroidal magnetic cores laminations at different range of magnetisations," *2015 50th International Universities Power Engineering Conference (UPEC)*, Stoke on Trent, 2015, pp. 1-5.

3- H. Hamzehbahmani, P. Anderson and A. **Eldieb**, "An overview of the recent developments of the inter-laminar short circuit fault detection methods in magnetic cores," *2015 50th International Universities Power Engineering Conference (UPEC)*, Stoke on Trent, 2015, pp. 1-7.

4- A. **Eldieb** and F. Anayi, "Evaluation of Loss Generated by Edge Burrs in Electrical Steels," in *IEEE Transactions on Magnetics*, vol. 52, no. 5, pp. 1-4, May 2016.

DECLARATION

This work has not been submitted in substance for any other degree or award at this or any other university of learning and is not being submitted concurrently in candidature for any degree or other awarded.

Signed   (candidate)

Date

Statement 1

This thesis is the result of my own work, except where otherwise stated other sources are acknowledged by footnote giving explicit reference. A bibliography is appended.

Signed   (candidate)

Date

Statement 2

I hereby give consent for my thesis, if accepted, to be available for photocopying and for inter-library loan, and for the title and summary to be made available to outside organisation.

Signed   (candidate)

Date

ABSTRACT

This thesis investigates the impact of edge burr faults on total power loss in electrical machine core laminations. Analytical techniques, experimental work and FEM modelling have been utilised to investigate the effect of the phenomenon from different aspects.

Measurements of overall specific total loss and analytical techniques were used to separate the power loss components over wide magnetising frequency ranges.

Two techniques were used in this project for edge burr simulation; these include (1) the short circuiting of two Epstein-size and three Epstein-size and large-size, non-oriented steel laminations by lead-free solder in the rolling and transverse directions and (2) the by clamping system method, which was designed for the application of edge burrs on toroid cores. Various sizes of artificial edge burrs were applied at set points and then in a random manner to confirm their effect and show the extent of their effect in different case scenarios and the tests were completely repeatable.

3-D FEM modelling for toroid cores was also used to study the impact of core geometry on the total core loss. This method provided a clear explanation for why smaller toroid cores have higher power loss than the larger ones.

The research presented in this thesis can be utilised by electrical steel manufacturers and electrical machine designers to evaluate the impact of edge burr faults on the properties of magnetic cores. The evaluation is beneficial because it could reduce the risk of local overheating of laminated magnetic material, which can lead to destruction of such an electrical machine.

ACKNOWLEDGEMENTS

TABLE OF CONTENTS

LIST OF FIGURES

ix

List of tables

ABBREVIATIONS

2-D FEM	Two dimension finite element modelling
3-D FEM	Three dimension finite element modelling
NO	Non-oriented electrical steel
GO	Grain oriented electrical steel
RD	Rolling direction
TD	Transverse direction
CGO	Conventional grain oriented electrical steel
P_{cu}	Copper losses
P_{me}	Mechanical losses
P_e	Eddy current losses
P_h	Hysteresis losses
P_a	Anomalous loss
H	Magnetic field strength
N	Number of turns
I	current
$\boldsymbol{\Phi}$	Magnetic flux
B	Magnetic flux density
μ_0	Permeability of free space
A	Surface area
μ_r	Relative permeability of the material
M	Magnetisation
p	Dipole strength
T	tesla
Oe	Oersted
G	gauss
l	distance
m	Magnetic moment
$\nabla.$	divergence
D	Electric flux
ρ_v	Volume charge density

ε_0	Permittivity of free space
E	Electric field
$\nabla\times$	Curl
J	Eddy Current density
m	Magnetic moment
χ	susceptibility
S	Power flux
n	Component normal the surface
R	reluctance
$\boldsymbol{F}$	magneto motive force
lm	magnetic path length
AC	Alternating current
DC	Direct current
R_{ct}	contact resistance of the laminations
U_{oc}	Open circuit voltage
R_{eq}	Equivalent resistance
I_{sc}	Short circuit current
U_{oc}	Open circuit voltage
R_{lam}	Lamination path resistance
ρ	Resistivity
δ	Skin depth
σ	Electrical conductivity of the material
B_z	instantaneous flux density in Z direction
w	Angular frequency
ß	phase angle
B_{pk}	peak value of the magnetic flux density
I_{pk}	peak magnetizing current
$\mu_Z{}'$	Absolute static permeability
γ	Propagation constant
k	Material constant
λ	Flux linkage
d	Sheet thickness
D	Material density 7650

K_h	Hysteresis loss coefficient
K_e	Eddy current loss coefficient
L	Half Spacing between domain walls
ɳ	Anomaly factor
K_{ex}	Excess loss coefficient

Introduction

The production of soft magnetic electrical steel material has reached almost 97% today for use in electrical steels [1-1]. Over 12 million tons are produced annually, around 80% of which are non-oriented electrical steel (NO) grade, and the rest are grain-oriented steel (GO) 3% silicon steel. There is an increasing demand for efficient electrical power generation and distribution equipment, which require high-standard electrical steels with low magnetic losses and higher permeability. The total loss in electrical steel cores account for 5 to 10% of all electrical power generated in developed countries [1-1]. Over the last few decades, there have been continuous improvements in the electrical steel industry, as illustrated in Fig 1-1, a rapid enhancement due to the introduction of new processes in the steel production and processing route [1-2]. Non-oriented electrical steel material contains roughly 0.2–3.3% silicon, has a thickness of 0.30–0.65 mm and is produced as wide strips. Due to low intrinsic coercivity, these silicon-iron alloys can be easily magnetised and demagnetised. As opposed to anisotropic grain-oriented steel, used in transformers subjected to unidirectional flux, isotropy makes non-oriented steel suitable for rotating machinery with revolving flux. It has almost the same magnetic properties in the rolling and transverse directions, and its main application is for building the cores of rotating electrical machines. Owing to its straight-forward production process, it has a lower cost compared to grain-oriented steel. Its value accounts for 53.0% of the total market [1-3].

Grain-oriented steel (GO) has approximately 3.2% silicon content and is mostly produced as 0.28–0.35 mm thick strips. GO steel has a larger grain size than non-oriented steel. Most of GO steel are produced with a [100] direction, which is approximately the same direction to the direction in which the strip is rolled (RD). The way in which GO steel is produced provides better magnetic properties because it is magnetised in the rolling direction (RD) rather than being magnetised in the transverse direction (TR) [1-2]. It is covered on both surfaces with electrical insulation coating, which ensures there is no electrical contact between the adjacent sheets. There are two types of GO steel, conventional grain-oriented (CGO) and highly grain-oriented (HGO) grades. The latter is produced via a complex production route which provides more controlled grain growth during the annealing process. The main application for grain-oriented steel is in energy-efficient transformer cores.

In general, the cores of electrical machines should be built from low-loss, high-permeability and high-saturation magnetisation steels. Consistent improvement and productivity is placed today, but there is a growing demand for reduced losses and increased permeability.
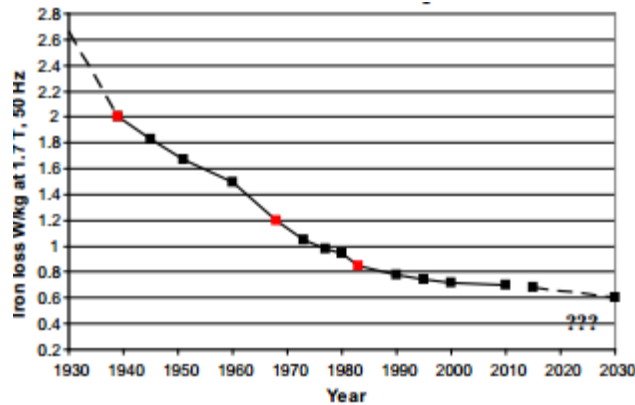
Fig 1-1. Losses at (1.7 T, 50 Hz) in the highest available grades of commercial electrical steels produced since 1930, showing occasional rapid improvement due to the introduction of new technology.

The improvement in soft magnetic materials for different uses started from incremental improvements in electrical steel technology, which then lead to being able to manipulate and control microstructure and composition.

1.2 Losses in electrical machine cores

Motors, generators and transformers play major roles in power systems; therefore, these machines should be designed efficiently to provide consistent power delivery with less power loss. Most recent studies regarding these machines largely focus on power loss optimisation. Power loss plays a significant part in machine design, and the material from which the core is made is normally characterised by its magnetic properties under specific frequencies. There is an increased competition between the material designers in order to provide the most efficient material with the lowest power loss. Power loss is generally divided into three different categories: copper loss P_{cu}, which occurs in machine winding; mechanical loss P_{me}, due to rotation of rotating parts in electrical machines or friction loss of an engine including bearing friction and magnetic core loss, which occurs in core laminations due to alternating magnetic field. Magnetic core loss originates from three main sources: eddy current power loss P_e, hysteresis loss P_h and anomalous loss P_a [1-4][1-5]. For this thesis, I have analytically and experimentally researched power loss in

machine cores, and the results show a significant increase in eddy current power loss for the material under investigation.

The cores of electrical machines and other magnetic devices play a significant role as magnetic field concentrators, which are required to contain as much magnetic flux as possible [1-6] because the magnetic flux changes over time. Therefore, an electromotive force is generated in the core lamination, which will lead to induced eddy currents, the energy lost in the form of heat along the eddy current path [1-7].

Eddy current power loss, P_e, is found to be the highest compared to other loss components, which in some cases has led to complete machine failure [1-8]. For this reason, some procedures have been put into place in order to minimise the impact of this loss. These include building the cores from a thin stack of laminations, typically 0.23–0.65 mm, based on the type of material and its application. The lamination of the material forces the eddy currents to flow in long, narrow paths, thus greatly reducing their values and the accompanying heating within the material. Moreover, the laminations are coated on both sides with insulating layers to prevent direct contact between the sheets [1-9]. First, it reduces the eddy current circulating in the core. Second, it provides a reduction on both hysteresis [1-10] and anomalous loss as a result of beneficial tensile stress [1-11]. Tensile stress applied to the material helps minimise the losses by reducing the size of the domains that are perpendicular to the magnetisation direction. Moreover, the tensile stress causes a narrowing of the domain wall spacing, which decreases the anomalous loss due to the reduction in average domain wall velocity. Finally, 3% high silicon content is added to the material to increase its resistivity, hence the reduced eddy current [1-6], which may provide efficient operation of modern electrical devices. Table 1-1 illustrates the effect of silicon content on power loss components at 50 Hz and 100 Hz.

Table 1-1 Range of variation of percentage of power loss components (per cycle) with silicon content and thickness in NO steels at 50 Hz and 100 Hz. The increased proportion of P_h and decreased P_e with decreasing thickness is clearly seen reproduced from [1-2].

Frequency (Hz)	Material specification	Hysteresis loss P_h (%)	Eddy current loss P_e (%)	Excess loss (%)
50	Low silicon	30–50	40–60	0–20
	High silicon	55–75	20–30	10–20
	Thin high silicon	80–90	1–2	5–15
100	Low silicon	20–30	50–70	10–20
	High silicon	25–35	40–60	15–25
	Thin high silicon	80–90	1–2	5–15

Table 1-2 Qualitative effect of some of the important parameters on traditional loss component (per cycle) in electrical steels, reproduced from [1-2].

P_h	P_e	P_a
High for increased defects, impurities, internal stress, high texture, poor surface topology	**High** for low resistivity and increased thickness	**High** for increased defects impurities ,internal stress
Low for thick material or large grains	**Low** for thin material or small grains	**Low** for narrow domain width and small grains
Decrease with increasing texture	**Probably** not texture dependent	Increase with increasing texture
Obtained from proportionality of measured static B-H loop or extrapolation of loss/cycle vs f curve to f=0	**Calculated** from Maxwell equations for thin sheet assuming linear B-H loop and no skin effect and flux harmonics	**Calculated** with empirical models or from difference between measured loss and (P_h+P_e)
Independent of frequency	**Proportional** to frequency	**Proportional** to (frequency)$^{0.5}$

1.3 Core fault

Core faults may occur anywhere in the core laminations of electrical machines, but these faults are more common in the stator core. They may occur on transformers as well but are more unusual there. This is due to lower leakage fields and more stable electrical, thermal and mechanical operating regimes [1-12]. One factor significantly influencing power loss is the manufacturing process. A fault may take place when two or more core laminations are electrically connected together, either because of an insulation failure between them or as a result of imposed short circuiting. This may happen due to different reasons, including edge burrs caused by the shearing and cutting processes for steel laminations. These connections lead to the circulation of additional currents, which leads to additional losses and heating. This causes further deterioration of the insulation layers, expanding the fault, which can cause the material to melt, which may lead to machine failure and damage.

Therefore, core faults are still very important issues; hence they have been under investigation by many authors.

1.4 Edge burrs in machine cores

Edge burrs are one of the manufacturer defects in laminations that lead to short circuits between the laminations. These defects are due to the cutting process, as will be further discussed in chapter 6. When edge burrs are present on both sides of the laminations, they form a closed electrical circuit; this leads to circulating eddy currents larger than in normal operating conditions. This type of fault in machine cores causes additional loss in the core in the form of heat, and the power losses occasioned by this heating thus reduce the efficiency of the device, whether it be a motor, generator or transformer. It has been indicated that [1-13] more localised heating may eventually cause burning or melting of the lamination, thus raising the potential for complete machine failure. This type of fault has caused some concern among the designers and manufacturers of electrical machine cores.

Owing to the role played by electrical machines in power generation and distribution, automation, transport engineering and industrial equipment [compressors, fans, etc.], the study of electrical steel is relevant. There is more focus on better performance and increased energy efficiency, along with remarkable competition between steel manufacturers. This emphasises the need for high-quality electrical steel at reasonable price.

1.5 Magnetic domain observation

In order to observe the magnetic domain structure, a magnetic field microscopy (*MFM*) was used in this project to obtain an image of magnetic domains on the surface of the material, which will in turn provide a closer look into the internal structure of the specimen. The same system uses AFM, which provided detailed information about the surface topology.

Kerr effect microscopy was used as well in this project; the specimen in this case went through different procedures of sample preparation. The whole procedure is time consuming, and it can it can have a destructive effect on the magnetic properties of the material. The coating must be removed, so chemical etching is used to remove it to reveal the grain size, but it does not provide any indication of orientation of individual grains.

Objectives

- Studying eddy current phenomenon in a ferromagnetic material this includes the impact of thickness, relative permeability and flux concentration based due to skin effect.
- Power loss and power loss separation into three components.
- Modelling the edge burrs faults on electrical steel laminations and toroid cores
- Using the available techniques to observe the magnetic domains of the material.

References:-

[1-1] A.J. Moses, Opportunities for exploitation of magnetic materials in an energy conscious world, Interdisciplinary Science Review (2002) 27 (2) 100-113, ISSN 0308-0188.

[1-2] A.J. Moses, Energy efficient electrical steels: magnetic performance prediction and optimization, Scr. Mater. 67 (2012) 560–565.

[1-3] O. Fischer, J. Schneider, "Influence of Deformation Process on the Improvement of Non-oriented Electrical Steel", Journal of Magnetism and Magnetic Materials, Vol 254-255, pp 302-306, 2003.

[1-4] Y. Zhang, M.C. Cheng, and P. Pillay, "A Novel Hysteresis Core Loss Model for Magnetic Laminations," IEEE Trans. Energy Convers. vol. 26, no. 4, pp. 993–999, Dec. 2011.

[1-5] Y. Chen and P. Pillay, "An Improved Formula for Lamination Core Loss Calculations in Machines Operating With High Frequency and High Flux Density Excitation," IEEE 37th IAS Annual Meeting, vol. 2, 13-18 Oct 2002, pp. 759–766

[1-6] B S Guru, H R Hiziroglu, "Electric Machinery and Transformers", Third edition, Oxford University press, 2001

[1-7] Z Popvic, B D Popovic "introductory electromagnetics" Prentice Hall, 1999

[1-8] M. Ibrahim and P. Pillay, "Advanced Testing and Modelling of Magnetic Materials Including a New Method of Core Loss Separation for Electrical Machines"IEEE Transaction on Industry Applications, Vol. 48, NO. 5, Sep/Oct 2012, pp. 1507 – 1515

[1-9] T. Wada, T. Nozawa, T. Takata, Method for producing a super low watt loss grain oriented electrical steel sheet, US Patent, vol. 3932236, January 13, 1976. [3] T. Yamamoto, T. Nozawa, Effects of tensile stress on total loss of single crystals of 3% Silicon–Iron, J. Appl. Phys. 41 (1970) 2981–2984.

[1-10] T. Yamamoto, T. Nozawa, Effects of tensile stress on total loss of single crystals of 3% Silicon–Iron, J. Appl. Phys. 41 (1970) 2981–2984

[1-11] V. Goel, P. Anderson, J. Hall, F. Robinson and S. Bohm, "Electroless Plating: A Versatile Technique to Deposit Coatings on Electrical Steel," in *IEEE Transactions on Magnetics*, vol. 52, no. 5, pp. 1-4, May2016.

[1-12] P. J. Tavner and A. F. Anderson, "Core faults in large generators," in *IEE Proceedings - Electric Power Applications*, vol. 152, no. 6, pp. 1427-1439, 4 Nov. 2005.

[1-13] S. B. Lee, G. B. Kliman, M. R. Shah, W. T. Mall, N. K. Nair, and R. M. Lusted, "An advanced technique for detecting inter-laminar stator core faults in large electric machines," IEEE Trans. Ind. Appl.., vol. 41, no. 5, pp. 1185–1193, Sep

2.1. Magnetism and magnetic materials

This chapter is an introduction to the history of magnetism and the physical laws governing electrical machines. It includes the most-used mathematical relationships, the magnetisation process in ferromagnetic materials used to build the cores of electrical machines and the hysteresis phenomena under AC magnetisation and the power loss caused as its result.

2.2. Historical background

Magnetism is one of the oldest physical phenomena observed and investigated; it is believed that magnetism was found in the 4th century BC, Chinese book of Guiguzi: 'The lodestone attracts iron' [2-1]. William Gilbert is thought to be the first person to conduct scientific study on magnetism by forming a picture of the earth's magnetic field and describing the movement of the magnetic needle when exposed to field [2-2]. By about 1800, Alessandra Volta, an Italian physicist, had developed his pile (or battery), which produced a constant motion of electrical charges in conducting materials. The transfer of these charges was called electric current [2-3]. In 1819, Hans Christian Oersted, a Danish physicist, discovered experimentally that the magnetic needle was deflected by a current in a wire passed over or below it; this was the earliest recorded experimental work in electromagnetism. It was almost immediately after that that Andre-Marie Ampere, a French physicist and mathematician, observed a force of the same nature between two conductors carrying currents. In the period 1820 to 1825, Ampere came up with a final hypothesis that an electric current is the source of every magnetic field. His assumption was that magnets comprised rotating electrodynamic molecules, about 80 years before the discovery of electrons and around 100 years before the Rutherford-Bohr model of the atom with orbiting electrons. In 1826, Ampere had managed to formulate one of the fundamental laws of physics, Ampere's circuital law [2-4]

$$\oint_c \boldsymbol{H}.\,d\boldsymbol{l} = NI \quad (2\text{-}1)$$

Equation (2-1) indicates that the magnetic field strength **H** in closed magnetic circuit C is due to the number of conductors (N) in the circuit carrying current I , dl incremental length of the loop, as illustrated in the below Fig **[2-1]** :
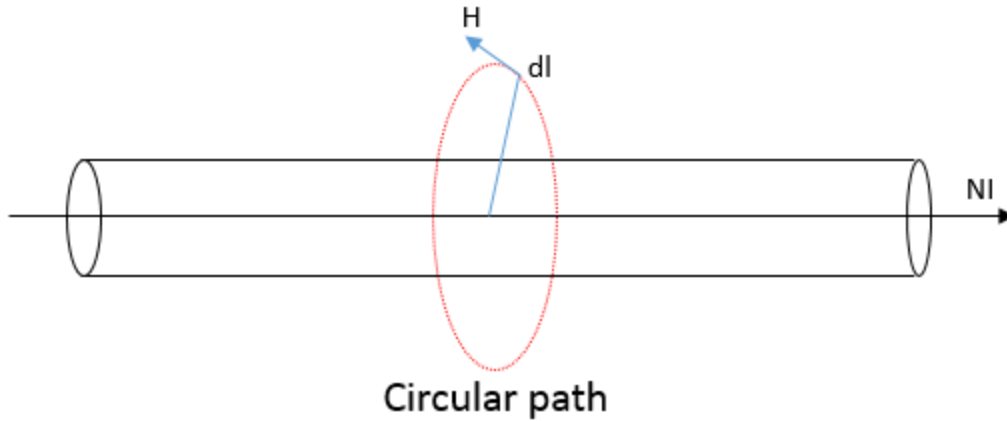
Fig 2-1 Ampere's circuital law

Michael Faraday discovered another fundamental law of magnetism in 1831. This law states that when the magnetic flux linking a circuit changes, an electromotive force (emf) is induced in the circuit proportional to the rate of change of the flux linkage [2-5].

$$v = -\frac{d\varphi}{dt} \qquad (2\text{-}2)$$

This is called electromagnetic induction. The minus sign in Equation (2-2) refers to Lenz's law, which states that the change in the magnetic flux according to (2-2), the polarity of the induced emf such that it produces a current whose magnetic field opposes the change which produces it.

At the end of the 19th century, in 1873, James Clerk Maxwell published a work 'A Treaties on Electricity and Magnetism', which proposed a set of 20 equations, later simplified to be a set of four equations: two by Gauss, and Ampere and Faraday's laws [2-5]. These equations provide full descriptions of how electric and magnetic fields are generated and affected by each other. Hence, the natural phenomena of electricity and magnetism were at long last united into one, the natural phenomenon of electromagnetism.

2.3. Electromagnetic terms

A magnetic flux $\boldsymbol{\Phi}$ in a cross-sectional area A is generated by a magnetic field **H** in a free space:

$$\boldsymbol{\Phi} = \mu_0 \mathbf{H} \text{A} \quad (2\text{-}3)$$

where μ_0 is the permeability of the free space and equal to $4\pi \times 10^{-7}$ Henry per meter (H m^{-1}). The magnetic flux is measured in wb (Weber), and the magnetic field is measured in A/m (Ampere per meter).

The magnetic flux density B (T, or Tesla) is a more commonly used quantity and is defined as:

$$\mathbf{B} = \frac{\Phi}{\text{A}} \quad (2\text{-}4)$$

(2-3) and (2-4) indicate the relationship between magnetic field strength **H** and the flux density **B** in the free space, which is:

$$\mathbf{B} = \mu_0 \mathbf{H} \quad (2\text{-}5)$$

The two parameters (the flux density **B** and the magnetic field) are most commonly used. Other parameters, such as permeability, losses, polarisation and magnetisation are all **B** and **H** dependent.

For any other medium, equation (2-5) can be written as

$$\mathbf{B} = \mu_0 \mu_r \mathbf{H}$$

Most units for the magnetic field intensity and the flux density are normally expressed in (SI) units T or Weber per square meter (Wb m^{-2}) and A/m. These units are sometimes expressed in G (Gauss) and/or Oe (Oersted) based on the centimetre-gram-second (CGS) systems in some countries, e.g. the USA.

In a free space, the magnetic field strength of 1 Oe corresponds with a magnetic flux density of 1 G.

Referring to Fig 2-1, a current-carrying conductor is the simplest method to generate a magnetic field. The circular current loop is also known as a magnetic dipole. At some distance away from the loop, the produced magnetic field is equivalent to the field produced by two hypothetical magnetic poles of strength p separated by a distance l. The dipole moment **m** for this arrangement would be:

$$\mathbf{m} = \text{p}\mathbf{l} \quad (2\text{-}6)$$

The pole strength is defined as:

$$\text{p} = \frac{\Phi}{\mu_0} \quad (2\text{-}7)$$

Based on that, a new quantity is defined: the magnetisation **M**, as the magnetic moment per unit volume of the material:

$$\mathbf{M} = \frac{m}{volume} \quad (2\text{-}8)$$

From (2-6), (2-7) and (2-8), the formula for magnetisation is set as

$$\mathbf{M} = \frac{\Phi l}{\mu_0 \, volume} = \frac{\Phi}{\mu_0 A} = \frac{\mathbf{B}}{\mu_0} \quad (2\text{-}9)$$

The magnetic flux density **B** in (2-5) and (2-9) has two contributions, one from the magnetic field in the free space $\mu_0 \mathbf{H}$, and the other one from the material magnetisation $\mathbf{M}\mu_0$. Therefore, the magnetic induction is the sum of these two vectors:

$$\mathbf{B} = \mu_0(\mathbf{H} + \mathbf{M}) \quad (2\text{-}10)$$

If no external field is present, in this case the induction inside the material is $\mathbf{B} = (\mu_0 \mathbf{M})$. If both the magnetisation and magnetic field are present, then their contribution can be assumed as $\mathbf{B} = \mu_0(\mathbf{H} + \mathbf{M}).$

The permeability is used to represent the impact of the magnetic field on the material, which is defined by:

$$\boldsymbol{\mu} = \frac{\mathbf{B}}{\mathbf{H}} \quad (2\text{-}11)$$

In practice, it is normal to use relative permeability instead of the permeability for material properties, which is expressed as:

$$\mu_r = \frac{\mu}{\mu_0} \quad (2\text{-}12)$$

The relative permeability μ_r of the materials can be treated as a measure of the material's capability to concentrate the magnetic field; its value in free space is 1. In fact, the magnetic materials are mainly classified based on the value of the relative permeability μ_r [2-6]. Materials with relative permeability slightly less than 1, such as silver, gold and copper, are called diamagnetic. Materials with relative permeability greater than 1 are called paramagnetic, e.g. aluminium, wolfram, and platinum. Materials with relative permeability much greater than 1 ($>10^3$) are called ferromagnetic materials. There are five ferromagnetic materials which exhibit ferromagnetic behaviour: iron (Fe), cobalt (Co), nickel (Ni), gadolinium (Gd) and dysprosium (Dy). Due to their higher permeability, ferromagnetic materials are adopted to build the cores of electrical machines, since they are the best magnetic field concentrators. However, when these materials are under alternating magnetisation, μ_r is no longer constant; it is a non-linear function due to many parameters such as magnetic field, temperature, frequency and

mechanical stress, which may themselves vary during the magnetisation process. Tables 2-2 and 2-3 illustrate the relative permeability for different material types.

In describing the magnetic behaviour of magnetic materials, the magnetic susceptibility χ is sometimes used instead of using magnetic permeability μ. The magnetic susceptibility is defined as the ratio between the material magnetisation **M** and the external magnetic field **H**:

$$\mathbf{M} = \chi\, \mathbf{H} \qquad (2\text{-}13)$$

The relation between the permeability and the susceptibility is therefore:

$$\boldsymbol{\mu} = \boldsymbol{\mu_0}(\boldsymbol{\chi} + \mathbf{1}) \quad (2\text{-}14)$$

The value of χ +1 is in fact equal to the relative permeability μ_r. χ and μ_r represent the response of the material when exposed to external magnetic fields. It is well known that the magnetic behaviour of the material is affected by the magnetic history of the same material; therefore χ and μ_r must be history dependent.

Table 2-2 Relative permeability μ_r of some diamagnetic materials [2-7]

Material	Relative permeability
Bismuth	0.999 981
Beryllium	0.999 987
Copper	0.999 991
Methane	0.999 969
Silver	0.999 980
Water	0.999 991

Table 2-3 Relative permeability μ_r of some paramagnetic materials [2-7]

Material	Relative permeability
Air	1.000 304
Aluminium	1.000 023
Oxygen	1.001 330
Manganese	1.000 124
Palladium	1.000 800
Platinum	1.000 014

The relative permeability of ferromagnetic materials is greater than unity and varies due to the aforementioned parameters.

For paramagnetic and diamagnetic materials, the relationship between **H** and **B** is linear, as shown in Fig [2-2]. For such materials, a low flux density of about (~ 0.1T) is produced by a very high magnetic field (~ 10^5 A/m). However, higher values of flux density are achieved in ferromagnetic materials with a lower magnetic field [2-8].

In fact, diamagnetic materials are for which χ is small and negative (10^{-5}). The magnetisation in such material opposes the applied magnetic field. The orbital motion of electrons creates tiny atomic current loops, which produce their own magnetic fields. When an external field is applied to diamagnetic materials, these current loops will tend to align in such a way to oppose the applied field.

Any conductive material will show a strong diamagnetic effect in the presence of a changing magnetic field; this is because the circulating currents will be generated in a conductor to oppose the change in the magnetic field. A superconductor would be a perfect diamagnetic, since there is no resistance to the forming current loops (χ = -1).

Paramagnetic materials are those containing microscopic magnetic moment, e.g. electron spin or orbital spin. When these materials are exposed to an external applied field, their orientation tends to rotate toward the direction of that field, causing a slight net material magnetisation. Their susceptibility is small (typically 10^{-5} to 10^{-3}) [2-11] [2-12].

Ferromagnetic materials, e.g. electrical steels, these materials when placed in a magnetic field, become strongly magnetised in the direction of the applied field. They exhibit the phenomena of remanence and hysteresis. The permeability of diamagnetic and paramagnetic materials is slightly different from that of free space; however, the permeability of ferromagnetic material is non-linear and multivalued. Values of 10 to 1,000 are quite common, and values up to 10^6 can be achieved.

Ferromagnetic materials respond very well to low magnetic field strength compared to paramagnetic and diamagnetic materials, which in consequence leads to non-linear magnetising characteristics, as described in Fig 2-4. Iron (Fe), cobalt (Co) and nickel (Ni) are the most important metals which exhibit ferromagnetic properties.

An electrical machine's core design is based on the magnetisation curve for specific ferromagnetic materials and magnetising conditions. Fig 2-3a illustrates magnetisation curve. Fig 2-3b illustrates the relative permeability of a material. Fig 2-4 illustrates magnetisation curves for several ferromagnetic materials [2-17].
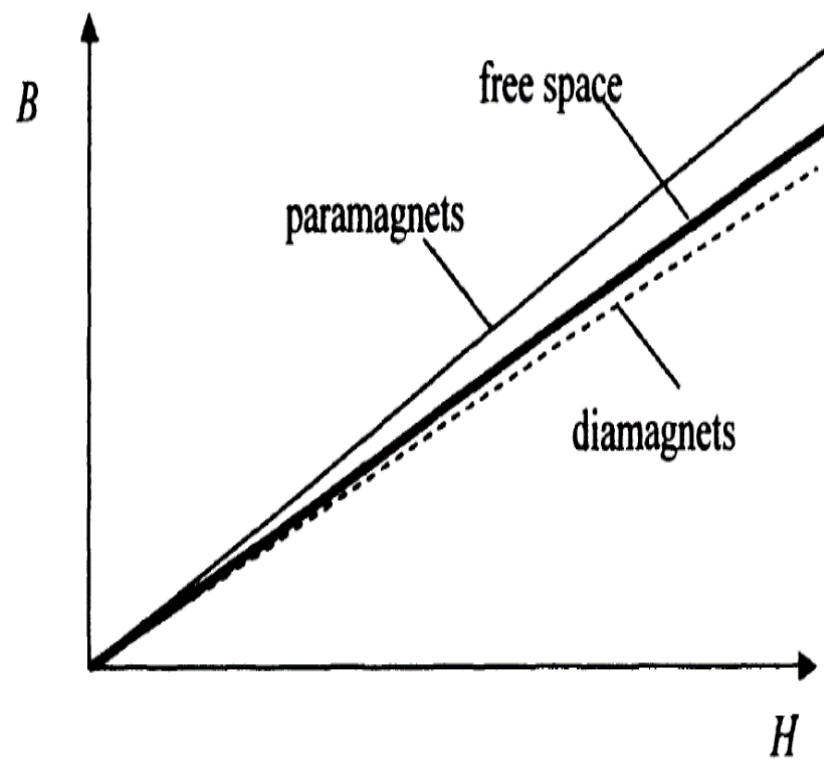
Fig 2-2 Magnetisation curve for para and diamagnetic materials.
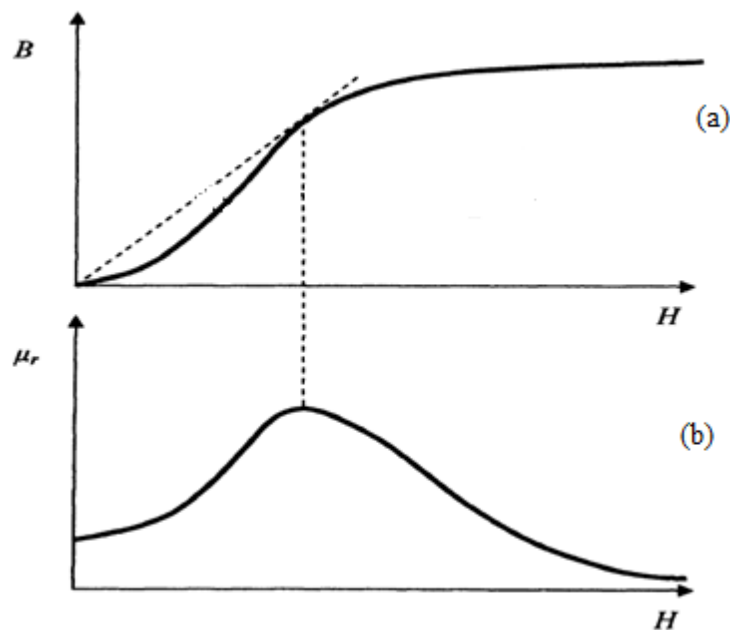
Fig 2-3 (a) B-H curves for ferromagnetic materials. (b) Variation with field strength.
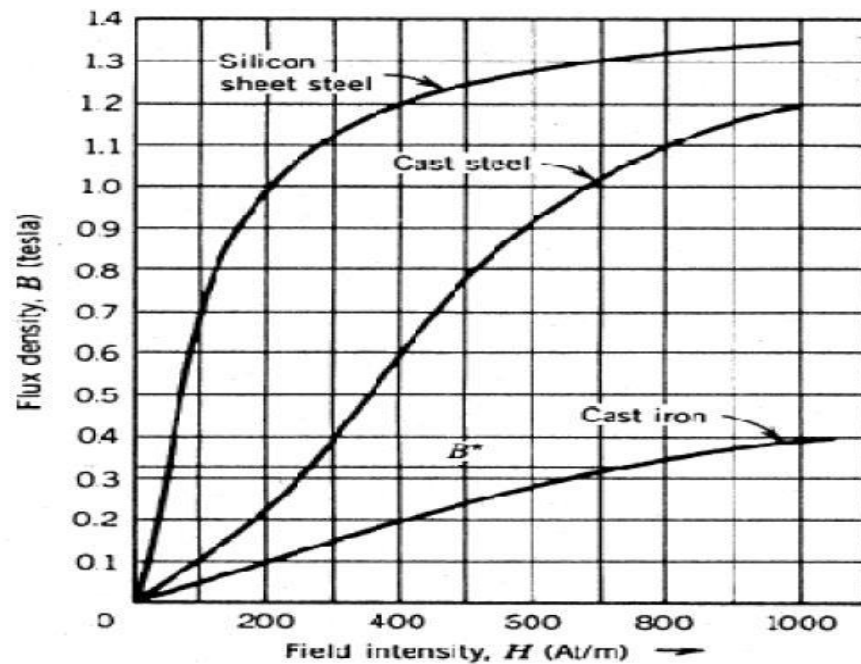
Fig 2-4: Magnetisation curves for some ferromagnetic materials. [2-17]

2.4. Applied electro-magnetic theory

The laminations in electrical machine cores are subjected to an alternating magnetisation and demagnetisation process. Therefore, it is essential to understand electromagnetism in order to analyse its behaviour under different magnetising conditions.

2.5. Maxwell's equations No table of figures entries found.

Maxwell's equations summarise the basic laws of electricity and magnetism. They were combined in 1865 by the Scottish mathematician and physicist James Clerk Maxwell. Maxwell managed to describe how oscillating electromagnetic waves interact with matter. In 1884, Heaviside and Gibbs reformulated the initial system formulated by Maxwell, which consisted of 20 variables, to a set of four equations based upon vector calculus. The first Maxwell equation (2-15) is derived from Gauss's law to an electric field. It provides a relationship between the electric charge enclosed in a surface and the electric flux emanating out of the surface

$$\nabla. D = \rho \quad (2\text{-}15)$$

where ρ the is the electric charge density and D is the electric displacement field, which is expressed in $C.m^{-1}$, the electric field is related to the permittivity of free space

ε_0 [F.m^{-1}], electric field E [v.m^{-1}] and polarisation density of the material P [c.m^{-1}], as given in (2-16)

$$D = \varepsilon_0 E + P \quad (2\text{-}16)$$

Maxwell's second equation (2-17) is obtained by applying Gauss's law to magnetism. It is assumed in the absence of magnetic monopoles within the enclosed volume of material.

$$\nabla . B = 0 \quad (2\text{-}17)$$

Maxwell's third equation is Faraday's law of induction (1831), a time-varying magnetic flux B flowing through a closed surface S [m^2] generates electromotive force (emf) of the opposite sign.

$$\nabla \times E = -\frac{\partial \mathbf{B}}{\partial \mathbf{t}} \quad (2\text{-}18)$$

Maxwell's fourth equation is based on Ampere's law that states an oscillating time-varying magnetic field **H** [Am^{-1}] in a closed circuit induces electric current, characterised by its density J in [A.m^{-2}], through the area confined to the loop. This law is similar to Faraday's law of induction. Maxwell noticed an inconsistency in its application to a charging or discharging capacitor; therefore, he modified this formula by introducing a time-derivative of electric displacement field D. Then the final form became:

$$\nabla \times H = J + \frac{\partial \mathbf{D}}{\partial \mathbf{t}} \quad (2\text{-}19)$$

2.6 Descriptive constitutive equations of the material

When the current is created by a magnetic field circulating through a conductive loop of area S, a magnetic dipole moment m associated with the electric circuit is equal to S^{2}J. The magnetisation M of a volume v of the material can be defined as the magnetic moment per unit volume.

$$M = \frac{\text{m}}{\text{v}} \quad (2\text{-}20)$$

The magnetic field strength H and the flux density B are related to the absolute permeability μ as provided in equation (2-21). The μ_0 is the permeability of free space, and the relative permeability of the material is μ_r.

$$\mathbf{B} = \mu \mathbf{H} = \mu_0 \mu_r \mathbf{H} \quad (2\text{-}21)$$

2.7 Poynting's vector

In 1884, John Henry Poynting managed to calculate the electromagnetic field in a material with a relative permeability μ_r by the means of the vector S. Its direction is coincident with the direction of energy flow, and its magnitude is expressed in power per unit area [W.m^{-2}]

$$S = E \times H = \frac{1}{\mu_0 \mu_r} E \times B \quad (2\text{-}22)$$

Where E is the electric field (V/m).

2.8. Electric and magnetic circuits

The magnetic system is considered as analogous to an electric circuit in the steady state, although a magnetic conductor and magnetic insulator are concepts not nearly so accurate as an electric conductor and insulator. The magnetic and electric circuits is that both the flux and the current are without sources and sinks; both are continuous around their respective loop. This means that the flux and the current through any closed surface both equal zero.

$$\oint B \cdot ndS \quad (2\text{-}22)$$

$$\oint J \cdot ndS \quad (2\text{-}23)$$

The concept of Ohm's law can also be applied in magnetism; therefore, where resistance is the ratio of the voltage to the current, the magnetic resistance is analogous to electrical resistance named as a reluctance R. Reluctance is a measure of the opposition to the magnetic flux driven by magneto-motive force. Because reluctance largely depends on geometrical parameters and the permeability of the material, the reluctance is a complex number that depends on frequency [2-16], which is defined as:

$$R = \frac{F}{\Phi} \quad (2\text{-}24)$$

Where F is magneto motive force (MMF) which equals to NI. Recall from (2-1), (2-4), (2-11) and (2-12) that the reluctance of the uniform, closed magnetic circuit of the magnetic path length l_m and cross sectional area A is:

$$R = \frac{lm}{\mu_0 \, \mu_r A} \quad (2\text{-}25)$$

Table 2-4 Values of the relative permeability μ_r for some paramagnets, diamagnetics and ferrimagnets [2-8] and [2-9]

Material	μ_r	B_{sat} (T)
Free space	1.000 000 00	-
Air	1.000 000 37	-
A1	1.000 02	-
Cu	0.999 99	-
96% Fe, 4% Si (non-oriented)	7 000*	1.97
97% Fe, 3% Si (grain-oriented)[2]	100 000*	2.00
50% Co, 50% Fe (Permendur)	5 000*	2.45
79% Ni, 16% Fe, 5% Mo (Super Malloy)	1 000 000*	0.79
97% Fe, 3% Si (monocrystalline)	3 800 000*	2.14

*For ferromagnetic materials

Table 2-5 Circuit analogies [2-9] and [2-9]

Electric	Magnetic
Current = electromotive force/resistance	Flux = magneto motive force/reluctance
Current = i	Flux = Φ
Electromotive force = e	Magneto motive force = ni (SI) (cgs)
Resistance = R = ρl/A = l/σA	Reluctance = l/μ_rA (SI) or l/μ A (cgs)
Resistivity = ρ	Reluctivity = 1/μ_r (SI) or 1/μ (cgs)
Conductance = 1/R	Permeance = μ_rA/l (SI) or μA/l (cgs)
Conductivity = σ = 1/ ρ	Permeability = μ_r (SI) or μ (cgs)

2.9. Magnetisation in ferromagnetic materials

Ferromagnetic materials can be easily magnetised, as they have a large magnetic permeability μ ranging from 10^2 to 10^6. Their magnetisation can change by the applied magnetic field in a complex way, which is described by the magnetisation curve.

2.10. Domain structure and magnetisation curve

Ferromagnetic materials are composed of a number of small regions (with physical dimensions of the order of 10^{-3} to 10^{-4} cm) called domains, each of which is magnetised

to saturation even though no external field is applied. Regions in ferromagnetic materials are formed by atomic dipole alignment. Each atomic dipole can be considered a north-south bar magnet with constant magnetisation, as shown in Fig 2-5, and a region comprised of magnetic moments all pointing in the same direction is called a magnetic domain. A layer of atoms called a domain wall separates them. These walls are 100 to 1000 atoms thick [2-8]. When the ferromagnetic material is subjected to an external magnetic field, the domain walls move, causing their size to change [2-10]. Each domain is magnetised to the saturation value. In fact, the magnetisation directions of the domains are randomly distributed, and further increase of the external magnetic field causes the domains to rotate and become closer to the direction of the applied field. The purpose of an applied field is to cause the assemblage of domains making up the magnetic moments of the dipoles to align themselves with the direction of the applied field.

The magnetisation process converts the ferromagnetic material from a multi-domain state into a single domain magnetised in the direction of the applied field.
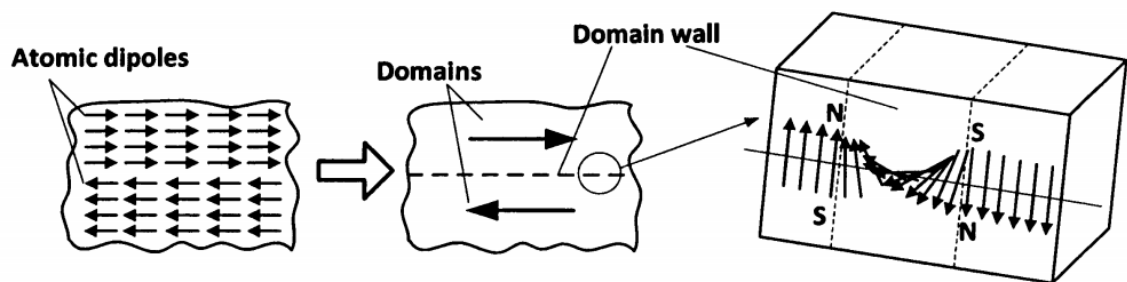
Fig 2-5 Domains and domain walls in ferromagnetic materials [2-8].

A single domain produces a large external field, so the domains re-distribute themselves to the state which has no external field and zero magnetisation, as illustrated in Fig 2-6. The domain walls separating two anti-parallel bar domains are called 180-degree domain

walls, and walls between the main bar domains and perpendicular flux-closure domains are called 90-degree domain walls [2-8].
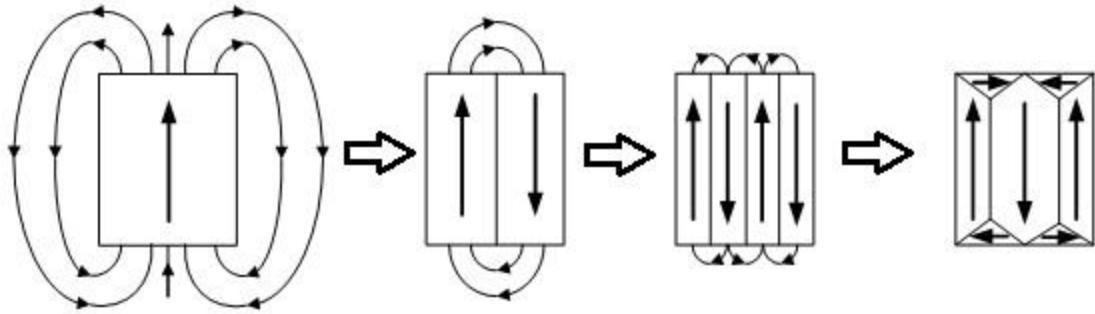
Fig 2-6 Re-distribution of domains to minimise the magneto-static energy [2-9].

The magnetisation curve represents a relationship between the flux density **B** and the magnetic field strength **H**. This curve provides fundamental information about a given magnetic material. The magnetisation process is schematically illustrated in Fig 2-7 and Fig 2-8 [2-11]. The squares in Fig 2-7 represent the crystalline structure of the material, shown as parts of four domains, and the solid line boundary separating them is called the domain wall. During the demagnetisation process, the four domains are magnetised in the opposite direction, so there will be zero net magnetisation for this crystal part, as it can be seen in Fig 2-8 part (a). When the material is subjected to magnetic field **H** (Fig 2-8 part b), that leads the upper domains to grow at the expense of the lower ones by the downward motion of the domain wall. For small applied magnetic fields, the material will return to its initial state without hysteresis. However, with larger applied fields, the domain wall movements are irreversible (Fig 2-8 part c). If the magnetic field is removed, the material will remain partially magnetised due to the new positions of domain walls (the hysteresis appears). With (Fig 2-8 part d) further increase of the magnetic field, the domain walls tend to disappear from the region, and the whole body of the material is a single domain. With magnetisation parallel to the direction of the applied field, the material is fully saturated, as illustrated in (Fig 2-8 part e)
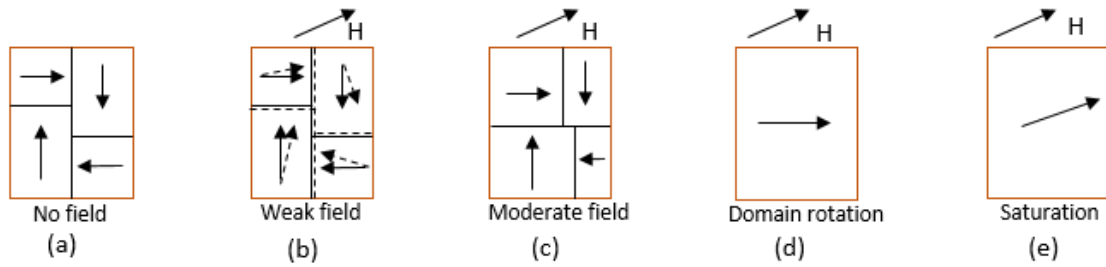
Fig 2-7 Change in domain pattern during magnetisation
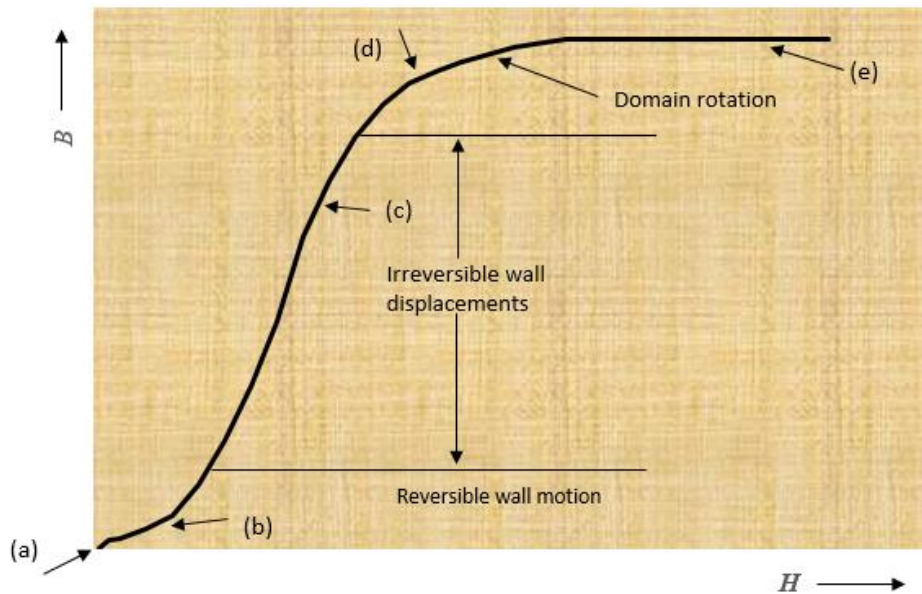
Fig 2-8 Magnetisation in ferromagnetic materials

2.11. Reversible and irreversible processes

The static hysteresis magnetisation has both reversible and irreversible processes. The reversible process is when the magnetisation changes with the applied field and returns to its original state when the field is removed. On the other hand, the irreversible process occurs or defines as that when the magnetisation takes a new value after removing the applied field. The slope of the curve (a b) in Fig 2-8 is the initial susceptibility, beyond this region, the processes of magnetisation are no longer reversible.

As shown in Fig 2-9 the magnetisation process for the soft magnetic material started from demagnetised state up to saturation, then, it is brought to the remnant when the applied field is removed. The final state for complete loop is achieved by applying a reversed field (coercive force)

2.12. Hysteresis loop

When ferromagnetic material is subjected to alternating magnetic field, the hysteresis loop will appear, it is also known as B-H loop or B-H curve, as shown in Fig 2-9. Starting from a demagnetisation point when (H=0, B=0), the curve follows the initial magnetisation path from 1 to 2 (dashed curve) B increases from zero up to the saturation. When **H** decreases, the return path will be different to the initial magnetisation curve, this is because of irreversible change of the domain wall locations. When the magnetic field **H** is zero, the value of **B** field is higher than that, this (point 3) is called residual or remnant flux density. The magnetic flux density becomes zero point 4 when an opposite direction magnetic field **H** is applied. This value of **H** is called coercive field or coercive force **H$_c$**. The portion 3 4, of the magnetisation curve is often referred to demagnetisation curve. Further increase in **H** field in the negative direction after coercive point, further increase of the magnetic field in the opposite direction, will gain negative saturation for the material point 5. When the **H** field changed to the positive value, the magnetisation will not return to the initial point from it had previously started (point 1), but it will close the loop at (point 2) forming the path 5 6 2, is called the *hysteresis loop*
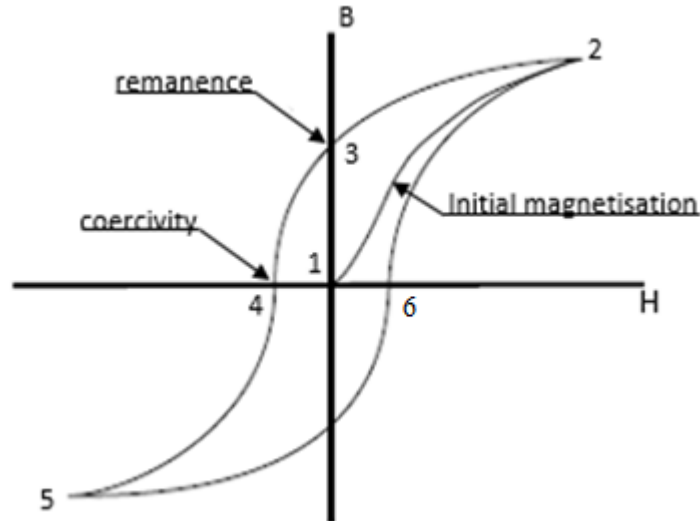
Fig 2-9 B-H loop for ferromagnetic material.

It can be seen from Fig 2-9 that one complete cycle of magnetisation yields B-H loop, The area enclosed by B-H loop is proportional to the energy loss dissipated in the material during one complete cycle, the loss is generated in ferromagnetic material can be

expressed as the sum of three components: static hysteresis loss, classical eddy current loss and anomalous loss.

The B-H loop provides information about ferromagnetic materials. For example, if the loop is narrow (low power loss generated and low stored magnetic energy) then such materials are called "soft magnetic material". The second case scenario is when the loop is wide (higher power loss generated and high stored magnetic energy), such materials are classified as "hard magnetic materials". Those materials (hard or soft) are also classified based on coercive force, hence materials with coercive force higher than 10 000 A/m are characterised as hard magnetic materials, and those with coercivity below 1000 A/m are considered magnetically soft. Coercivity depends on the heat treatment and deformation of the material such as cold rolling as well as the addition of non-magnetic elements such as carbon [2-6].
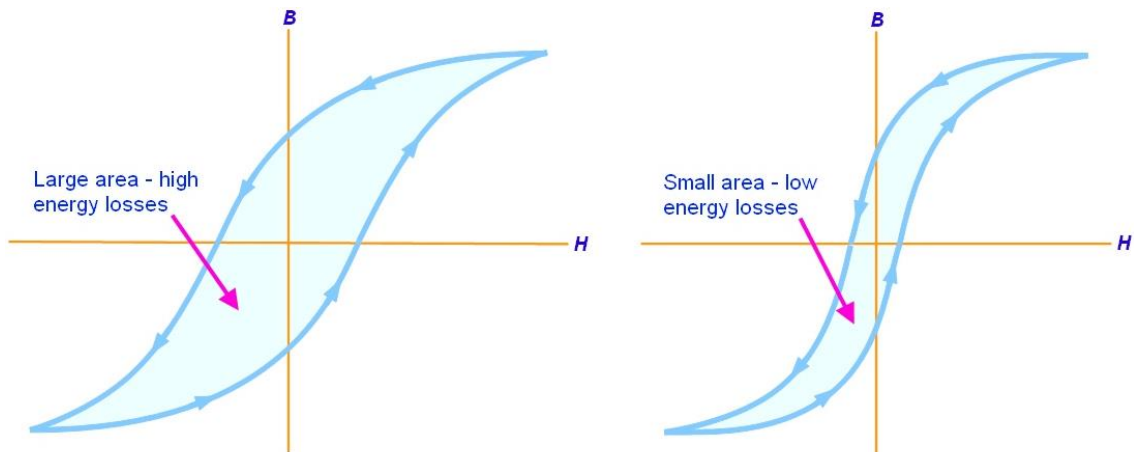
Fig 2-9 B-H loop for ferromagnetic material

The origin of B-H loop is the work required in order to align the magnetic domains to the direction of the applied magnetic field. The domain walls under the applied field are believed to be impeded by pinning sites which are caused by impurities in the magnetic material or inhomogeneous strain caused by dislocations. Based on the impact of the pinning sites, more energy is needed in order to gain full alignment of the domains, and the loss of energy associated with this work is dissipated in the form of heat.

The static hysteresis loss is proportional to the area enclosed by B-H loop and also the magnetising frequency. Though Steinmetz hysteresis loss formula is widely used, but it has been found that the Steinmetz exponents varies with flux density, which constitutes some restriction on its application [2-12], [2-13]. The eddy current power loss is the induced currents due to the main magnetic flux density B, this type of loss is highly

proportional to the square product of material thickness, flux density and the magnetising frequency. Hence the core laminations are build-up with stacked up thin laminations which provides restriction to the induced current to flow in smaller surface area therefore lower power loss. The anomalous loss, or the excess loss there has been always known as the difference between the measured power loss and the sum of the calculated hysteresis and classic loss. It has been found that this discrepancy in grain oriented electrical steel has reached up to 50 % of the total core loss at operating frequency [2-14]. The anomalous loss is thought to be proportional the domain wall spacing and inversely proportional to the lamination thickness [2-15]. More details about the three power loss components will be presented in chapter 5.

In addition, under DC/quasi-static magnetisation, there is only hysteresis loss component. But when the material is under AC magnetisation, the B-H loop will become wider, due to the impact of conventional eddy current and the anomalous loss. As a result, the total power loss is higher under AC magnetisation than that under DC quasi-static magnetisation condition.

2.13. Saturation and hysteresis

This is known as unwanted side effect of ferromagnetic core, though it has advantages, this effect is known as the saturation, this happens when the applied field is larger than the permeability of the core material, when the permeability starts to drop.

If the applied field is past the saturation further, the permeability eventually drops to that of the free space [2-16]. This state (saturation) the material is no longer able to increase its internal microscopic alignment, in other words, the domains are fully aligned.

Summary

In this chapter, the electromagnetic terms, unit systems and the relationship between different parameters have been presented, followed by classification of the materials and the development of electromagnetism. The magnetisation process in ferromagnetic materials was described using domain structure theory. Hysteresis loss and the accompanying power losses under AC magnetisation were also discussed in this chapter. The background knowledge in this chapter providing the base for the upcoming chapters on studying different phenomenon occurs and affects the electrical steel cores.

References :-

[2-1] L.Shua-hua,"Origine de la boussole ll.Aimant et boussole, "lsis, vol.45, no. 2, p.175.Jan.1954

[2-2]W. Gilbert and P.F.Mottelay, De magnete. New York: Dover Publication, 1958, p.368

[2-3] W. Boast, principles of electric and magnetic fields" second edition, USA Harper and brotherS.1956

[2-4] D. Ball," Maxwell's equations, part VII," Spectroscopy, vol. 27, no.6, pp.20-27, 2012

[2-5] F.T. Ulaby, E. Michielssen, and u. Ravaioli, fundamentals of applied electromagnetics. Boston: Prentice Hall, 2010, p.298

[2-6] B.D. Cullity and C.D. Graham, introduction to magnetic materials. Hoboken, NJ, USA: John Wiley & Sons, Inc., 2008

[2-7] B S Guru, H R Hiziro, "*Electric Machinery and Transformers*" Third edition, Oxford University Press, Inc. 2001

[2-8] D. Jiles, Introduction to magnetism and magnetic materials, Chapman & Hall, London, UK, 1991

[2-9] B. D. Cullity, Introduction to Magnetic Materials, Addison-Wesley, Reading, Massachusetts, 1972.

[2-10] Seely S. "introduction to electromagnetic fields" McGraw-Hill Book Company, Inc.USA, 1958

[2-11] C.E. Webb" The power losses in magnetic sheet material at high flux densities*," Electr. Eng. J. Inst.*, vol.64, no352, pp.409-427, 1926

[2-12] F. Brailsford, "Investigation of the eddy-current anomaly in electrical sheet steel,*"Electr. Eng. -Part I Gen.J.Inst., vol.95, no.88, pp.175-177, 1948*

[2-13] M.J. Heathcote, the J & P transformer book: a practical technology of the power transformer. Amsterdam; London; Oxford: Elsevier; Newness, 2007.

[2-14] R. H. Pry and C.P Bean, "calculation of the energy loss in magnetic sheet material using a domain model, J .Appl. phys.," vol.29, no.3, pp.532-533, 1958

[2-15] K. G. N. B. Abeywickrama, T. Daszczynski, Y. V. Serdyuk and S. M. Gubanski, "Determination of Complex Permeability of Silicon Steel for Use in High-Frequency Modeling of Power Transformers," in *IEEE Transactions on Magnetics*, vol. 44, no. 4, pp. 438-444, April 2008.

[2-16] R. Schmitt. Electromagnetics explained: a handbook for wireless, RF, EMC, and high-speed electronics, (2002)

[2-17] P.C. Sen. "Principle of Electric Machines and Power Electronics", 2nd Edition, John Wiley and Sons, 1997.

3.1. Introduction

This chapter summarises the previous studies related to edge-burrs in the electrical steel materials, hence different techniques have been applied to study the impact of this phenomena.

3.1.1. Effect of edge-burrs defect on the magnetic properties of electrical steel

Moses and Aimonitois have studied the impact of edge burrs on total power loss of single phase transformer core by introducing artificial burrs along the edges of the core [3-1], the core under investigation was assembled from grain oriented 3% silicon iron, the power loss were firstly measured at 1.3 T, 1.5 T and 1.7 T at magnetising frequency of 50 Hz. Fig [3-1] shows edge burrs simulated by drilling 0.3 mm holes close the edges of the laminations and inserting a steel pin or rod to short out the required number of laminations under test. Fig 3-1(a) illustrating the location of pins in one of the limbs and Fig 3-1 (b) shows the method of applying artificial burrs.

(a)   (b)
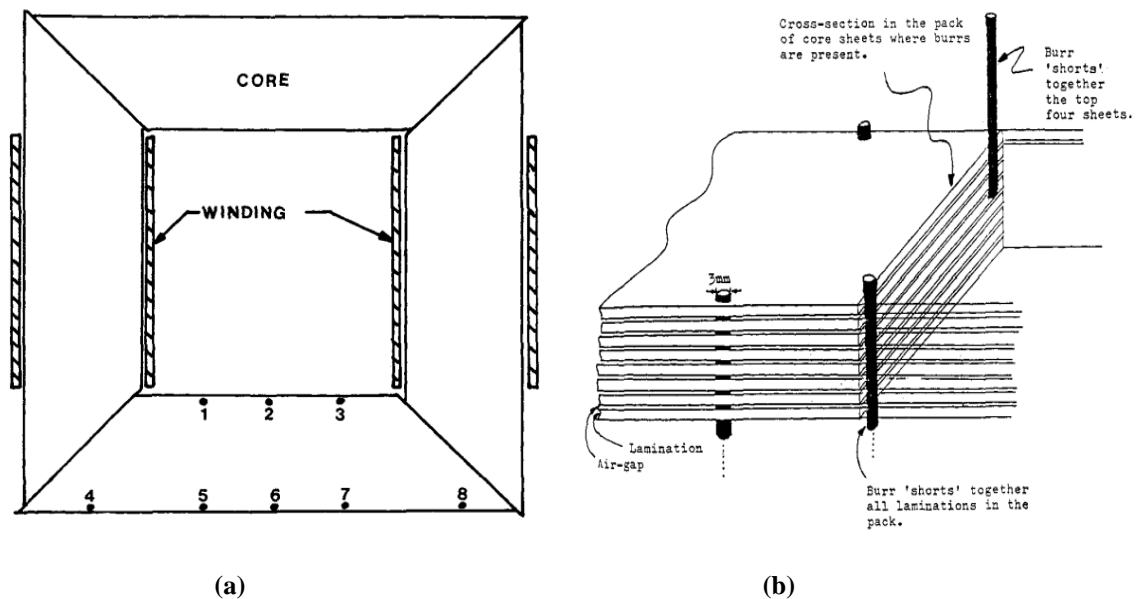
Fig 3-1(a) Schematic plan view of single-phase core showing positions of artificial burrs. [3.1]

Fig 3-1(b) Method of producing artificial burrs. [3.1]

The transformer core with various combinations of artificial burrs (, the points 2, 3 & 7and 2,3,&7 and 1,2,3,6&7). was energised and then the total power loss was measured, the obtained results were compared with burrs-free core. Results are shown in Fig 3-2
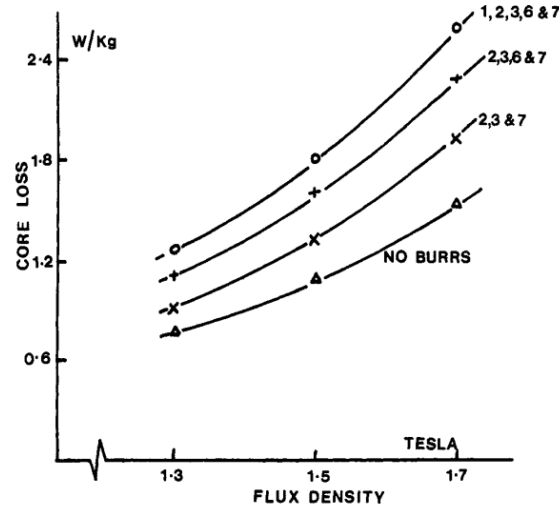
Fig 3-2 Total core loss variation with flux density for different burr configurations.[3-1]

The localised loss was measured at 32 points on specific laminations using initial rate of rise of temperature technique, a microprocessor controlled thermocouples bridge was designed to scan through the array of 32 thermistors and evaluate the loss Fig 3-3(a) shows the location of thermistors on the core laminations for measuring the power loss and Fig 3-3 (b) shows measured power loss.
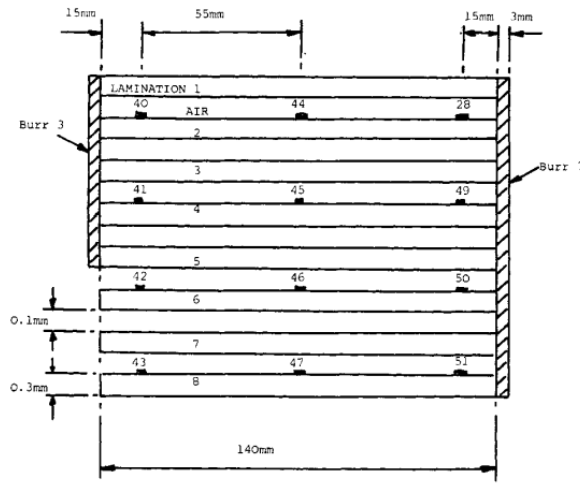
Fig 3-3(a) Position of thermistors in stack of laminations.[3-1]
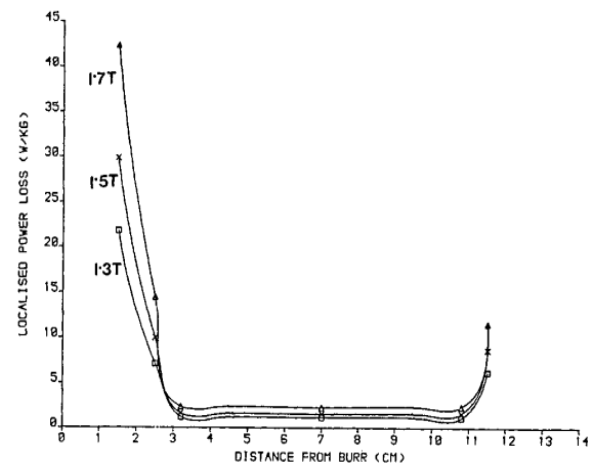
Fig 3-3(b) Variation of localised loss on a line between burrs 3 and 7 at 1.3T, 1.5T and1.7T.[3-1]

The results have shown a high increase in power loss based on the number of shorted laminations, a further increase in power loss when more laminations shorted together. This is due to closed path between the burrs introduced resulted in localised loss close to burrs was very high.

Another study was conducted by Aimoniotis and Moses in 1993, in which they have employed finite element program to evaluate the linear steady state eddy currents induced in a core [3.2]. By applying Maxwell's equation for time varying electromagnetic fields, number of laminations were shorted on either sides. Fig 3-4(a) shows the end part of core model that contains eight laminations being electrically connected Fig 3-4(b) shows the contour of the equivalent surface which illustrates the eddy current path in the core. The variation of current density is along line located just below the surface of the third lamination in the core parallel to the surface,

Based on the obtained results, eddy currents are very high at the burrs and their surroundings and these drop down by moving 2.5 mm away from the burrs. The value of eddy current increases with increased number of shorted laminations. The model has also concluded that the effect of edge burrs only occurs when burrs appear on both sides of the core, so shorting one side of the core has no impact on the total power loss.
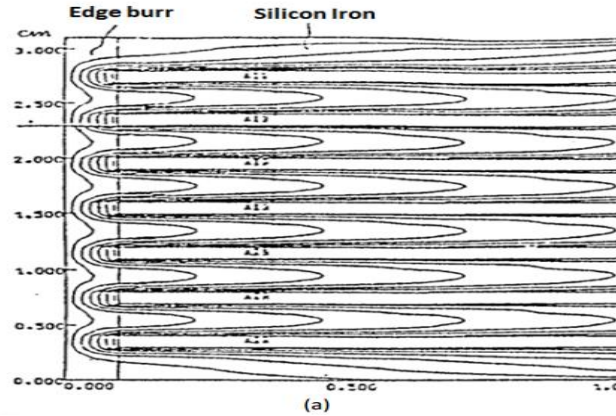
Fig 3-4(a) end part of model having 8 laminations shorted on both sides.[3-2]
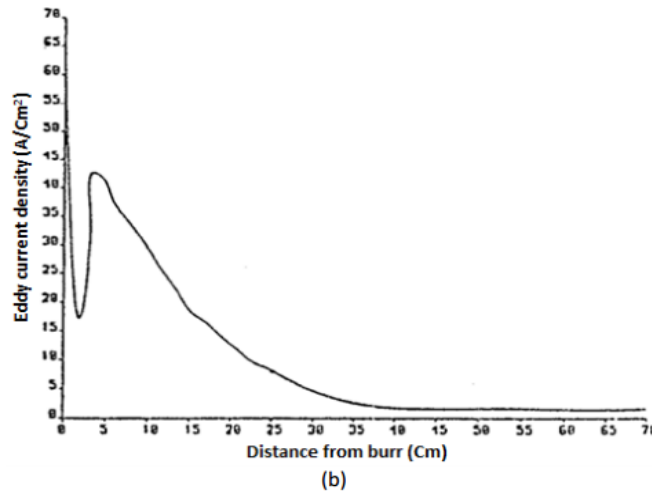
Fig 3-4(b) variation of current density along the laminations (third from the top) of the core consisting of 8 laminations [3-2]

In 2010, Schulz et al have studied the impact of short circuit between a pair of magnetic sheets, the work is elementary based on introducing insulation fault on opposite sides of the sheets. Hence when insulation fault (short circuit) is applied on one side only, it showed no effect on the total power loss. This is because this type of faults does not introduce closed path for the current induced perpendicular to the component of flux density vector **B** [3.3]. The below schematic illustrates two laminations with short circuit on one side only Fig 3-5(a) and on two sides Fig 3-5(b), Their model is based on Thevenin equivalent circuit, Fig [5-c], and Fig [5-d] respectively. R_{eq} is the equivalent resistance of the lamination R_{ct} is the contact resistance caused by edge burrs. This experimental work has determined the U_{oc} and

R_{eq} by applying alternating magnetic field to a pair of artificially shorted transformer sheets 30 mm wide, from CGO 0.3 mm thickness,
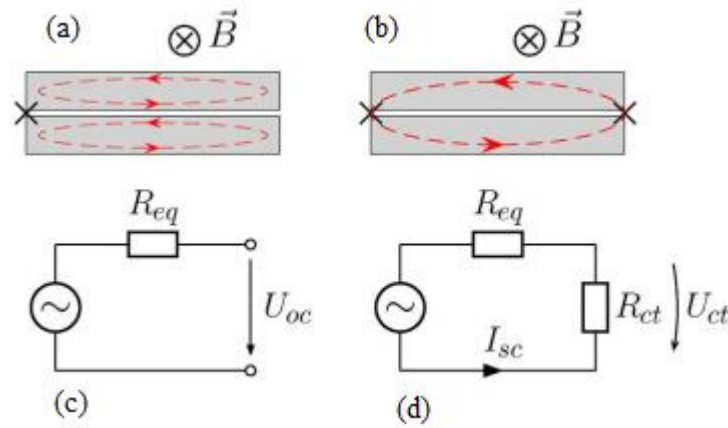
Fig 3-5(a) Cross-section of pair of lamination with fault short circuit at one side, 3-5(b) Cross section with fault current path 3-5(c-d) equivalent electric circuit with and without contact point respectively.[3-3]

The tests were firstly performed in an open circuit condition then in a short circuit condition and the voltage drop across the contact resistance R_{ct} is also measured. The worst case is given when $R_{ct} = R_{eq}$ leading to maximum power dissipation in the burrs area. On the other hand, higher short circuit current occurs when $R_{ct}=0$

The obtained results for R_{eq}, U_{oc} and I_{sc} as a function of flux density are depicted in Fig 3-6 for different core widths.
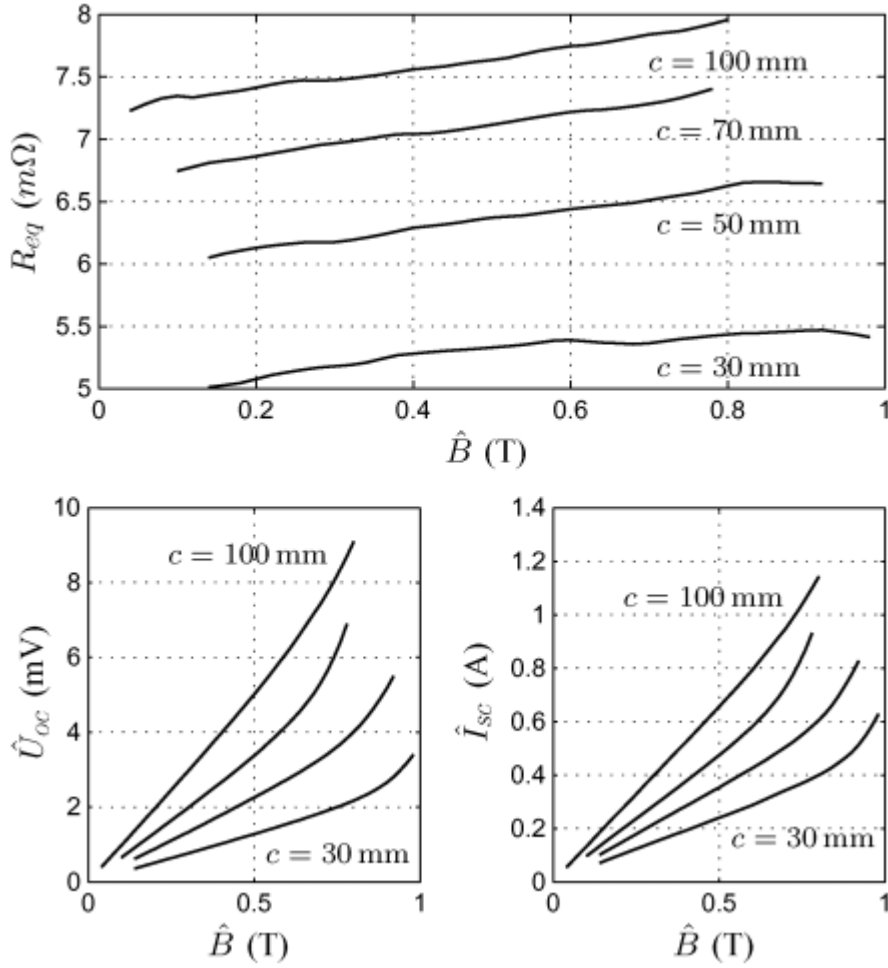
Fig. 3-6. Behaviour of an inter-laminar short as a function of flux density and for different core widths C.[3-3]

It has been found that U_{oc}, I_{sc} and R_{eq} are proportional to the flux density, the short circuit current I_{sc} increased when applying zero contact resistance. Moreover, if the material is homogeneous, the linear increase R_{eq} is constant for different core width. The linear increase in R_{eq} shows that the equivalent resistance of an inter-laminar short depends on the complex interaction between the eddy currents circulating in the individual laminations and the short circuit current circulating between the shorted laminations. As a result, the eddy current distribution caused by an inter-laminar short circuit forms a complex problem, involving the anisotropic magnetic properties of the material, electric properties and many geometric parameters.

In 2011, Lamprecht and Graf had investigated the effect of the electrical short circuit caused by edge burrs on the power loss of a ring core specimen [3.4]. A short circuit between the lamination was simulated by using galvanic nickel with a thickness of approximately 0.1 mm. the below Fig 3-7(a) illustrates the dimensions of the core sample while Fig 3-7 (b) is the cross section of the core sample with galvanic nickel.
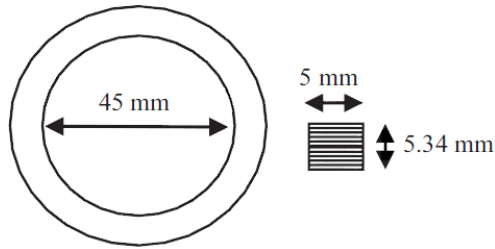
Fig 3-7(a) Dimension of core ring sample.[3-4]
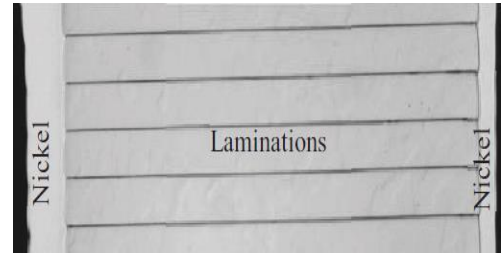
Fig 3-7(b) Cross-section of galvanically coated ring core sample.[3-4]

The analysis of eddy current paths in the core samples and the loss was conducted by using "ANSYS Maxwell 3-D" simulation tool. A fine mesh was used in order to visualize the eddy current paths which in turn will provide a reliable calculation of the specific eddy current loss. Fig 3-8 illustrates a model of three laminations shorted at the edges.
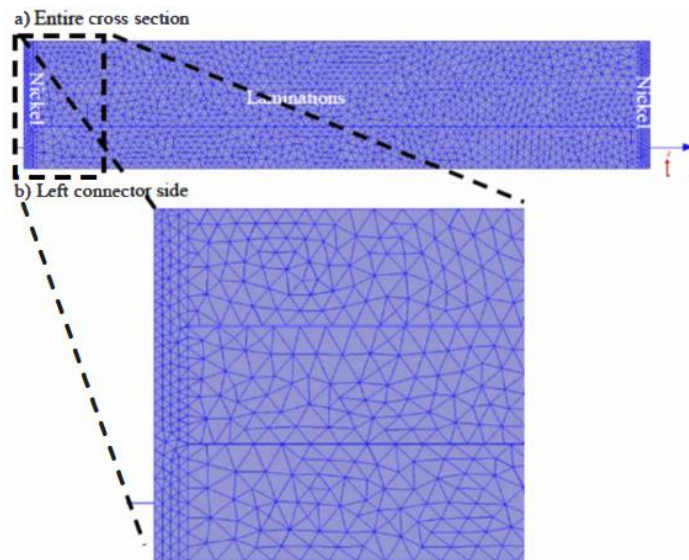
Fig 3-8 Finite element model with mesh, three laminations: a) entire cross section; b) left connector side.[3-4]

Fig 3-9 illustrates Finite element modelling (FEM) eddy current circulation in a stack of four laminations, as it can be seen the eddy current circulates in one entire loop, while in the

middle of the stack no eddy current induced. A simple equivalent circuit for the model is shown in Fig3-10, the model is simulated based on that.
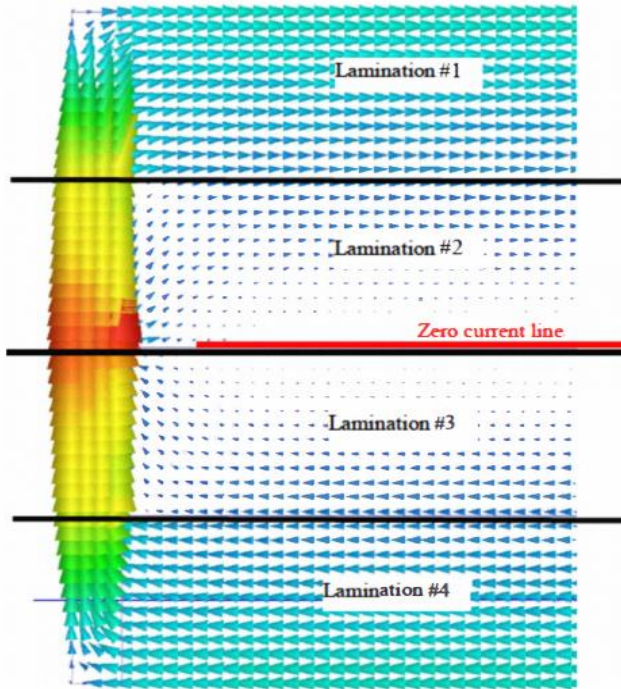
Fig 3-9 eddy current density direction in four shorted laminations [3.4]
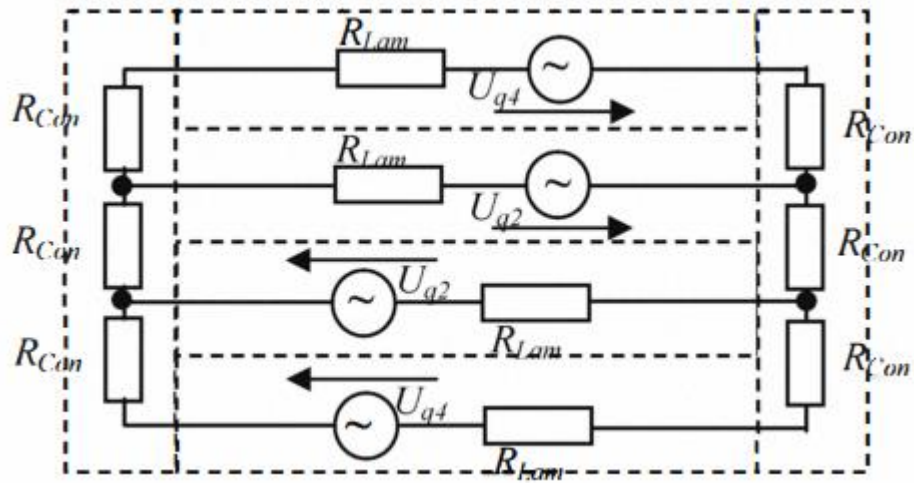
Fig 3-10 Equivalent electric circuit model of a stack of four shorted laminations reproduced from [3.4]

The obtained results of the eddy current power loss based on analytical analysis (electric circuit model) model are roughly 10 % higher than the numerical analysis (FEM). The results are compared in Fig 3-11.
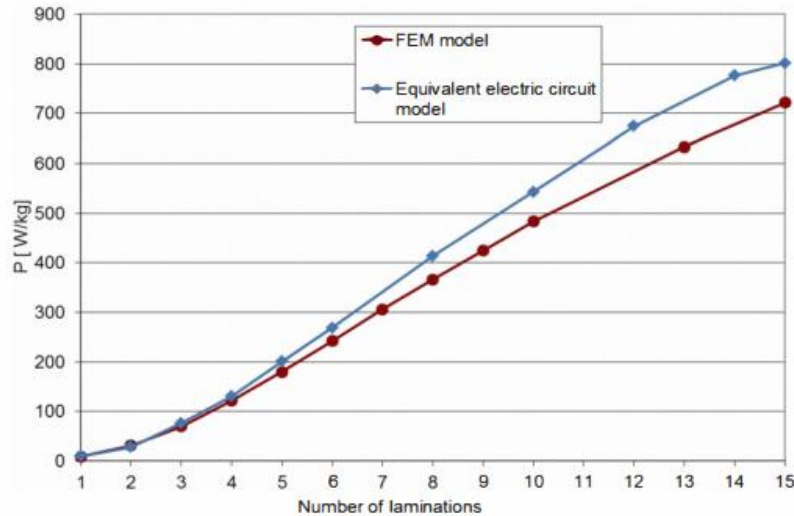
Fig 3-11: Variation of finite element and modelling of eddy current losses vs. number of laminations reproduced from [3.4]

A comparison had been made between the FEM, calculation and measured results for the eddy current power loss of a pack of 15 burred laminations at magnetising frequency of 400 Hz and flux density of 1.0 T, the table 3-1 shows this comparison.

Table 3-1 Comparison of specific eddy current losses at B=1 T at f = 400 Hz

Method	Specific eddy current losses B=1.0T, [W/kg]
Finite element analysis (Maxwell 3D)	722
Equivalent electric circuit model	801
Measurement	1038

It has been noticed that higher values of eddy current power loss is obtained by experimental measurement than through simulation and the calculated methods. This difference is believed to be due to the impact of the galvanic coating process. Hence, the coating thickness varies between 0.1 mm and 0.4 mm, while in the FEM modelling a constant thickness of 0.1 mm

was considered, moreover, the impact of the anomalous loss related to domain structure of the specimen might lead to higher power loss which was not considered in these two methods.

Bielawski et al. in 2012 had studied the impact of a short circuit fault (specifically edge burrs) on the efficiency of a transformer core. Some assumptions have been made in this study. The first is by assuming that the electrical conductivity between the centers of two laminations is very low. The second is the contact points are random, therefore they separate the faults into two different categories, one of which does not create current loops and the other create extra current loops, which lead to additional losses and hotspots. The purpose of their study was to estimate the currents flowing in the edge burrs to visualise the current line in the core laminations, a 3-D numerical simulation has been applied. Fig 3-12(a) illustrates a simulation of edge burrs on two small blocks connecting the two sheets on each side. The modelling results in Fig 3-12(b) has shown that current lines converge towards the contacts which explains the hotspots occurrence caused by edge burrs. This study have also concluded that the short circuit current is significantly high when the contact points are in front of each other and also when one contact is shifted in z- direction, the current decreases.
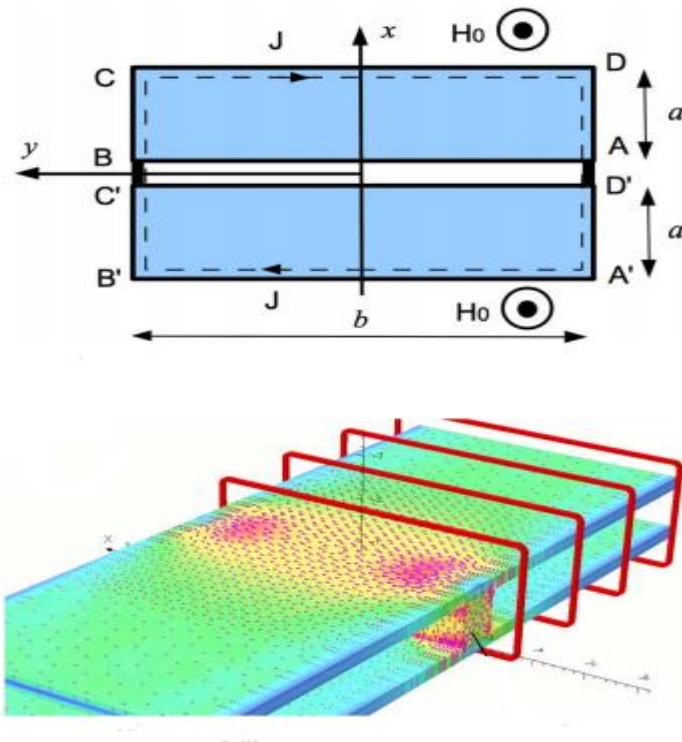
Fig 3-12(a) A detrimental effect caused by two burrs. (b) 3-D numerical simulation of an elementary short-circuit.[3-5]

The obtained results by FEM has shown that when low contact resistant formed by edge burrs, the induced current forms a large loop inside the two laminations; the set of two laminations acts as a double thickness sheet.

In 2012 Mazurek et al. conducted an experimental work on the impact of inter-laminar fault on a 350 kVA three-phase transformer core. Fig 3-13(a, b) shows a clamping device which was used to apply artificial burrs, hence 10 mm, 15 mm and 20 mm lengths shorting out approximately the top 33, 50 and 66 laminations respectively. For simulating real edge burrs, 8 μm thick copper tape, pressed against the sides of the stack of laminations by wooden block and then firmly clamped by torque meter. In this experimental work, the thickness of copper tape was chosen to be comparable with actual edge-burrs dimensions. Moreover, the clamping device did not have an impact on the power loss.
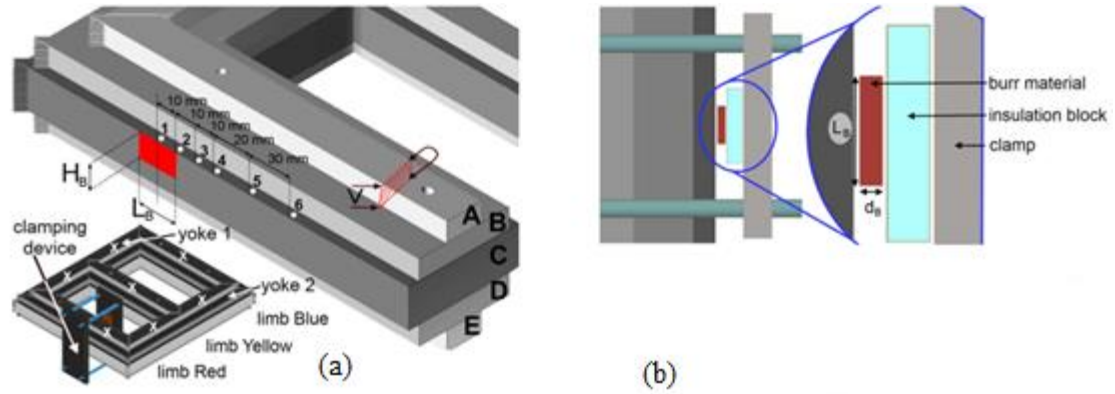
Fig 3-13(a) Experimental core showing clamping rig for applying artificial burrs, thermocouples and needle probe measurement positions. (b) Top view of the burr clamping showing the insulation block, burr (copper tape) length and thickness.[3-6]

The total power loss was measured using power analyser, and the localised losses with and without burrs was measured by initial rate of rise of temperature technique. The results are shown in Fig 3-14(a, b)
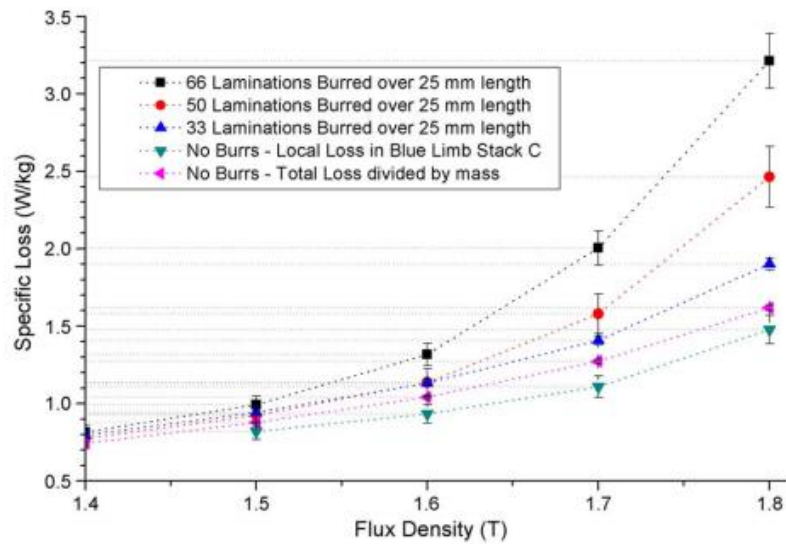
Fig 3-14 (a) Variation of specific loss with overall flux density of the core for burrs of different heights compared with the non-burred core.[3-6]
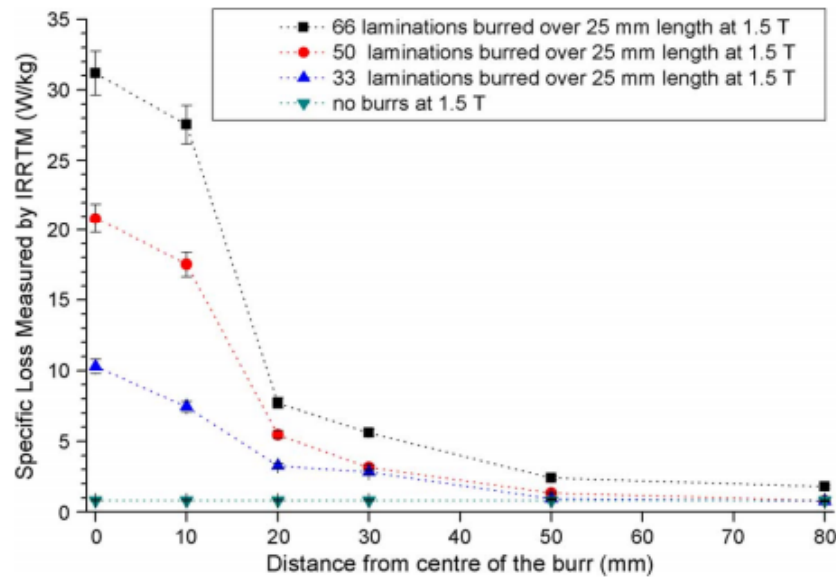
Fig 3-14(b) Variation of local specific total loss with distance to the center of the artificial burr for burr height HB = 10 mm, 15 mm and 20 mm. [3-6]

This experimental work has shown that the effect of edge burrs is largely proportional to the number of burred laminations, as burr region covers 66 laminations, 13% increase in the power loss at 1.5 T and by 100 % increase at 1.8 T. Furthermore, the presence of edge burrs had caused a higher increase in temperature and hence higher local loss. It had been noticed that the local power loss increase occurs as far as 70 mm from the edge of the burred region.

3.2. Toroid cores

Zurek et al, in 2008 had conducted both experimental and a 2-D FEM of wound toroids. A commercially available FEM software Finite-Element Modelling, "Mag Net" with three types of solver: magneto-static, transient and time harmonics was used. A test specimen as shown in Fig 3-15(a, b) 2-D core with 55 turns was modelled, the inner and outer diameter were set to 70 mm and 102 mm respectively. The core material was chosen as conventional grain oriented electrical steel (grade M4) of thickness equal to 0.27 mm, with 20 μm air gap between laminations. A uniformly distributed exciting coil with 12 turns was modelled [3.7].

a)   b)
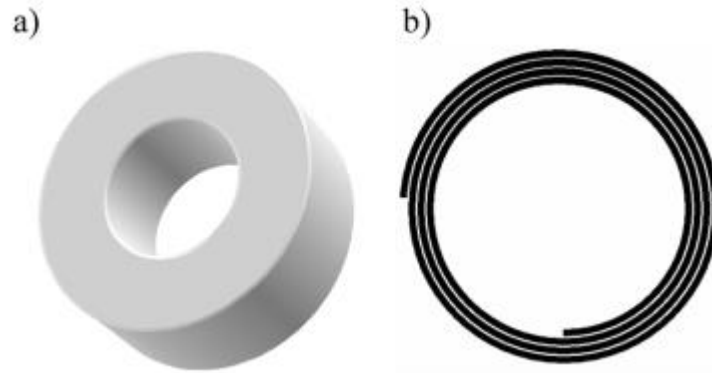
Fig 3-15 Wound toroid core (a) general view; (b) simplified cross-section through a four-turn showing spiral structure.[3-7]

The measurements for the power loss of the sample were performed according to specifications, the full procedure for the measurement is fully explained in chapter 5. The flux density was controlled to vary sinusoidally with time to peak values up to 1.5 T at 50 Hz. The test sample is a wound toroid having dimensions of $70\times104\times40$ commercially produced grain oriented electrical steel (grade 4). The search coils encloses every five turns (55 turns in total, 11 search coils as seen in Fig 3-16.
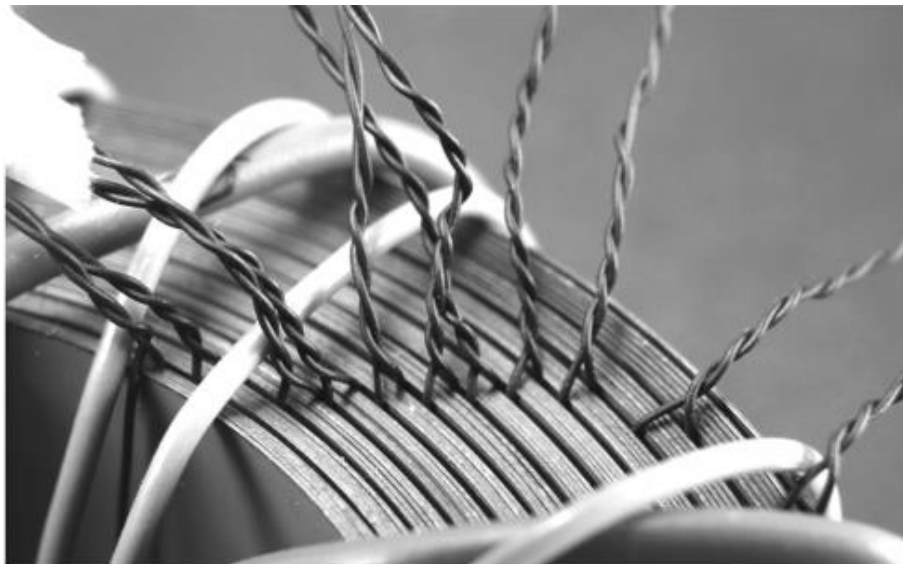
Fig 3-16 close up of the set of search coils in the toroid core under test.[3-7]

The search coils were placed close to each other rather than at random position. The obtained results are presented in Fig 3-17 where it shows radial distribution of the flux density. The

flux density B decreases towards the outer diameter, a distortion is noticed in measured B which can be attributed to the non-uniformity of core winding. At 400 Hz, the difference between inner and outer diameters is more slightly pronounced.
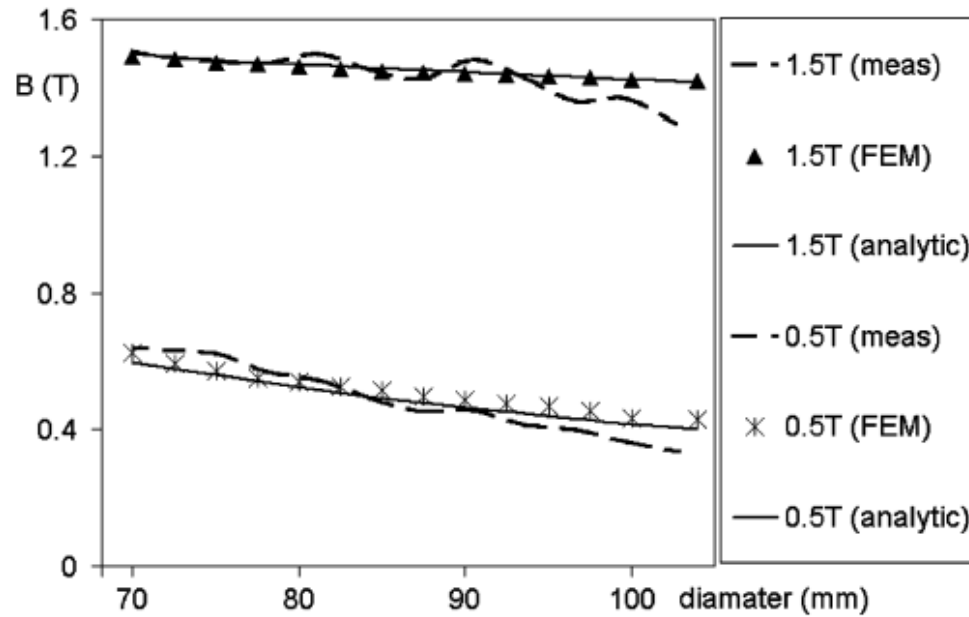
Fig. 3-17. Comparison of results for: a) 50 Hz, b) 400 Hz (measured and FEM—for 55-turn wound core, respectively, analytic—calculated for solid core with the use of analytical equation and B-H data as for the FEM solution).[3-7]

References:-

[3.1] A J Moses and M B Aimoniotis, "*Effects of Artificial Edge Burrs on the Properties of a Model Transformer Core*," Physica Scripta, VOL. 39, 1989, pp. 391–393

[3.2] M B Aimoniotis and A J Moses, "*Evaluation of Induced Eddy Currents in Transformer Sheets Due to Edge-Burrs, Employing Computer Aided Design Programs*," in Athens Power Tech '93 Proc., 1993, VOL. 2, pp. 847–849

[3.3] C A Schulz, D Roger, S Duchesne, and J N Vincent, "*Experimental Characterization of Interlamination Shorts in Transformer Cores*," IEEE Trans Magn. vol. 46, no. 2, Feb. 2010, pp. 614–617,

[3.4] E Lamprecht and R Graf, "*Fundamental Investigations of Eddy Current Losses in Laminated Stator Cores Created Through the Impact of Manufacturing Processes*" Proceeding of 1stInternational Electric Drives Production Conference (EDPC), 2011, pp. 29-35

[3.5] J P Bielawski, S Duchesne, D Roger, C Demian and The Belgrade, "*Contribution to the Study of Losses Generated by Inter-Laminar Short-Circuits*", IEEE Trans On Magn, Vol. 48, No. 4, April2012, pp 1397-1400

[3.6]R. Mazurek, P. Marketos, A. Moses and J. N. Vincent, "Effect of Artificial Burrs on the Total Power Loss of a Three-Phase Transformer Core," in *IEEE Transactions on Magnetics*, vol. 46, no. 2, pp. 638-641, Feb. 2010.

[3.7] S. Zurek, F. Al-Naemi and A. J. Moses, "Finite-Element Modeling and Measurements of Flux and Eddy Current Distribution in Toroidal Cores Wound From Electrical Steel," in *IEEE Transactions on Magnetics*, vol. 44, no. 6, pp. 902-905, June 2008.

4.1. Introduction

The core of an electrical machine is the main part in which the magnetic flux is circulating, and the main purpose of the core is to concentrate the magnetic flux at as maximum a value as possible [4-1]. According to Faraday's law of induction, emf is induced in the windings by the magnetic flux flowing through the core. However, the cores of electrical machines are normally built from electrically conductive soft magnetic materials; hence an emf is induced in the core. The induced emf inside a magnetic core sets up losses $i^2 R$ along the path, called the eddy current [4-1], where i the eddy current and R is the resistance of the portion of the magnetic core through which the current flows. The induced eddy current along the path in the magnetic core causes heating due to path resistance. This heating represents the power loss known as eddy current power loss [4-2]. Different techniques have been used to minimise eddy current power loss, such as assembling the core from thin laminations so the induced current will be restricted to flowing in smaller surface areas, small amounts of silicon are added to the material to increase its electrical resistivity at the expense of reduced permeability. The laminations are then coated on both sides to provide electrical insulation between the laminations, which ensures the current will flow into each lamination, not including the adjacent lower and upper laminations [4-3], [4-4].

4.2. The effect of eddy current

Provided that the specification of the lamination sheet is available, the effect of the eddy currents on lamination thickness can be studied. Fig 4-1 shows the cross section of a sheet with thickness 2a, which is smaller than the width C. Moreover, AÁ and CĆ' have equal distances from the center OÓ. A portion of the total magnetic flux in the sheet passes through the electrical circuit formed by the thin elemental sheets of thickness dx. An electromotive force (emf) will be induced in this area AÁ CĆ; therefore an alternating eddy current flows around the path indicated by dx. The magnetic flux equals zero when x is zero and a maximum when x=a; hence, eddy current density in the material varies from zero at the centre of the lamination to the maximum value at the surface of the lamination.

Chapter 4: Eddy Current Phenomena In Ferromagnetic Materials
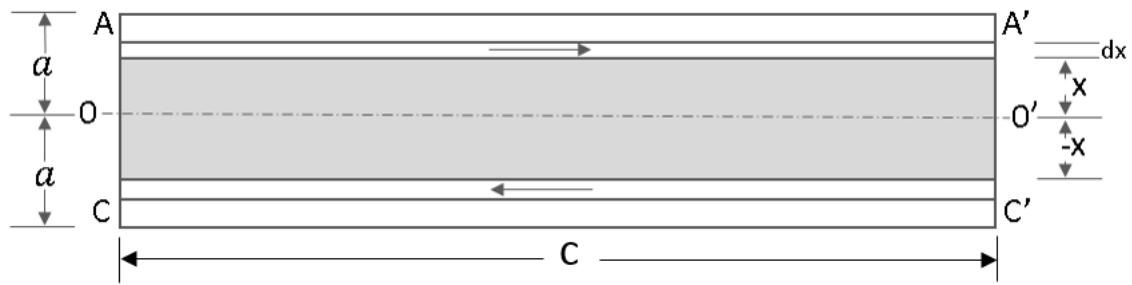
Fig 4-1 Eddy current in a thin lamination sheet

The arrows in Fig 4-1 represent the induced eddy currents. These currents have two different effects, since they flow in a resistive circuit; therefore, eddy current loss of energy in the form of heat in the lamination will occur in addition to the hysteresis loss. Moreover, the material inside the sheet indicated by AÁ and CĆ is subjected not only to the externally applied alternating magnetic field but also to the sum total of the eddy currents flowing between AÁ and the surface on one side of the central plane and between CĆ and the other surface. It must be noted that the magnetic field produced by the eddy currents has an opposite reaction towards the applied field—normally, the magnetic field is maximum at the centre of the lamination and zero at the surface. These eddy currents have the effect of reducing the internal flux density, which in turn will have minimum value at the centre and maximum at the surface, known as the skin effect. As a result, the net flux density obtained by the applied magnetic field will be reduced by eddy currents. It must be noted that the total flux in the lamination is sinusoidal, i.e. the flux density at any internal point will be of distorted wave form [4-5]. The same is the case for the internal eddy current and the effective field strength at any point.

In fact, the exact calculation of the distribution of eddy current and flux density inside a lamination is not possible because of the non-linear relation between **B** and **H** for any ferromagnetic material. The only way to make this calculation is by assuming that the relative permeability of that material is constant, and this assumption ignores the non-linearity of **B** and **H**. So for a sinusoidal total flux, or sinusoidal applied field, all other quantities are also sinusoidal. Some other assumptions are made in this calculation as well, such as that the material is a homogeneous medium, which ignores any possible complications that may be caused by the ferromagnetic domain structure.

Chapter 4: Eddy Current Phenomena In Ferromagnetic Materials

In order to apply the mathematical solution, the instantaneous eddy current per unit volume at distance x from the centre is $\frac{i}{volume}$. Magnetic induction and related phenomena inside a piece of steel lamination subjected to an external magnetic field can be derived from Maxwell's equations [4-6]. It is assumed that the displacement current density is neglected in comparison to the conducting current. To understand the nature of eddy current and eddy current power loss in accordance with Faraday's law of induction, when a time varying magnetic field is applied to conducting medium, an electromagnetic force is induced in that medium, taking into account the electrical conductivity of the material. The induced (emf) along a closed path inside the material sets up a current along this path to circulate and penetrate the conducting parts [4-7]. The direction of the eddy current is perpendicular to the direction of the magnetic field, while the distribution pattern depends on the shape of the conductor. Fig 4-2 (a, b) shows the distribution pattern of the eddy current for two different shapes. It can be seen from these shapes that the current density has a maximum value at the conductor surface, and it has a minimum value towards the center of the conductor, which will be analytically explained later in this chapter. The decline of the current density is known as the skin depth, which is a measure of the depth at which the current density falls to e^{-1} (approximately 0.367) of the value near the surface [4-8].
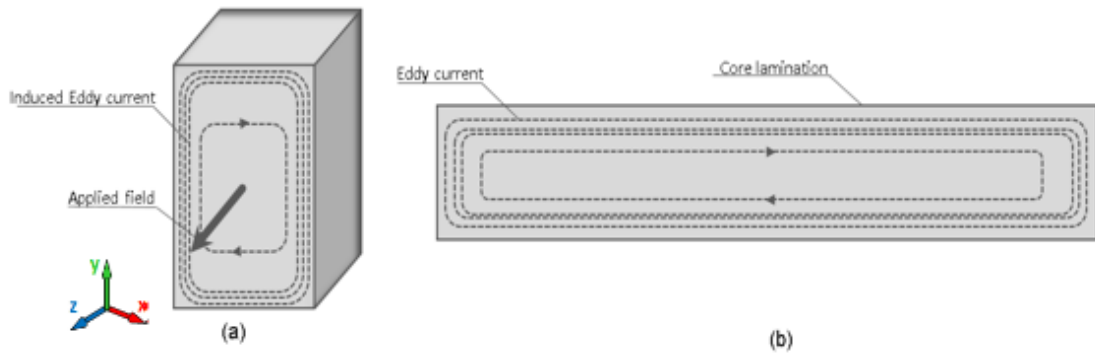
Fig 4-2 (a, b). Induced eddy currents in conducting medium caused by time varying magnetic field.

The skin depth of any conducting material can be calculated by using the below formula:

$$\delta = \frac{1}{\sqrt{\pi \mu f \sigma}} \quad (4\text{-}1)$$

Where f is frequency in (Hz); μ is permeability in (H/m) and σ is conductivity in (S/m). When the properties of the material are available, it is easy to calculate the skin depth. It

should be noted that the effect of the skin effect is negligible at low frequency; however, at higher frequencies where the skin depth is smaller, the effective cross section is reduced, which will increase the resistance of the conductor and hence the characteristics of the conductor. As a rule, the eddy current losses should be kept as low as possible. This can be achieved by keeping the eddy current low.

It has been indicated by [4-5] that the frequency-dependent magnetic flux density distribution is the main factor affecting eddy current power loss determination along the thickness of the lamination. Referring to Fig 4-1 lamination thickness t=2a in a time-varying magnetic field B_S cos ωt. (B_S : flux density at the surface) applied in the rolling direction.

Fig 4-2a illustrates a 3-D view of the single sheet lamination, with the z and y directions representing both directions of magnetisation either in rolling direction or transverse direction, which is at a 90-degree to the rolling direction. If the eddy current loops are assumed to be large enough in the transverse direction, the field problem becomes 1-d and can be reduced to a single equation for the z- component of the magnetic flux density B_z (x,t) that depends on (x,t) [4-5].

$$\frac{\partial^2 B_z \text{ (x,t)}}{\partial \text{x}^2} = \mu_0 \mu_z \, \sigma \, \frac{\partial^2 B_z \text{ (x,t)}}{dt} \quad (4\text{-}2)$$

Where μ_z is the permeability of the material at the particular flux density B_z , Equation 4-2 is a differential equation that defines the flux density B_z as a function of distance x and the time t, and it has the value B_S cos ωt. When x is ± a, this equation is applied for particular relative permeability and magnetic flux density as stated in [4-5].

The instantaneous flux density B_z at any point inside the lamination is given by:

$$B_z = B_s \; \left(\frac{\cosh 2px + \cos 2px}{\cosh 2pa + \cos 2pa}\right)^{0.5} . \; \text{Cos} \; (\omega t - ß) \; (4\text{-}3)$$

$$\text{where tan ß} = \frac{\sinh p(a-x).\sin p(a+x) + \sinh p(a+x).\sin p(a-x)}{\cosh p(a-x).\cos p(a+x) + \cosh p(a+x).\cosh p(a-x)} \quad (4\text{-}4)$$

and p = $^1/_\delta$

Where δ is the skin depth, which was defined by (4-1), and ß is the phase angle of the flux density and can be obtained by (4-4). Formula in (4-3) defines the flux density along the thickness of the lamination of distance x from the centre line of the lamination.

4.3. Flux density dependence of the relative permeability

Equation (4-2) can be extended to a wider range of flux density which includes the non-linear relation between **B** and **H**. By assuming that the material is ideal, i.e. no leakage flux is present around the magnetic core, the effective relative permeability μ_r can be obtained using the following equation [4-9].

$$\mu_r = \frac{B_{pk} \; l_m}{\mu_0 \; NI_{pk}} \quad (4-5)$$

Where B_{pk} is the peak value of the magnetic flux density, l_m is the mean magnetic path length, μ_0 is the permeability of free space, N is the number of turns of the magnetising coil (primary) and I_{pk} is the measured peak magnetising current. Based on that, the relative permeability of single sheet lamination can be calculated at different flux densities from 0.1 to 1.8 Tesla at 50 Hz by utilising a single strip tester. The obtained results would indicate that the relative permeability of the lamination varies accordingly with flux density.

Fig 4-3 illustrates flux density dependence of the effective permeability on non-oriented silicon steel at the magnetising frequencies of 50 Hz, 100 Hz, 200 Hz, 400 Hz, 500 Hz, 800 Hz and 1 kHz in rolling direction, while Fig 4-4 illustrates the dependence in the transverse direction.
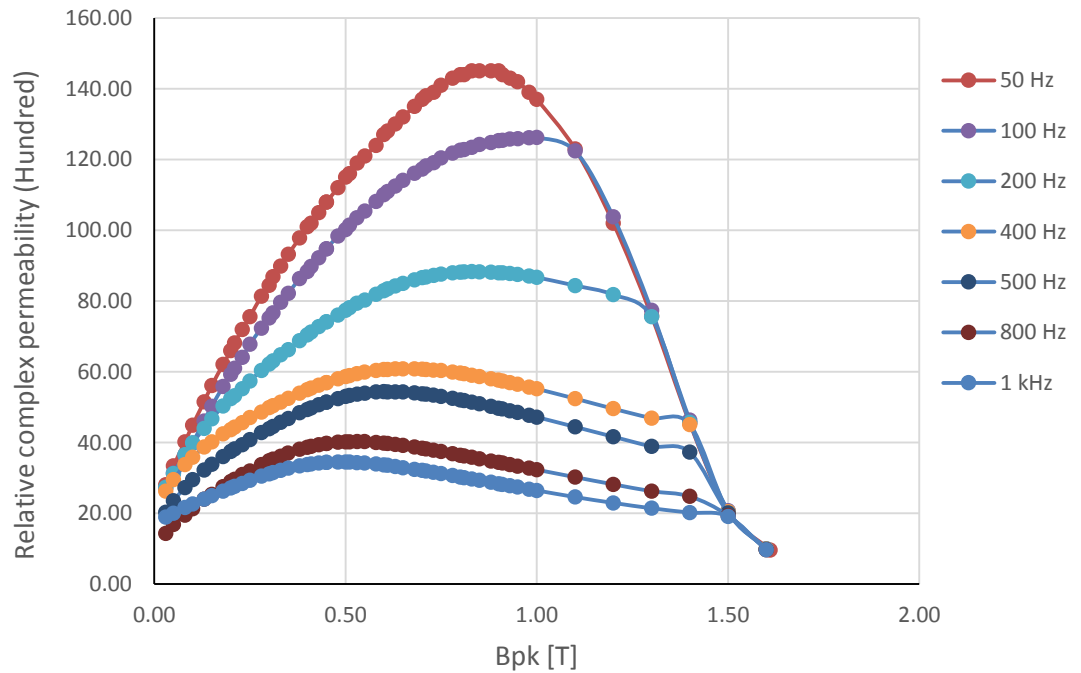
Fig 4-3 Measured relative complex permeability of lamination sample BL32 in the rolling direction.
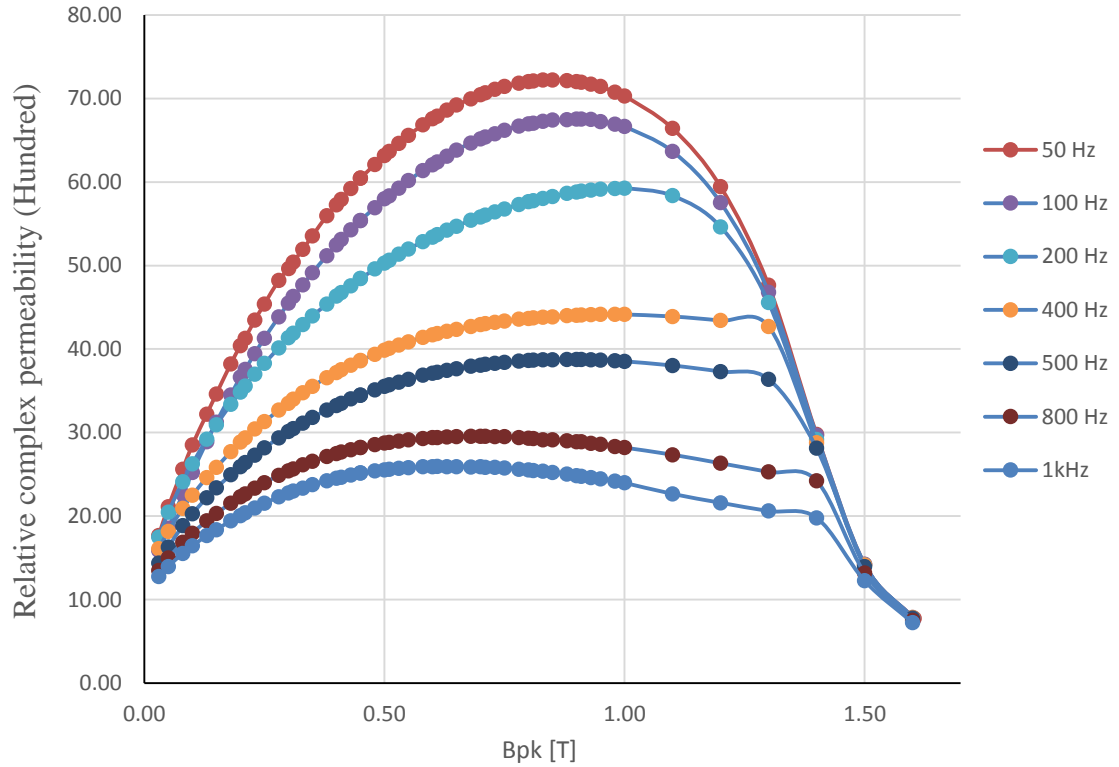
Fig 4-4 Measured relative complex permeability of lamination sample BL32 in the transverse direction.

As can be seen from the curves, for any value of B, the absolute permeability is obtained by the formula $\mu = \frac{B}{H}$. The relative permeability μ_r is plotted against the flux density **B** for these samples. Figs [4-3] and [4-4] show that permeability is a complicated function of the flux density. This complication is referred to as the effect of hysteresis.

4.4. Complex relative permeability at high frequency

Due to the inductive nature of electrical steel materials, there is a time lag between magnetic flux density **B** and the magnetic field strength **H** [4-7]. This lag is negligible at low frequencies, but at higher frequencies, it might be significant and should be taken into consideration. To analyse this phenomena in magnetic cores, it is generally assumed that the relative magnetic permeability is a complex quantity, which consists of real and imaginary parts as a function of frequency f. [4-10]

$$\mu_Z{}^{eff} = \mu_Z' - j\,\mu_Z'' = \mu_Z\,\frac{\tanh(a\gamma)}{a\,\gamma} \quad (4\text{-}6)$$

Hence, μ_Z is the static permeability of the magnetic material either in rolling or transverse direction, and γ is the propagation constant which is directly related to the skin depth δ [4-10].

$$\gamma = \frac{(1+j)}{2\delta} \quad (4\text{-}7)$$

Fig 4-5 shows the real and imaginary parts of the effective complex permeability as a function of frequency in rolling and transverse directions for the material under investigation.
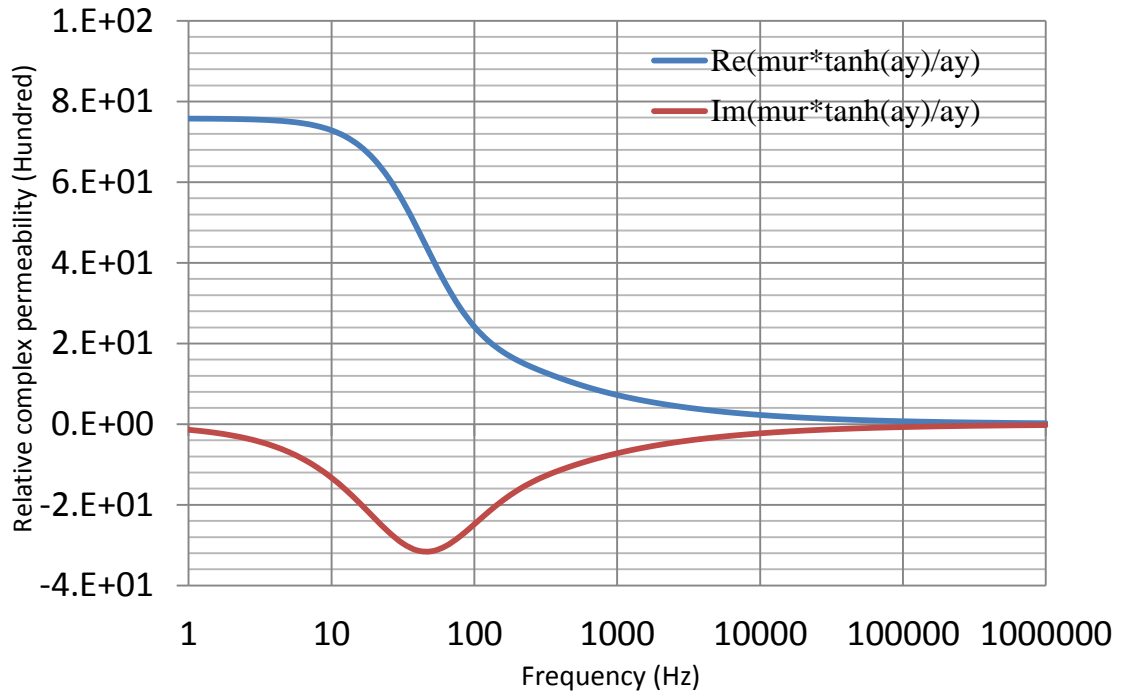
Fig 4-5 Real and imaginary parts of the relative complex permeability of a single strip tester lamination sample BL32 in the rolling direction at a peak flux density of 1.3 T, μ_z= (7580).
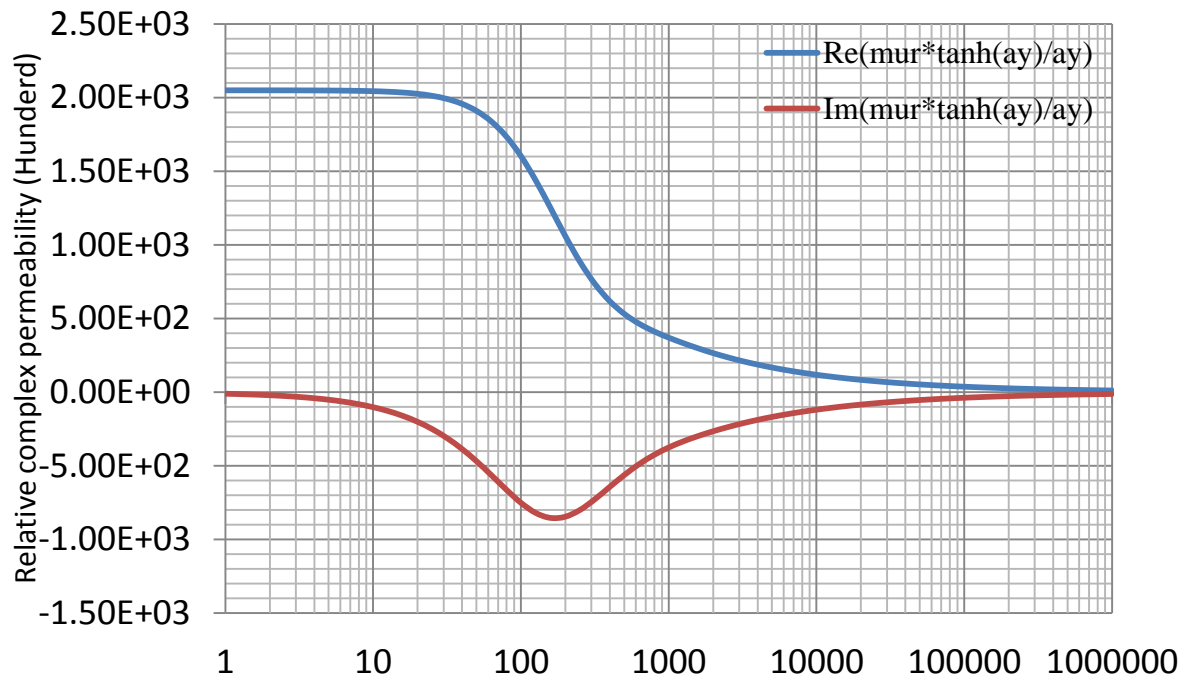
Fig 4-6 Real and imaginary parts of the relative complex permeability of a single strip tester lamination sample BL32 in the rolling direction at a peak flux density of 1.5 T, μ_z= (2050).
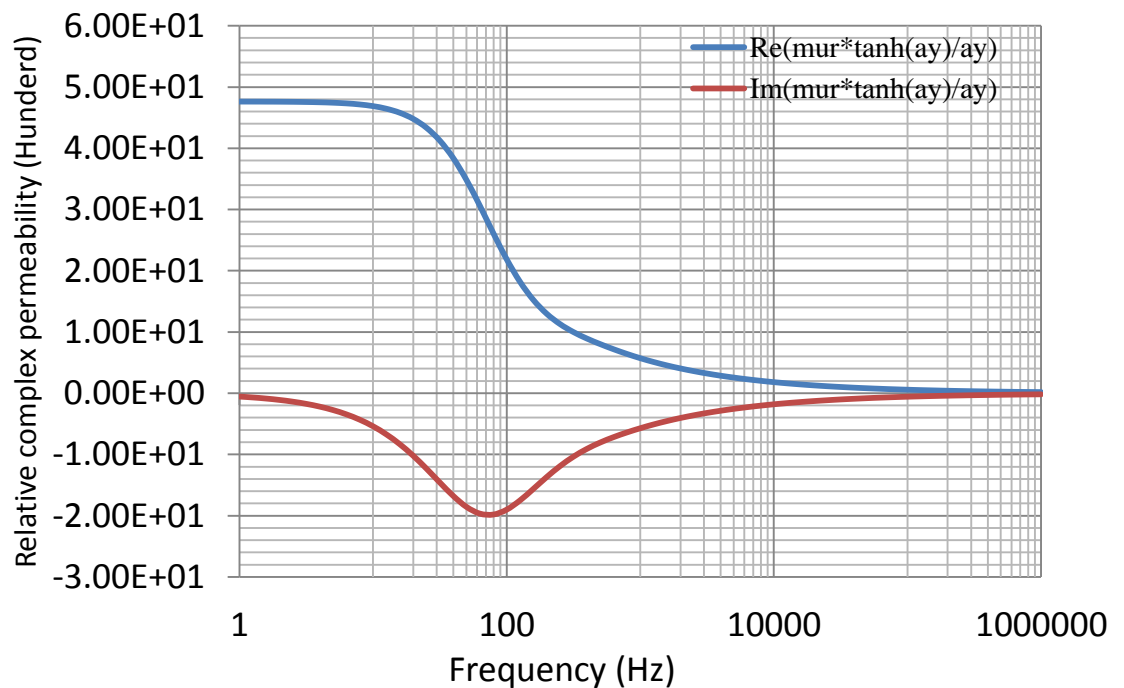
Fig 4-7 Real and imaginary parts of the relative complex permeability of a single strip tester lamination sample BL32 in the rolling direction at a peak flux density of 1.3 T, μ_z= (4763).
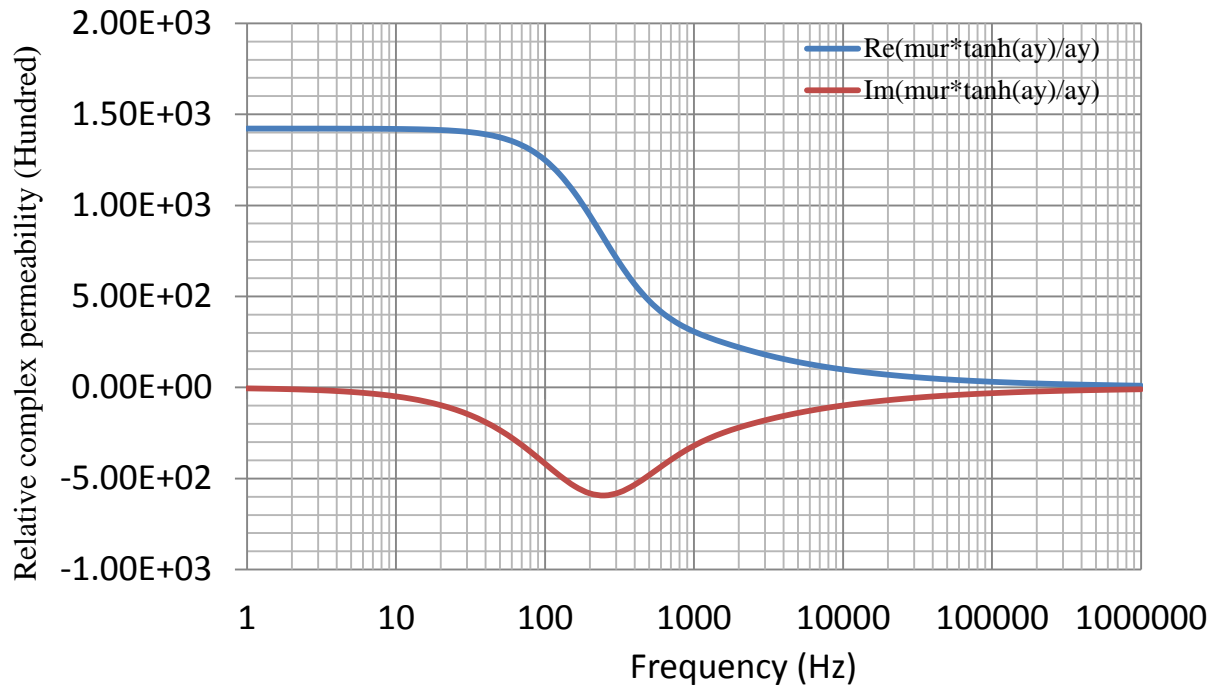
Fig 4-8 Real and imaginary parts of the relative complex permeability of a single strip tester lamination sample BL32 in the transverse direction at a peak flux density of 1.5 T, μ_z= (1422).

Figures 4-5, 4-6, 4-7 and 4-8 demonstrate the calculation for the real and imaginary parts of the relative complex permeability of the lamination sample BL32 in the rolling and transverse directions. These figures were obtained by using the following parameters for 3.0% non-oriented silicon steel material of 0.5 mm thickness, resistivity 51 micro Ohm-cm at 25 °C relative permeability in rolling and transverse directions at peak flux density of 1.3 T , $\mu_Z = 7580$, at 1.5 T $\mu_Z = 2050$ while in transverse direction at 1.3 T, $\mu_Z = 4763$ and 1422 at 1.5 T (these values are derived from figures 4-3 and figure 4-4).

Magnetic flux density distribution (normalised by the value at the surface) along the thickness of the lamination at different values of magnetising frequencies and by assuming that the relative complex permeability is constant as it ignores the non-linearity of **B** and **H**. Some other assumptions are made, as the material is a homogeneous medium, which ignores any possible complications that may be caused by the ferromagnetic domain structure.

Fig 4-9, 4-10, 4-11 and Fig 4-12 are obtained by using the specific properties of lamination material B32L in the rolling and transverse directions at 1.3 T and 1.5 T. The resistivity of the material is 51 micro Ohm-cm at 25 °C, the material thickness is 0.5 mm and the relative permeability is derived from figures 4-3 and 4-4 at 1.3 and 1.5 T in the

rolling and transverse directions, respectively. Then the normalized flux density B_x / B_S at the specific value of magnetising frequency is calculated by using the formula in (4-3).

In order to study the local flux density distribution while the lamination material is magnetised at transverse direction, the same procedure is followed as for in the rolling direction, apart from that the values of the relative permeability at specific flux densities are different. These are shown in Fig 4-11 and Fig 4-12.
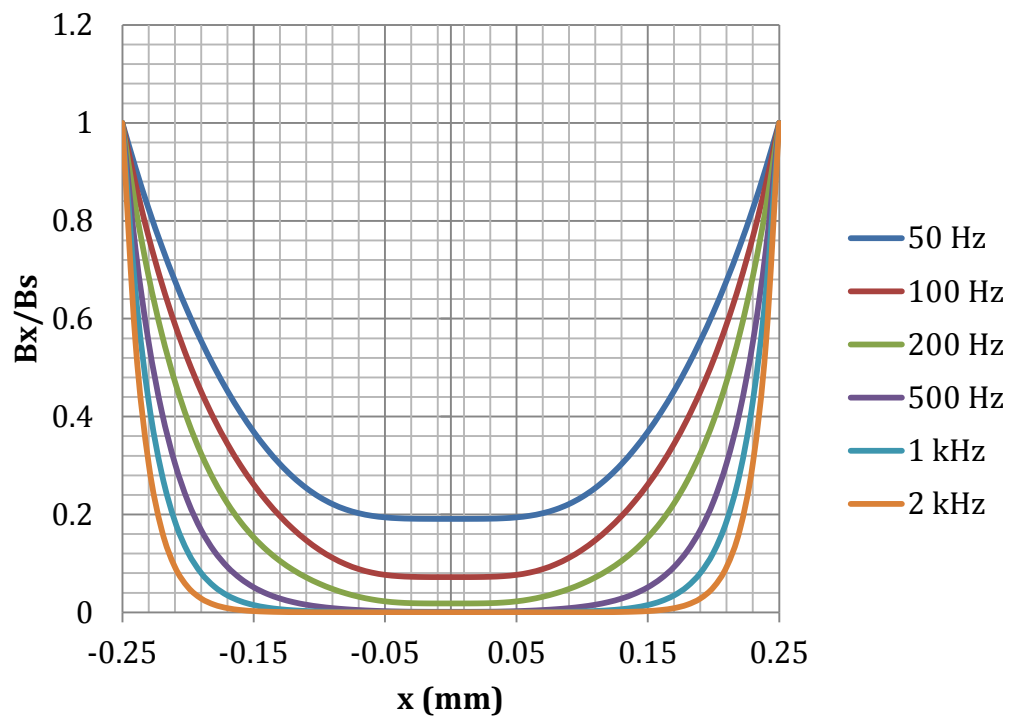
Fig 4-9 Normalised magnetic flux density penetration into magnetic lamination at different frequencies at 1.3 T in the rolling direction.
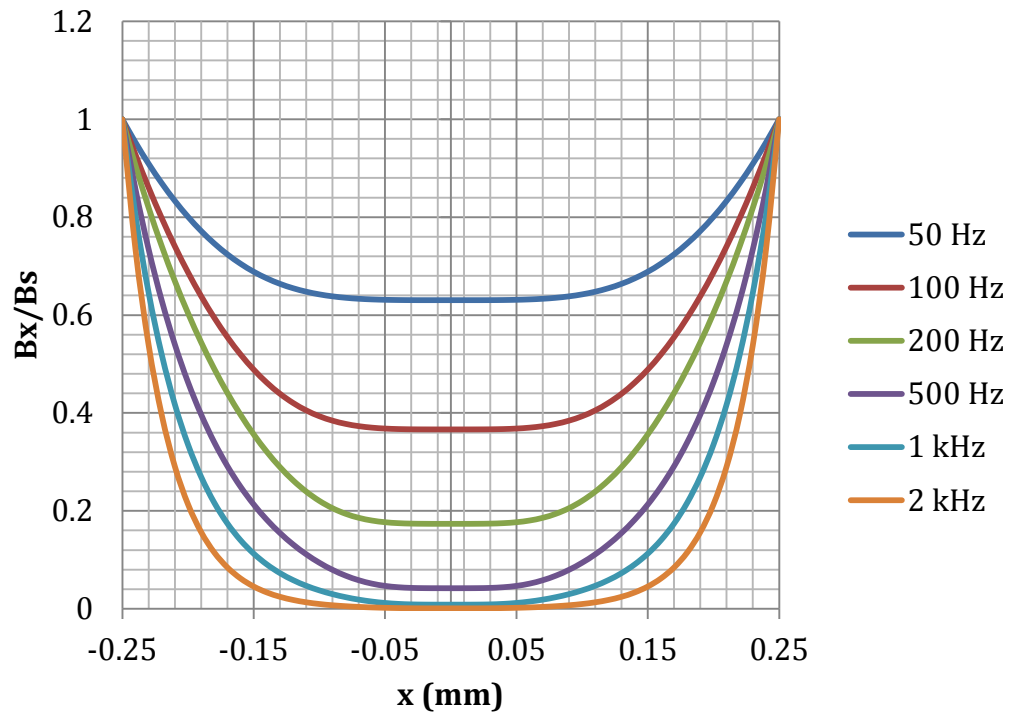
Fig 4-10 Normalised magnetic flux density penetration into magnetic lamination at different frequencies at 1.5 T in the rolling direction.
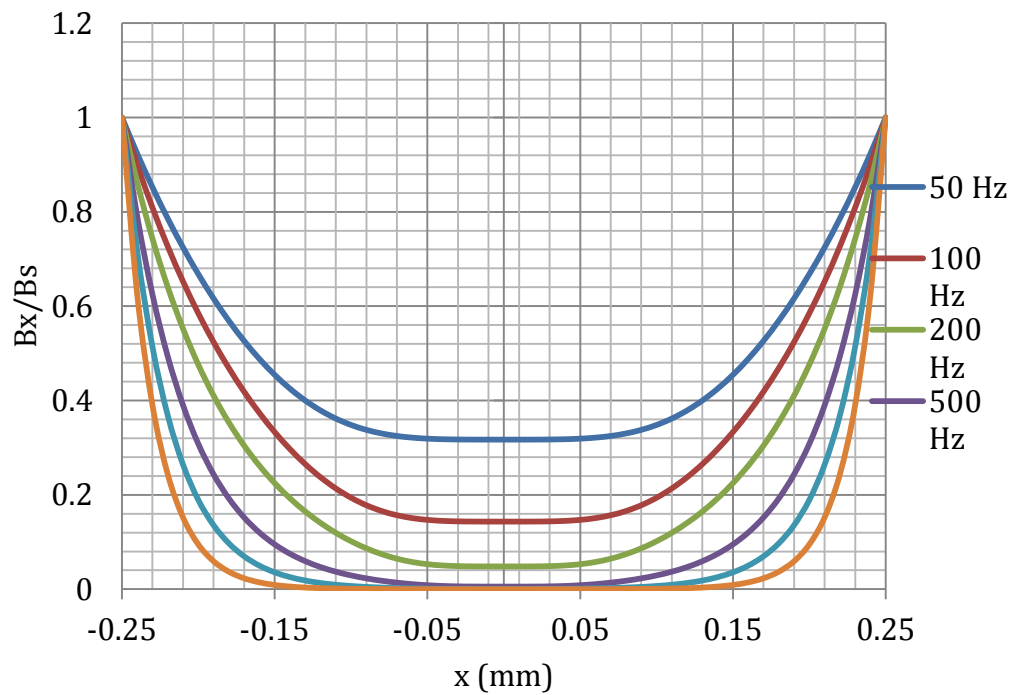
Fig 4-11 Normalised magnetic flux density penetration into magnetic lamination at different frequencies at 1.3 T in the transverse direction.
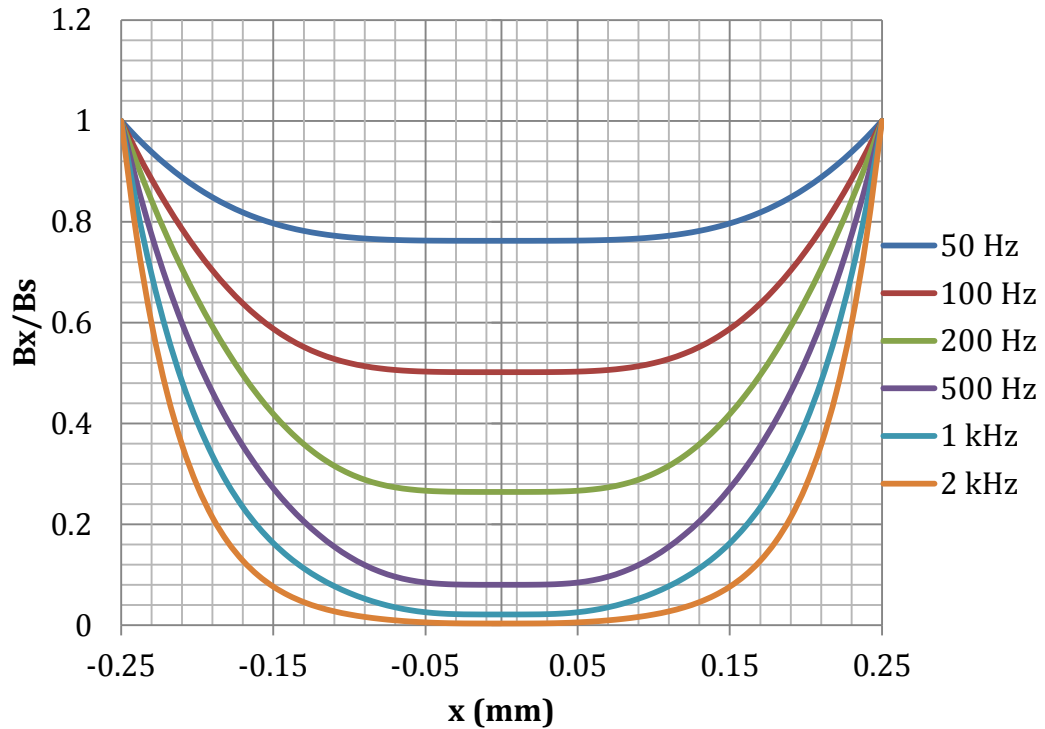
Fig 4-12 Normalised magnetic flux density penetration into magnetic lamination at different frequencies at 1.5 T in the rolling direction.

Based on the obtained results, it is important to notice the flux distribution along the thickness of the lamination. From (4-3) and (4-4), half of the lamination thickness 'a' and skin depth δ are two determinant factors in the qualification of the flux density distribution along the lamination thickness [4-7]. However, at low frequency, where δ ≫ a, flux density is distributed uniformly. But at higher frequencies, where δ ≪ a, it leads to reducing the internal flux density, which in turn has a minimum value at the centre and maximum at the surface.

A closer look at the obtained results shows the variation of the flux density along the thickness of the lamination. This variation is small at 50 Hz, and the whole material of the lamination is nearly fully utilised, but the other variations are at 200 Hz and up. When the skin depth becomes large enough, the magnetic flux is carried mainly by the material near the surface or skin, the interior being shielded by the eddy currents which also flow near the surface. From this point it is quite clear that the effect does not depend only on lamination thickness but also on permeability, frequency and electrical resistivity. This is proved by the above calculation; hence, at 1.3 T, the relative permeability has different values compared to that at 1.5 T, which would have a significant effect on the flux density distribution along the lamination thickness. This also can be applied to the effect of the

frequency. The higher the frequency and permeability, the greater is the need to reduce the thickness of the lamination in order to have good use of the material.

As indicated by [4-11], the value of the measured average flux density would no longer be accurate if the skin effect were significant, because significant skin effect causes the actual flux density inside the laminations to be different in magnitude at each point across the lamination thickness. The variation in magnitude due to skin effect also causes phase difference in the flux density waveform at different points across the laminations; therefore, the measured average flux density is not necessarily the average value of these peak flux densities.

4.5. The effect of lamination thickness

Electrical machine cores are generally built up of laminations. These laminations have thicknesses of 0.35 mm, 0.5mm, 0.65mm and 1 mm. Rotating machines have thicknesses of 0.5 mm, which is the standard thickness for the lamination sheet material. As mentioned earlier, it is very important to use thin laminations, not only to guarantee the best magnetic utilisation of the material, but also to reduce the eddy current power loss. When operating these thin laminations at mains frequency, the flux density is approximately uniform across the cross section of the lamination.

In order to investigate the effect of the thickness on the flux distribution at surface flux densities 1.3 T and 1.5 T at the mains frequency of 50 Hz, different thickness values have been used from 0.25 mm up to 1 mm. Results are shown in Fig4-13, Fig 4-14, Fig 4-15 and Fig 4-16. Almost full utilisation is obtained with smaller thickness lamination. However, when the thickness is increased at the same flux density and magnetising frequency, half of the thickness 'a' becomes greater than the skin depth, which causes a decline to the flux density from the edge of the laminations to the centre line.
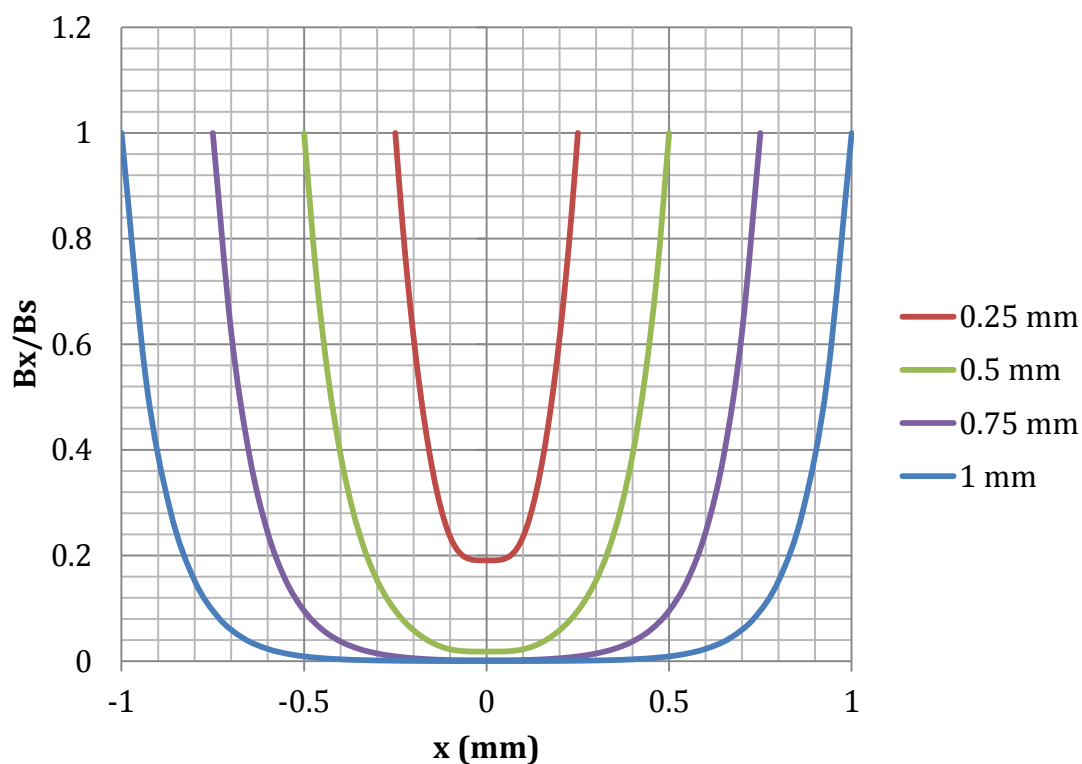
Fig 4-13 Distance from the centre of the lamination (mm) sample BL32 L at 1.3 Tesla, μ_z= (7,580) in the rolling direction RD.
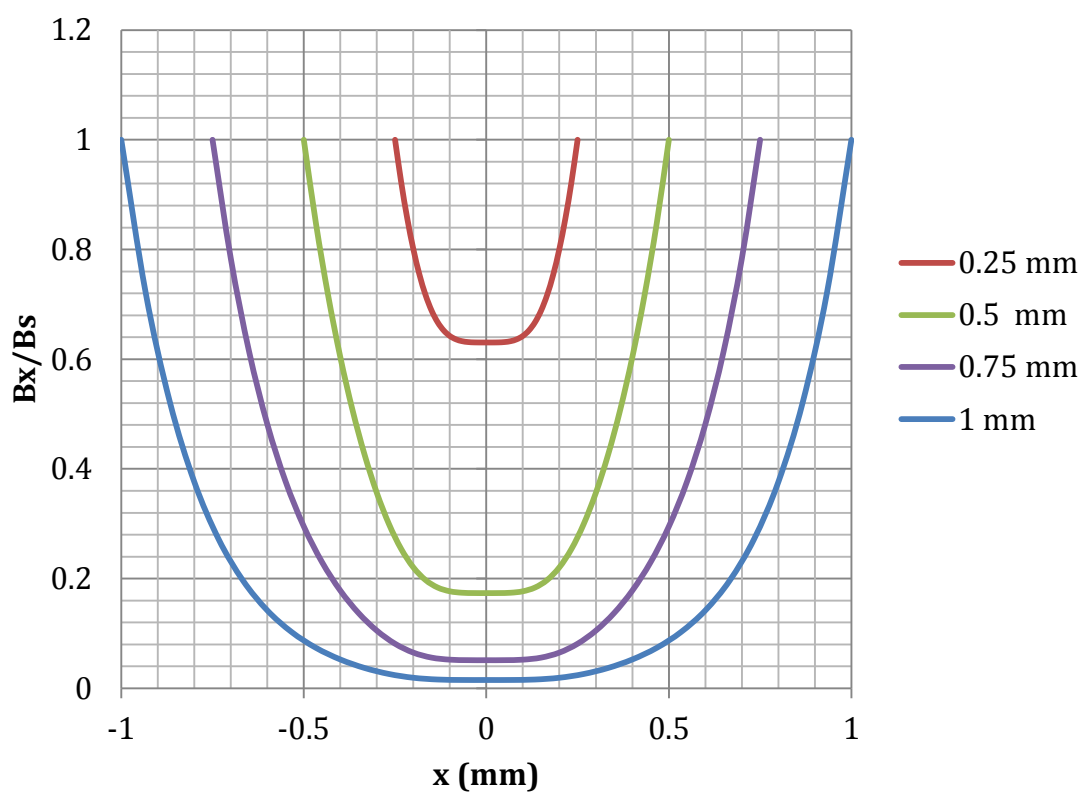
Fig 4-14 Distance from the centre of the lamination (mm) sample BL32 L at 1.5 Tesla, μ_z= (2,050) in the rolling direction RD.
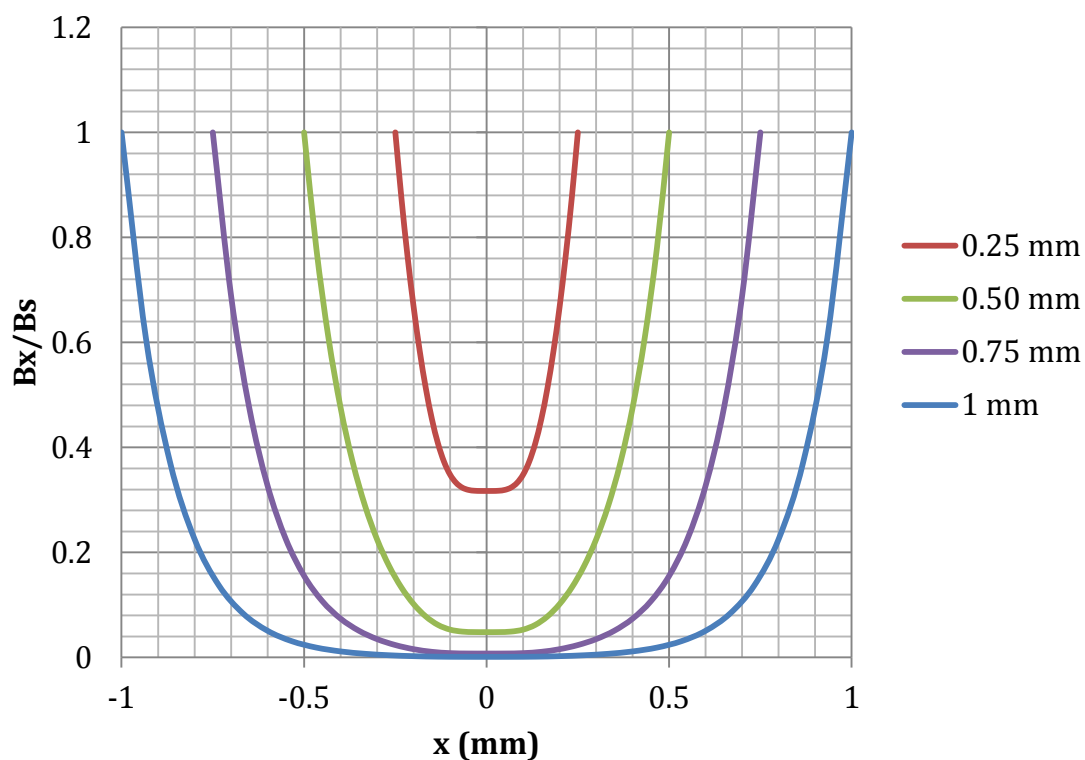
Fig 4-15 Distance from the centre of the lamination (mm) sample BL32 L at 1.3 Tesla, μ_z =(4,763) in the transverse direction TR.
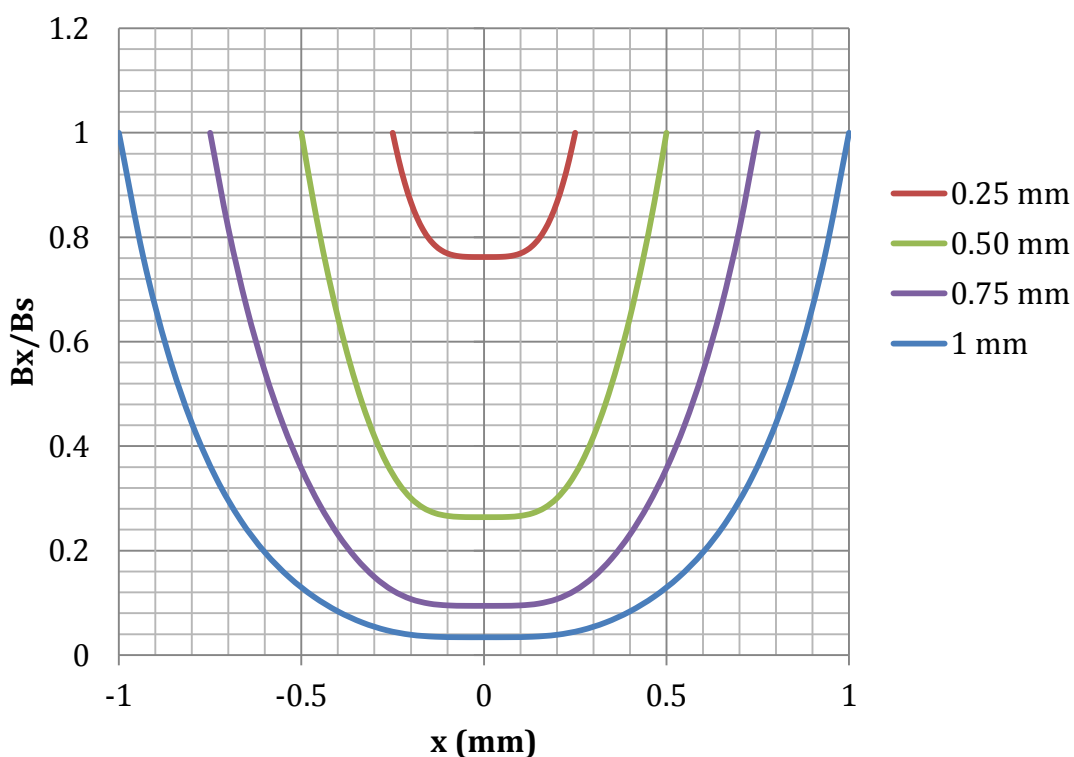
Fig 4-16 Distance from the centre of the lamination (mm) sample BL32 L at 1.5 Tesla, μ_z= (1,422) in the transverse direction TR.

The flux density distribution in the lamination is largely dependent on the magnetic permeability, which varies along the **B-H** curve depending on the flux density level. The variation of magnetic permeability affects the distribution of the flux density across the laminations. It becomes non-uniform at higher values of magnetic permeability and uniform for low values of magnetic permeability at low fields and near the saturation [4-11].

4.6 Governing equations for eddy current

The eddy current effect in electromagnetism is governed by a series of laws showing the relationship between the electric and magnetic fields known as Maxwell's equations [4-12].

4.6.1. Differential form of Maxwell's equations

Ampere's law $\qquad \nabla \times H = J + \frac{\partial D}{\partial t}$ (4.8)

Ampere's law in differential form stated in (4.8), relating the magnetic field **H** produced by a current in a conductor.

Faraday's law $\qquad \nabla \times E = -\frac{\partial B}{\partial t}$ (4.9)

Faraday's law in differential form in equation (4.9) states that the changing magnetic flux density **B** produces circulating electric field density, E.

Gauss's law for magnetic fields $\quad \nabla . B = 0$ (4.10)

The differential form for Gauss's law for magnetic fields in equation (4.10) states that the divergence of magnetic flux density B at any point equals zero.

4.6.2. The integral form for Maxwell's equations

Ampere's law $\quad \oint_c H. \, dl = \int_s [\, J + \frac{\partial D}{\partial t} \,]. \, ds$ (4.11)

Ampere's law in (4.11) states that the electric current flowing through a surface area produces circulating magnetic field **H** around the surface.

Faraday's law $\quad \oint_c E. \, dl = -\frac{\partial}{\partial t} \int B. \, ds$ (4.12)

The integral form for Faraday's law in (4.12) states that the changing magnetic flux density through a surface area induces a changing electromotive force (emf) on the boundary of that surface. The negative sign in (4.12) indicates that the eddy currents induced by changing the magnetic flux oppose the change in the flux (Lenz's law).

Lenz's law for magnetic field states that $\oint_s B.\,ds = 0$ (4.13)

The integral form for Gauss's law in equation (4.13) says that the net magnetic flux density passing out of a surface is zero.

For static (dc) cases, magnetic flux leakage phenomena, all the time derivatives are zero, therefore $(\frac{\partial}{\partial t})$ is cancelled.

$$\nabla.A = \frac{\partial A_X}{\partial t} + \frac{\partial A_y}{\partial t} + \frac{\partial A_z}{\partial t} \quad \text{is divergence in a Cartesian coordinate}$$

$$\nabla \times A = \begin{vmatrix} i & i & K \\ \frac{\partial}{\partial x} & \frac{\partial}{\partial y} & \frac{\partial}{\partial z} \\ A_X & A_y & A_z \end{vmatrix} \quad \text{is the curl operator in the Cartesian coordinate system, showing}$$

how the vector field circulates around a point. Equations (4.14) and (4.15) are the

constitutive equations for a linear material.

$$B = \mu_0\,\mu\,H = \mu\,H \text{ (4.14)}$$

$$J = \sigma\,E \qquad \text{(4.15)}$$

Where μ_0 the permeability of is free space, and μ_r is relative permeability of the material.

Chapter 4: Eddy Current Phenomena In Ferromagnetic Materials

SUMMARY

This chapter is based on the physical dimensions of the sheet laminations, the electrical and magnetic properties of the core material and mathematical models. Different parameters have been modelled, including the relative permeability of the material at higher frequencies, the skin effect and non-uniform flux density distribution. These have shown that the magnetic properties of the core material are largely affected by the magnetising frequencies: the skin effect is found to be larger with higher frequency, and the relative permeability of the material decreases with increasing frequency. Hence, both the skin effect and the permeability are largely related to each other. Further, since the core material is non-linear, the relative permeability of the material depends on the amplitude of the peak flux density. Therefore, at each specific magnetising frequency, the magnetic material has different responses to different induction values.

The skin effect was shown to be negligible at low frequency; therefore, the flux density along the sheet thickness is almost uniformly distributed, while an increase in the frequency caused a non-uniformity in the flux density that caused less flux at the centre of the lamination of nearly zero and higher flux towards the surface of the lamination.

Modelling for eddy current power loss over a wide frequency range and higher induction should take into account the impact of skin effect and non-uniformity of flux distribution.

Chapter 4: Eddy Current Phenomena In Ferromagnetic Materials

References:-

[4-1] S. Bhag. Guru, R. Huseyin. Hiziroglu, *"Electric Machinery and Transformers",* Third edition, Oxford university press, 2001

[4-2] J Lammeraner, and M Stafl "*Eddy currents*", ILIFFE Books Ltd., London, 1966

[4-3]P. Beckley, *Electrical steels for rotating machines*: Institution of Electrical Engineers, 2002.

[4-4] B. D. Cullity, *Introduction to Magnetic Materials*, 1 ed. Reading: Addison-Wesley Publishing Company, Inc., 1972.

[4-5] F. Brailsford, *Physical Principles of Magnetism*. New York: Van Nostrand, 1966.

[4-6] Laminations for Transformers and Inductors—Part 1: Mechanical and Electrical Characteristics, BS EN 60740-1:2005, 2005.

[4-7] H. Hamzehbahmani, P. Anderson, J. Hall and D. Fox, "Eddy Current Loss Estimation of Edge Burr-Affected Magnetic Laminations Based on Equivalent Electrical Network—Part I: Fundamental Concepts and FEM Modelling," in *IEEE Transactions on Power Delivery*, vol. 29, no. 2, pp. 642-650, April 2014.

[4-8] Z. Popovic and B. D. Popovic, *Introductory Electromagnetics*. Upper Saddle River, NJ: Prentice-Hall, 2000.

[4-9]M. B. Balehosur, Ph. Marketos, A. J. Moses, and J. N. Vincent, "Packet-to-packet variation of flux density in a three-phase, three-limb power transformer core," *IEEE Trans Magn.*, Feb. 2010.
vol. 46, no. 2, pp.642–645,

[4-10] K. G. N. B. Abeywickrama, T. Daszczynski, Y. V. Serdyuk and S. M. Gubanski, "Determination of Complex Permeability of Silicon Steel for Use in High-Frequency Modeling of Power Transformers," in *IEEE Transactions on Magnetics*, April 2008 vol. 44, no. 4, pp. 438-444,.

[4-11]M. Ibrahim and P. Pillay, "*Advanced Testing and Modelling of Magnetic Materials Including a New Method of Core Loss Separation for Electrical Machines*", IEEE Transaction on Industry Applications, Vol. 48, NO. 5, Sep/Oct 2012, pp. 1507 – 1515

[4-12] N. Ida, *Numerical Modelling for Electromagnetic Non-destructive Evaluation*.
London: Chapman & Hall, 1995.

5.1 Introduction

Core loss is an important factor in the grade and price of electrical steel. Loss is largely dissipated in the form of heat. Studies on power loss estimation have shown that the cost of the no-load core losses in transformers in the UK alone was approximately £110 million during 1987 and 1988 [5-1]. Today, there are over 1 billion barrel units of electricity wasted each year in the UK's distribution transformers, which requires at least 7 million barrels of oil and releases 4 million tons of Co_2 and 35,000 tons of So_2 into the atmosphere [5-2]. These gases have large impact on the environment.

In fact, the study of power loss of electrical steel used to build electrical cores has been under investigation for a long time in order to obtain lower power loss and largely improve the economic and environmental benefits.

As [5-3] states, power loss studies over the past 100 years have successfully played a major role in reducing the power losses to 0.4 W/kg from the initial 15 W/kg at 1.5 T magnetisation and 50 Hz. During that period, remarkable changes have been made, for example, the addition of Si in 1900, Goss texture in 1934, high grain-oriented steel in 1970 and, finally, amorphous material in 1980.

The modelling of core loss has been a subject of interest since the 19th century. In 1892, Steinmetz [5-4], [5-5] started his experimental study which had resulted in formulation of core loss. His study had concluded that the core loss in magnetic materials consists of two loss components added together: hysteresis loss, P_h (also referred to as static losses), which is proportional to the enclosed loop and the frequency, and eddy current loss, P_e. P_h loss is characterised by the material, and it is a function of peak flux density. Hysteresis loss is incurred as a result of cumulative lagging behind of the flux density inside the material when an external magnetic field is applied to the material [5-6]. Another description of hysteresis loss is related to domain walls. These domain walls move in jumps known as Barkhausen jumps, which by nature are correlated and localised by means of one jump at a particular site increasing the probability of another jump occurring in the vicinity [5-7]. The product of the number of jumps and the average energy loss due to a single jump constitutes hysteresis loss [5-8], broadly speaking. Power loss in electrical steel largely depends on four different parameters: frequency (f), maximum flux density (B_{pk}), lamination thickness (t) and the material resistivity (ρ). Then the eddy current is also split into classical and anomalous loss (also called excess loss) [5-9]. Finally, the total loss is expressed in its final format as follows:

$$P_T = P_h + P_e \ (\text{Wkg}^{-1}) \ (5\text{-}1)$$

Where P_h is the hysteresis loss, P_e is the eddy current loss and P_a is the anomalous loss, all are measured in (Wkg^{-1}).

The hysteresis loop is defined as the area within the B-H loop that represents the energy expended when an alternating field is applied to the material, as illustrated in Fig 2-4. Using this method assumes that eddy currents are negligible and hysteresis is the measure of wall pinning effects.

It is believed that hysteresis loss is due to the micro eddy currents induced when domain walls 'flick' free of inclusion or are suddenly nucleated [5-9], but, in fact, the main cause of the dissipated energy is domain wall motion through the material during magnetisation. This loss is largely attributed to stress, impurities, dislocations, surface roughness, etc. Hence, these factors have a significant impact on the magnitude of the material permeability.

Referring to the equation (5-2), the hysteresis loss depends on the maximum flux density (B_{pk}) and the frequency (f) [5-10].

$$P_h = kf \ (B_{pk})^{\ x} \quad (\text{Wkg}^{-1}) \ (5\text{-}2)$$

Where k is a constant for the material at a given flux density and x is the Steinmetz index with a value range of 1.6 to 2.0 for electrical steel.

P_e (*dynamic losses*) [5-6], or eddy current power loss, is largely attributed to the fact that when a time-varying magnetic field is applied to conductive material, it induces time-varying electromotive force, which causes eddy currents to circulate. The induced eddy currents in steel lamination causes phase lag between the applied field and magnetisation. The energy is dissipated in the form of heat due to the ohmic resistance of the laminations. Eddy currents increase with increasing material thickness, magnetising frequency and material conductivity. According to Lenz's 1833 law for determining the sense of the induced emf, the direction of the induced emf is such that any current that it produces tends to oppose the change of the flux that produces it. In other words, eddy currents generate their own magnetic field that opposes the magnetising field. This is in turn has a demagnetising impact, causing a reduction in flux density from its surface value to minimum value at the center of the material.

$$v = -\frac{d\lambda}{dt} = -N\frac{d\phi}{dt} \ \text{Volts} \qquad (5\text{-}3)$$

Where v is the induced emf in volts and λ is the flux linkage in weber turns. The minus sign takes into account the sense of the induced emf.

Generally, the eddy current power loss for thin laminations can be obtained according to their geometry and the magnetising frequency and can be calculated as follows:

$$P_e = \frac{\pi^2}{6.\rho.D} d^2 f^2 B_{pk}{}^2 \qquad \text{[W/kg]} \quad (5\text{-}4)$$

Where B_{pk} is peak flux density, [T]; f is frequency, [Hz]; ρ is resistivity [Ω. m]; D is density, [kg/m^3]; and d is the thickness of the lamination [m]; [5-11]. The resistivity and the thickness of the lamination have a large influence on the eddy current power loss; hence, small thickness and high resistivity will reduce P_e, as shown in Fig 5-1.
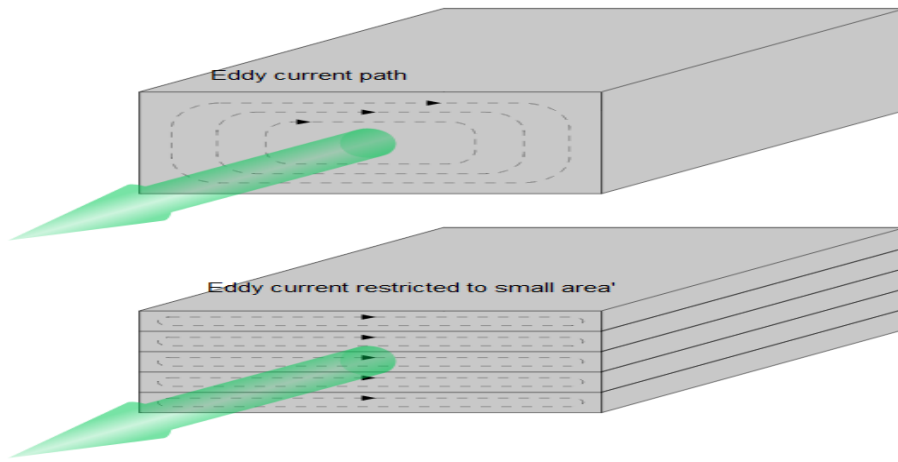
Fig 5-1 Schematic diagram of the eddy current path in a solid core and a laminated core.

Then the total core loss is expressed by:

$$P_c = P_h + P_e$$
$$= K_h f B^n + K_e f^2 B^2 \qquad \text{[W/kg] (5-5)}$$

where f is the magnetising frequency [Hz], B is the peak flux density [T], K_h and K_e indicate the hysteresis and eddy current loss coefficients, respectively, which can be obtained by extraction from experimental data, n is Steinmetz constant equal to 1.6 and n varies with flux density [5-12]. Most electrical machine designers are still using this formula to calculate core loss. It should be noted that the Steinmetz hysteresis loss flux density exponent n depends on material type as well as the flux density.

The fundamental theory of electromagnetic field is based on Maxwell's equations

$$\nabla \times \vec{E} = -\frac{\partial \vec{B}}{\partial t} \qquad (5\text{-}6)$$

$$\nabla \times \vec{H} = \vec{J} + \varepsilon \frac{\partial \vec{E}}{\partial t} \qquad (5\text{-}7)$$

$$\vec{J} = \sigma \vec{E} \qquad (5\text{-}8)$$

Where $\vec{E}, \vec{B}, \vec{H} \, and \, \vec{J}$ are the electrical field intensity, the magnetic flux density, the magnetic field and the current density, respectively. In order to apply Maxwell's equation to solve for a magnetic circuit model, it is generally assumed the magnetic field distribution is uniform. The eddy current loss coefficient K_e can be expressed as a function of the electrical conductivity σ and the lamination thickness 2 L as

$$K_e = \frac{(2L)^2 \pi^2 \sigma}{6} \qquad (5\text{-}9)$$

This is based on the estimation of eddy current losses using both the classical theory and the domain theory by assuming uniform wall motion. However, when both losses are added together, their sum is found to be less than the measured total loss. The difference between the measured losses and the sum of the estimated hysteresis and eddy current losses, as illustrated in Fig 5-2, has been called anomalous or excess loss P_a. This loss had not been defined well until the domain wall model was proposed by Pry and Bean in 1958 [5-12]. The below Fig 5-2 illustrates domain wall spacing 2L and inversely proportional to the thickness d. The anomalous loss is related to continuous re-arrangement of domain configuration (domain structure and domain dynamics) [5-4] [5-11]. Based on this, an additional loss (excess losses) was added by [5-13]. Then the equation (5-1) became the ratio of the total eddy current power loss $(P_a + P_e)$ to the value of the classical eddy current loss P_e, called the anomaly factor, η.
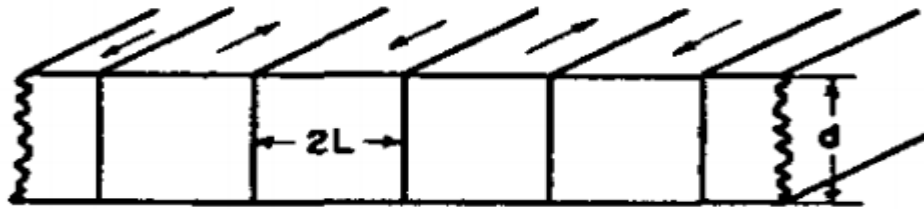
Fig 5-2 Domain wall for anomalous loss eddy current.

$$P_c = P_h + P_e + P_a$$
$$= K_h f B^n + K_e f^2 B^2 + K_{ex} f^{1.5} B^{1.5} \qquad (5\text{-}10)$$

Where K_{ex} is the excess loss coefficient, the new term K_{ex} depends on the material microstructure, conductivity and the cross-sectional area of the lamination. The three

coefficients (K_h, K_e, K_{ex}) given in equation (5-10) can be easily obtained from the measured core losses at different frequencies and flux density ranges. To achieve more accurate results at high flux densities and higher frequencies, a newly developed model by [5-6] is used. It has been indicated by [5-14] that excess losses are mainly related to the non-uniform distribution of the magnetic field inside the lamination, as shown in Fig 5-3. This non-uniformity of the magnetic field is attributed to the skin effect and the non-linear diffusion of the magnetic flux [5-15], [5-16]. This phenomena has been explained fully in chapter 4.
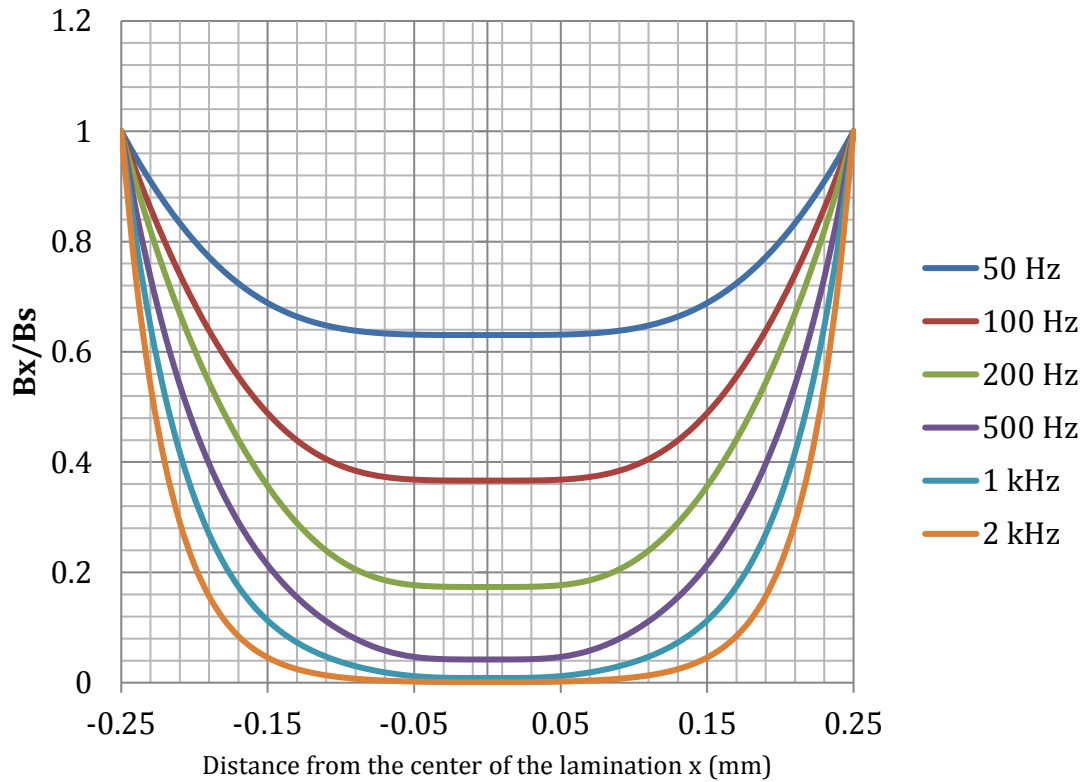
Fig 5-3 Normalised magnetic flux density penetration into magnetic lamination at different frequencies and 1.5 T

Moreover, another approach is demonstrated in [5-17] for calculating eddy current loss while taking into account the impact of the skin effect. However, using this formula (5-4) is only applicable at low flux densities not beyond the knee point.

William et al. were the first to calculate the power loss in ferromagnetic material by the behaviour of domains using a single moving wall in an infinite medium [5-18]. It is believed that anomalous loss contributes 50% of the total loss in grain-oriented 3% silicon iron, which has led to more investigation to deduce the cause of this difference [5-19].

Therefore, all investigation into power loss now takes the domain motion into consideration.

5.2. Power loss measurement

There are two different ways to study and evaluate the magnetic properties and power losses of electrical steel materials. In studying the properties of sheet laminations, Epstein frame measurements and single strip testers are used. These two measurement systems are mostly preferred to specify catalogue values and to compare characteristics of sheet laminations between different manufacturers.

5.2.1. Measurement with Epstein frame

The Epstein frame was originally proposed as a 50 cm square by Epstein in 1900. Later, Burgwin proposed a smaller 25 cm version in 1936. This measurement technique had been standardised in IEC 60404-2. The Epstein frame is schematically shown in Fig 5-4 as a standard Epstein strip (305) mm long and 30 mm wide to be placed between the yokes. In this setup, the flux continuity at the square corners is ensured by double-lapped joints, as illustrated in Fig 5-4. A force of 1N is placed in each corner joint and provides good and reproducible flux enclosure.

There are four fixed windings composed of four coils connected in a series. The primary winding is connected to the power source to provide the magnetising current. The secondary winding is connected to a voltmeter to measure the peak flux density.
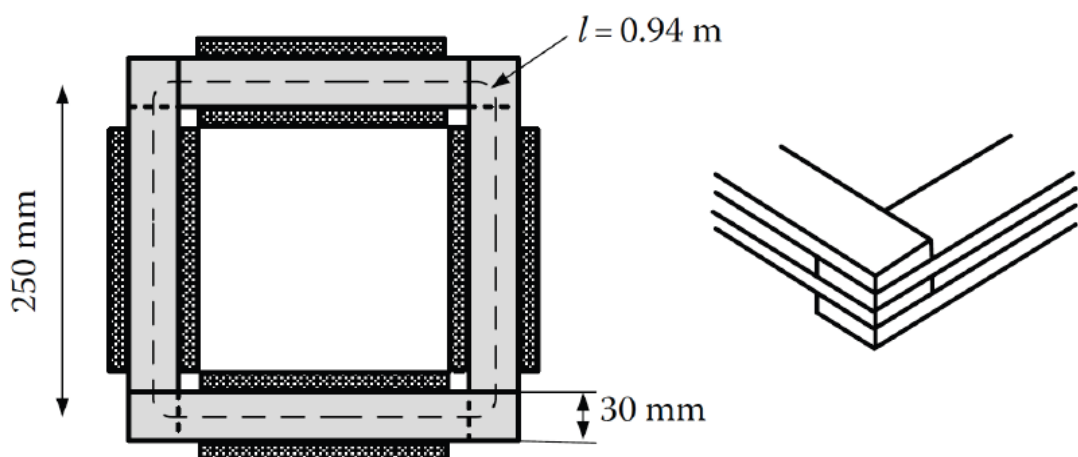
Fig 5-4 Schematic Epstein frame and double overlapped corner arrangement.

In the closed sample, the magnetic path length l_m is 0.94 m, as specified in standard IEC 60404-2, and the instantaneous magnetic field H(t) is derived by using (5-11) and simplified as in equation (4.1), knowing i(t) is the magnetising current and N_1 is number of primary windings.

$$H(t) = -\frac{N_1 i(t)}{l_m} \quad (5\text{-}11)$$

The instantaneous flux density B (t) is also derived from (2-2), where A is the lamination cross-sectional area, N_2 is the number of turns in the secondary winding and v (t) is the voltage measured across the secondary winding.

$$B(t) = -\frac{\int v(t)dt}{AN_2} \quad (5\text{-}12)$$

By using this method, there will be a choice for selecting the most suitable material under different frequencies.

The below Fig 5-5 and Fig 5-6 show the Epstein frame used to measure power losses. This system consists of a computer with a pre-installed LabVIEW version 8.5 software from National Instrument, an NI PCI 6120 data acquisition card (DAC)[5-20],[5-21], a power amplifier, a 1 ohm resistor R_s and an Epstein square frame. LabVIEW was chosen for this system because it runs a specialised data acquisition software that uses mathematical analysis to process measurements and display the desired output in real time. Moreover, this software is capable of saving data instantaneously.
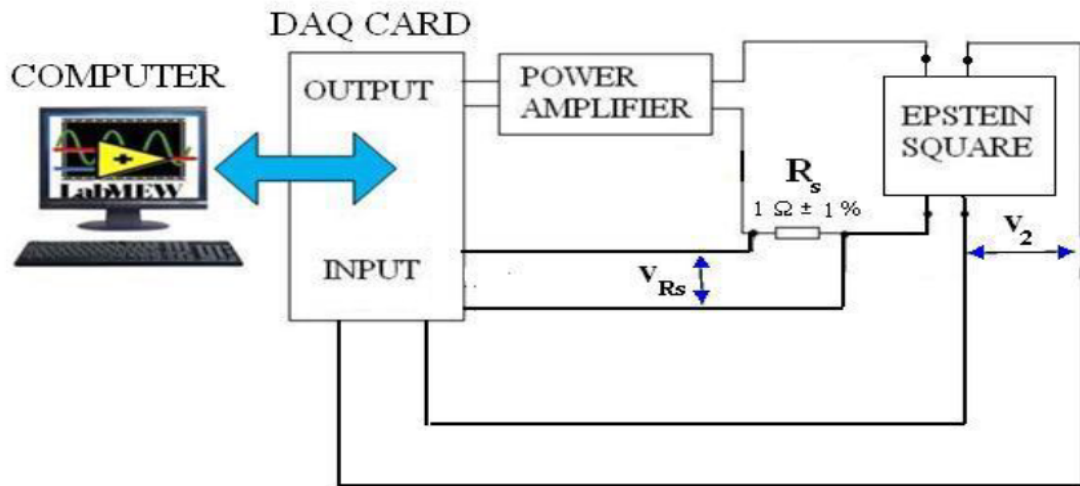
Fig 5-5 Schematic diagram of computer controlled Epstein frame reproduced from [5-15].
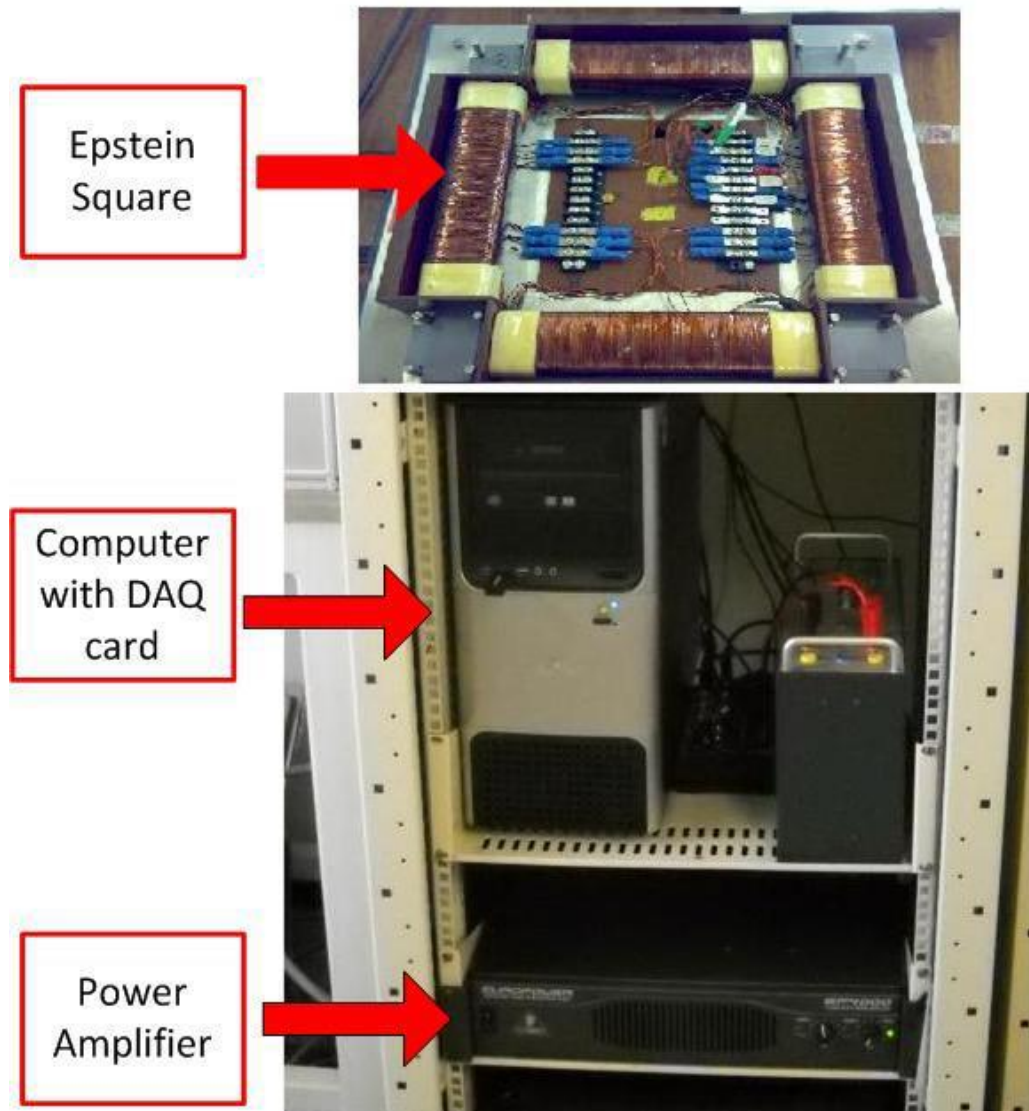
Fig 5-6 Schematic diagram of computer controlled Epstein frame reproduced from [5-15]

This frame is suitable for core loss testing at high frequencies and high flux densities. In measuring core losses with Epstein frames, it is assumed that all the excitation currents are responsible for core losses [5-22].

The number of strips also plays a major role in this test. It is recommended to use 12 to 24 strips, but in the test for this study, 12 strips were used with a total weight of 391.68 gm. In the above Fig 5-6, a square area at the four corners can be seen. These are used as places for plastic weights of about 100g. These are used to ensure that the sample has good contact at corners, which minimises error caused to reluctance.

5.2.2. Single strip tester

Properties of silicon steel are usually determined by means of the Epstein frame method or a single sheet tester (SST), as recommended by IEC-Standards (IEC 404-2) [5-24] and (IEC 404-3) [5-25]. This type of measuring system focusses on specific power loss (W/kg) and the permeability at different magnetising frequencies. The single strip tester (SST) system has been developed within the 'Wolfson Centre for Magnetics', providing high accuracy and automatic measurement. The (SST) is similar to the Epstein frame system apart from the frame itself. Today it is used more often than the Epstein frame, as it has many advantages such as being inexpensive and time saving for sample preparation and insertion [5-13].

Fig 5-7 illustrates the system which consists of a PC with pre-installed LabVIEW version 8.50, an NI PCI -6210 data acquisition Card (DAC), a power amplifier, a 1ohm shunt resistor (R_{sh}) and an air flux compensated single strip tester [5-21],[5-26]. Double vertical yokes are used, both of which are made of grain-oriented silicon steel or nickel iron alloy, as recommended by (IEC 404-3). A 250 turn secondary coil (N_2) is wound around the plastic frame, and a 865 turn primary winding (N_1) is wound around the secondary winding. A standard Epstein strip size sheet, (305) mm long and 30 mm wide, is placed between the yokes. This type of arrangement offer low reluctance path.
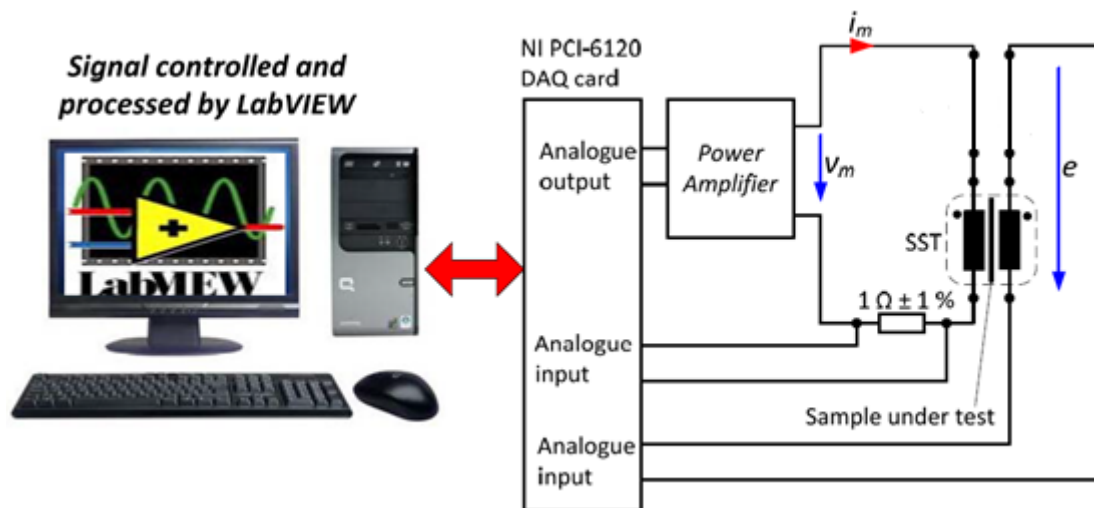
Fig 5-7 Schematic diagram of computer-controlled AC magnetic property measurement system [5-21].
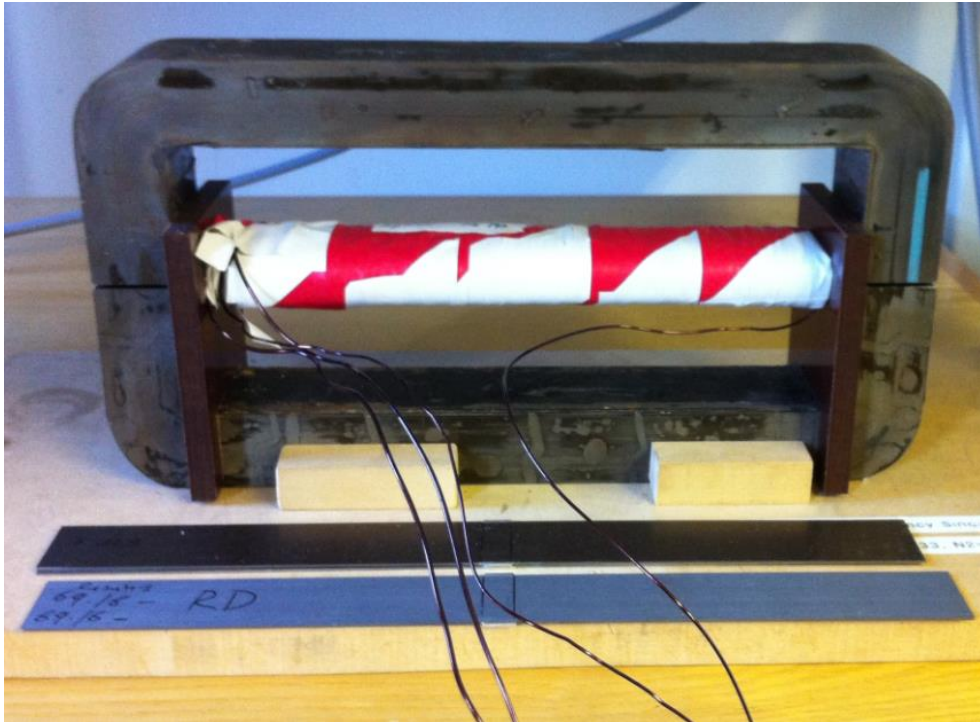
Fig 5-8 Single strip tester side view.
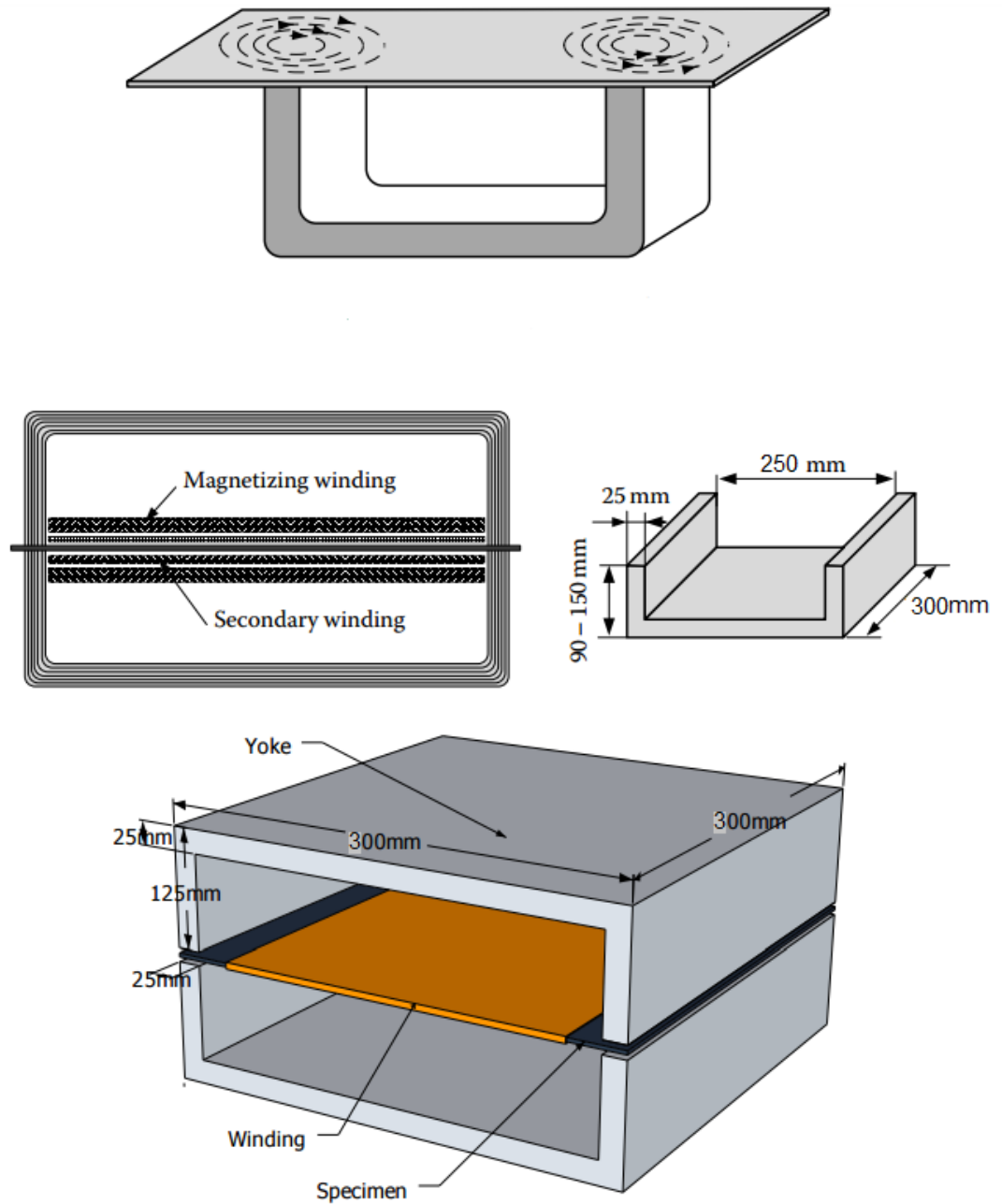
Fig 5-9 Schematic for large-scale single strip tester (300*300) mm.

5.3. Power loss in electrical steel laminations

Power loss in electrical machines is the most important parameter in magnetic materials used for AC applications, which always determines the grades and the prices of the material. These losses largely depend on four different parameters: frequency (f), maximum flux density (B $_{pk}$), the thickness (d) and the material resistivity (ρ). Loss can be split into hysteresis and eddy current loss components. Then the eddy current is also split into classical and anomalous loss (also called excess loss) [5-9]. Then the total loss is expressed in its final format as follows:

$$P_T = P_h + P_e + P_a \ \ (\text{W/kg}^{-1}) \ (5\text{-}13)$$

5.3.1 Core loss separation

This approach provides a method for core loss component separation (hysteresis and eddy currents) in the laminations under different values of magnetising frequencies and at specific flux densities. The lamination under investigation for this study is NO steel; therefore, the magnetising frequency would not exceed a few hundred hertz.

5.3.2 Core loss separation method

The static hysteresis loss per cycle is normally defined by measuring the area enclosed by the B-H loop under DC excitation (static), which represents the energy expended when material is magnetised in a slowly changing magnetic field, as illustrated in Fig [2-9]. However, using this method of measurement requires special instrumentation [5-27].

When time-varying magnetic fields are applied to magnetic material, the area enclosed by the measured hysteresis B-H loop represents the total core loss per cycle. The total loss includes both components, hysteresis and eddy current loss. Currently, an alternative method is used to calculate the hysteresis loss per cycle. This method is based on measuring core loss at different frequencies. The hysteresis loss per cycle then is separated by extrapolating core loss per cycle versus magnetising frequency curves at different flux densities to zero frequency, which represents the hysteresis energy loss per cycle [5-6].

$$\frac{P_c}{f} = K_h B^n + K_e B^2 f \ \ \ (5\text{-}14)$$

This is a linear equation as a function of magnetising frequency at peak flux density **B.** Then the core loss data are used to plot curves of P$_c$ /f versus f. The curves are straight lines, and their equation can be written as:

$$\frac{P_c}{f} = D + Ef \qquad (5\text{-}15)$$

Where $D = K_h\, B^n$ refers to hysteresis loss per cycle and $E = K_e\, B^2$. More detailed information for calculating these coefficients are available [5-28] [5-29] [5-30].

To apply the extrapolation method, it should be noted that the hysteresis energy loss per cycle is frequency independent, and the total hysteresis loss is found by multiplying the static hysteresis energy by the magnetising frequency. This assumption is valid only at low frequency; at higher frequencies, it would cause non-uniformity of the magnetic field across the lamination, which would make the calculation more complicated. Hence, the magnetic field distribution is maximum at the surface and minimum at the centre, known as the skin effect (chapter 4) [5-31]. At lower frequencies, the generated eddy currents are small, so the skin effect is neglected and vice-versa at higher frequencies. Previously, this was illustrated in Fig 5-3, which showed that magnetic field distribution along the thickness of the lamination is strongly affected by the magnetising frequency. Therefore, the hysteresis loop and hysteresis energy loss per cycle vary at each point inside the lamination. For this reason, it is strongly recommended to apply the calculation for the separation of core loss by extrapolation method at a low frequency; otherwise, the skin effect should be taken into consideration [5-32].
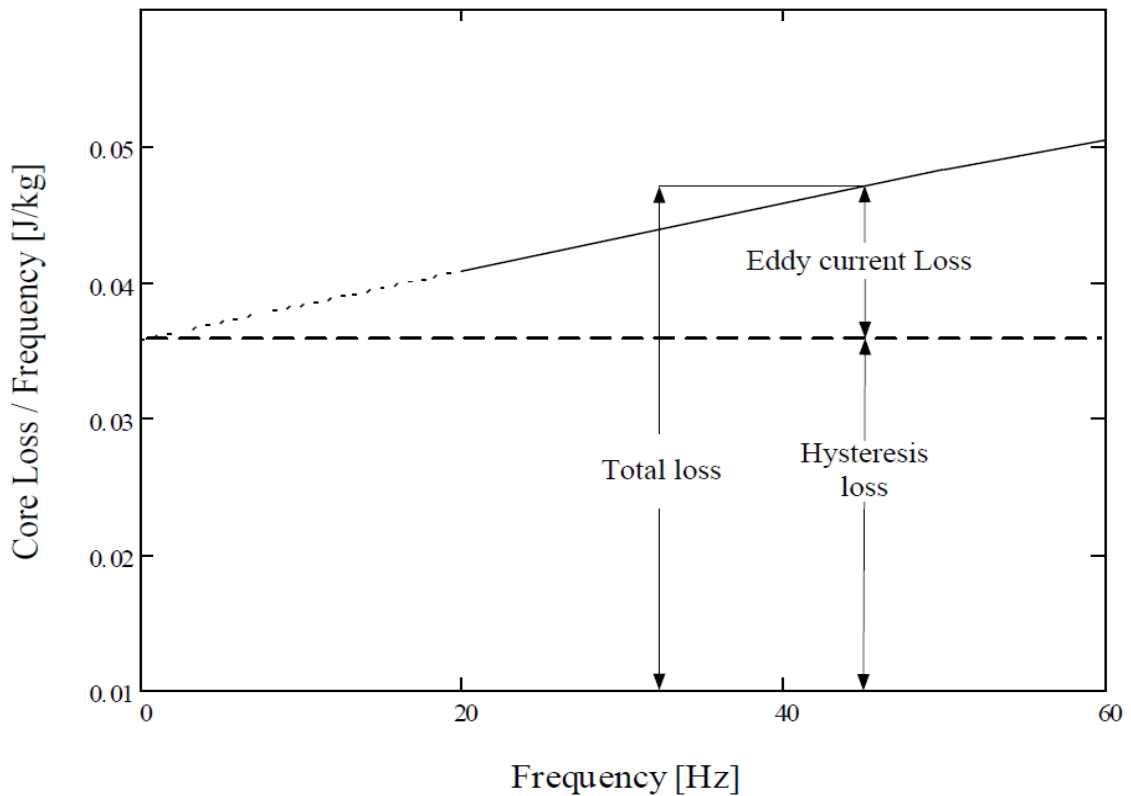
Fig 5-10 Core losses separation by the extrapolation method reproduced from [5-21].

It is quite clear from Fig 5-10 that the extrapolation method is fundamentally based on a static (constant) hysteresis loop per cycle and a linear relation of eddy current power loss at all frequencies.

5.3.3 Core loss separation based on a three-term formula

This follows the same procedures used for separation of loss based on the two components, hysteresis and eddy current losses. But in this case, a third term is added that represents the excess loss (5-10). This method is achieved by dividing (5-10) by the magnetising frequency that will lead to (5-16).

$$P_c = P_h + P_e$$

$$\frac{P_c}{f} = K_h\, B^n + K_e\, fB^2 + K_{ex}\sqrt{f}\, B^{1.5} \quad (5\text{-}16)$$

This approach follows the one used for two-term separation, where the first right hand (P_h) is the hysteresis loss component, the second (P_e) is for the eddy current loss component and the last term represents the excess or anomalous loss component (P_a). The latter is largely influenced by intricate phenomena related to microstructural interaction, magnetic anisotropy and non-homogenous locally induced eddy current [5-30], so the constant coefficients can be represented as:

$$\frac{P_c}{f} = D + Ef + G\sqrt{f} \quad (5\text{-}17)$$

A More feasible method can be implemented to obtain the coefficients by plotting the core loss per cycle vs. the square root of frequency $\sqrt{f}$, not the frequency f, for different values of flux density B from the lowest frequency to the highest frequency [5-28]. Therefore, (5-17) can be modified by

$$\frac{P_c}{f} = D + E\left(\sqrt{f}\right)^2 + G\sqrt{f} \quad (5\text{-}18)$$

D, E and G can be obtained by nominal curve fitting, with P_c/f on the y-axis and $\sqrt{f}$ on the x-axis. By comparing (5-16) and (5-18) we have

$$D = K_h\, B^n$$

$$E = K_e\, B^2$$

$$G = K_{ex}\, B^{1.5}$$

Therefore, applying this method for given flux densities, the loss coefficients K_h, K_e and K_{ex} can be obtained.

In summary, equations (5-15) and (5-18) emphasise that by using the extrapolation method, the eddy current power loss per cycle is assumed to be a linear function of frequency. Moreover, hysteresis loss per cycle is assumed to be frequency independent.

5.3.4 Experimental results:

This method of determining power loss separation is based on measuring the power loss of an Epstein-size lamination of non-oriented electrical steel for two samples at rolling and transverse direction. All the measurements for power loss are obtained by using the SST system as described in [5-15] and [5-18]. Normally, power loss of non-oriented steel is measured at a peak flux density of 1.5 T and magnetising frequencies from 25, 50, 100, 200, 400, 500, 800 Hz up to 1 kHz together with total power loss per cycle, as shown in table [5-1].

Table 5-1 Eddy current power loss of an Epstein-size lamination at 1.5 T at different magnetising frequencies.

Magnetising frequency Hz	Measured power loss (W/kg)	Power loss per cycle (W/kg).sec
25	0.84	0.033
50	2.02	0.040
100	5.49	0.054
200	16.3	0.081
400	53.6	0.134
500	80.25	0.160
800	189.9	0.237
1000	289	0.289

The obtained power loss per cycle is plotted against the square root of frequency, as shown in Fig 5-11. From this curve, it is quite easy to obtain the coefficients of the power loss components by applying a polynomial curve fitting in Microsoft Excel.
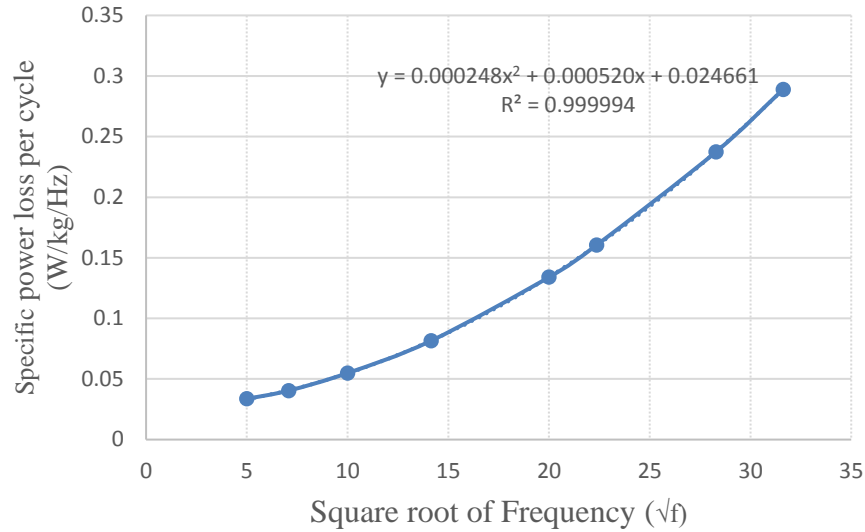
Fig 5-11 Total power loss per cycle of an Epstein-size magnetic lamination of NO steel versus the square root of frequency √f at flux density of 1.5 T.

Typically, the values of the fitting residual of the equation are very close to unity, i.e., R^2 ≈ 1, indicating a very good approximation. Based on the coefficients of Fig 5-11, the power loss components were calculated at different frequencies, and the results are shown in Table 5-2.

$$D = K_h \, B^n = 0.000248$$
$$E = K_e \, B^2 = 0.000520$$
$$G = K_{ex} \, B^{1.5} = 0.024661$$

By applying these coefficients in equation (5-18), the power loss components are automatically calculated, as shown in table 5-2. The eddy current power loss and the hysteresis power loss versus the magnetising frequency at 1.5 tesla are shown in Fig 5-12. The value of hysteresis loss is deduced from the static hysteresis loops, while the eddy current power loss per cycle is a linear function of magnetising frequency, which can also be calculated by using equation (5-4).

Table 5-2 Loss components of an Epstein-size lamination of NO steel at a peak flux density of 1.5 [T] and different magnetising frequencies in the rolling direction.

Frequency (Hz)	Measured power loss (W/kg)	P_e (W/kg)	P_h (W/kg)	P_a (W/kg)	$P_e = P_e + P_h + P_a$ (W/kg)	Error%
25	0.84	0.15	0.61	0.06	0.83	-0.41
50	2.02	0.62	1.23	0.18	2.03	0.83
100	5.49	2.48	2.46	0.52	5.46	-0.43
200	16.3	9.92	4.93	1.47	16.32	0.14
400	53.6	39.61	9.86	4.16	53.70	0.19
500	80.2	62	12.33	5.81	80.14	-0.13
800	189.9	158.70	19.71	11.76	190.21	0.16
1000	289	248	24.62	16.44	289.10	0.03
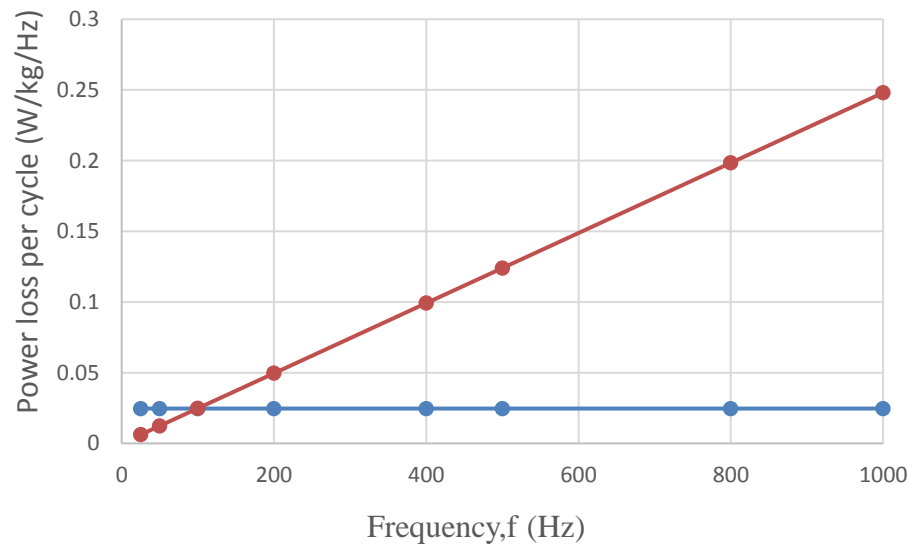
Fig 5-12 Eddy current and hysteresis loss per cycle versus frequency.

The results below represent the power loss separation for the same material in the transverse direction (TD).

Table 5-3 Eddy current power loss of an Epstein size lamination at 1.5 T at different magnetising frequencies in the transverse direction

Magnetising frequency Hz	Measured power loss (W/kg)	Power loss per cycle (W/kg).sec
25	1.047	0.041
50	2.53	0.050
100	6.54	0.065
200	18.7	0.09
400	57.2	0.14
500	83.83	0.16
800	193	0.24
1000	290	0.29
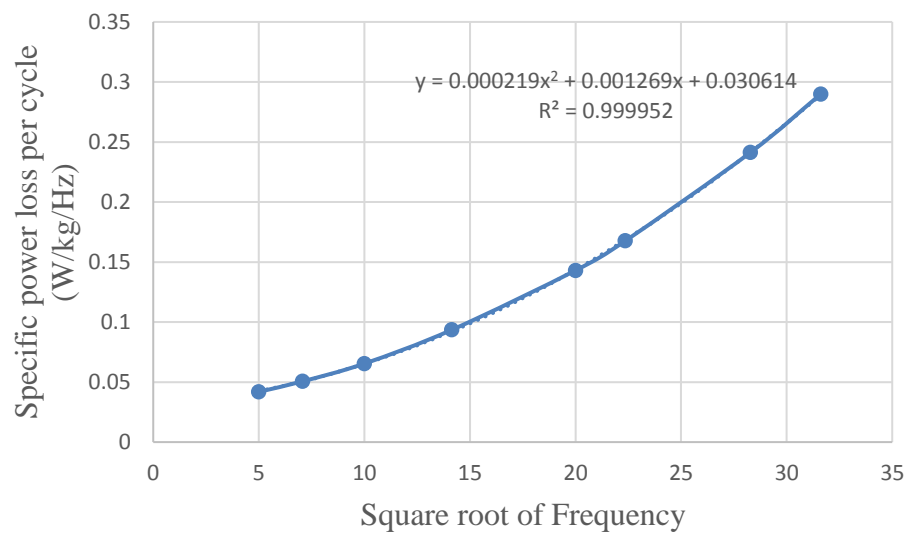
Fig 5-13 Total power loss per cycle of an Epstein-size magnetic lamination of NO steel versus the square root of frequency √f at a flux density of 1.5 T.

Table 5-4 Loss components of an Epstein-size lamination of NO steel at a peak flux density of 1.5 [T] and different magnetising frequencies.

Frequency (Hz)	Measured power loss (W/kg)	P_e (W/kg)	P_h (W/kg)	P_a (W/kg)	$P_t = P_e + P_h + P_a$ (W/kg)	$Error_\%$
25	1.047	0.13	0.76	0.15	1.06	1.32
50	2.53	0.54	1.53	0.44	2.52	-0.12
100	6.54	2.19	3.061	1.269	6.52	-0.29
200	18.7	8.76	6.122	3.58	18.47	-1.21
400	57.2	35.04	12.24	10.15	57.43	0.415
500	83.83	54.75	15.30	14.18	84.24	0.49
800	193	140	24.49	28.71	193.36	0.18
1000	290	219	30.61	40.12	289.74	-0.08
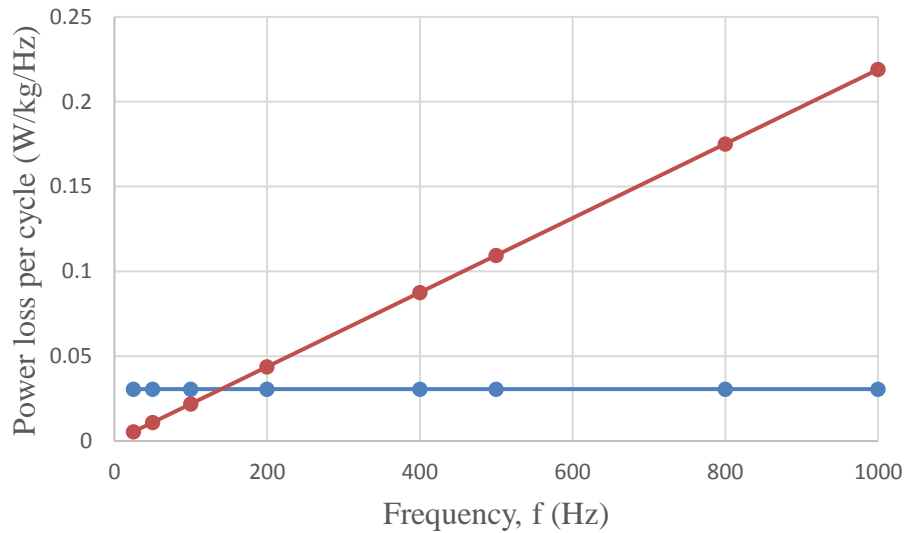
Fig 5-14 Eddy current and hysteresis loss per cycle versus frequency.

A comparison has been made between eddy current power loss obtained by the extrapolation method and eddy current calculated by the conventional formula. It has been noticed in this study, that the eddy current loss in a lamination calculation at low induction and low frequency is almost exactly the same as the one observed by extrapolation method. Most of the extra loss varies with frequency and the field in the same way as the eddy current power loss. In [5-32] it was indicated that the classical calculation of eddy current power loss is invalid when the distance between domain walls is comparable with sheet thickness.

Table: 5-5 Eddy current power loss of an Epstein-size lamination at a peak flux density of 1.5 T and different magnetising frequencies obtained from extrapolation method and equation [5-4].

Magnetising frequency Hz	Eddy current power loss (W/kg)by extrapolation method	Eddy current power loss (W/kg) by equation (5-4)
25	0.155	0.188
50	0.62	0. 59
100	2.48	2.37
200	9.92	9.48
400	39.68	37.9
500	62	59.28
800	158.72	151.78
1000	248	237.15

5.4. COMSOL Multiphysics Model

The purpose of using this software is to explore the behaviour of the magnetic flux and the generated power loss within the material. Therefore, the model was built within the context of the physical world and was explored in the first principle technique.

The primary purpose in combining the experimental results and the simulation is to try as many different approaches to the solution of the problem as needed in order to get it right or at least close to right.

The eddy current power loss for the Epstein frame size lamination was simulated. The system geometry was similar to the actual single strip tester described in section 5-2-2. Fig 5-15 shows the mesh for the SST, including the coils and the sample under investigation, while Fig 5-16 shows the flux distribution, the magnitude of the magnetic field and the flux density.
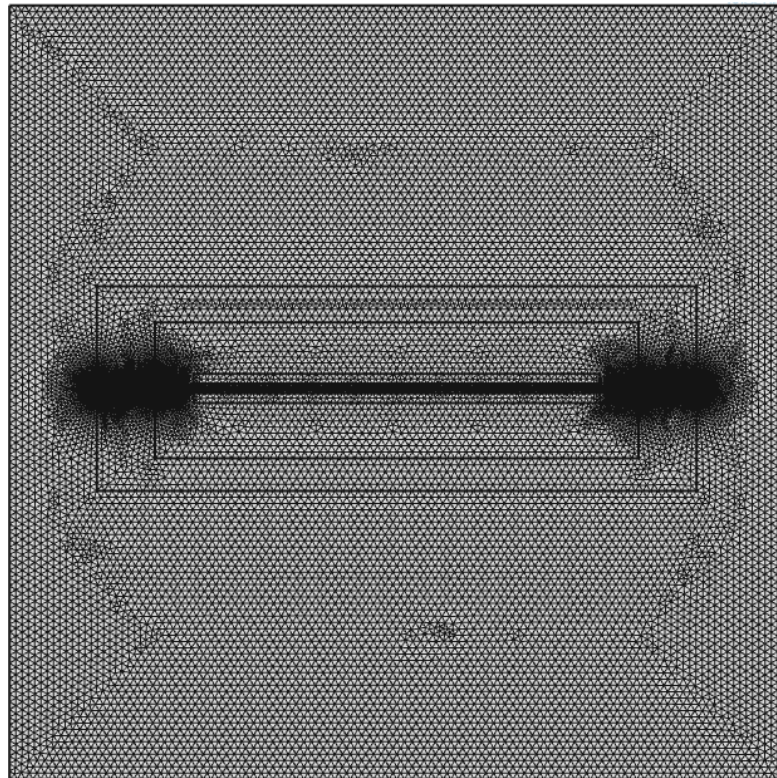
Fig 5-15 FEM mesh for the model.
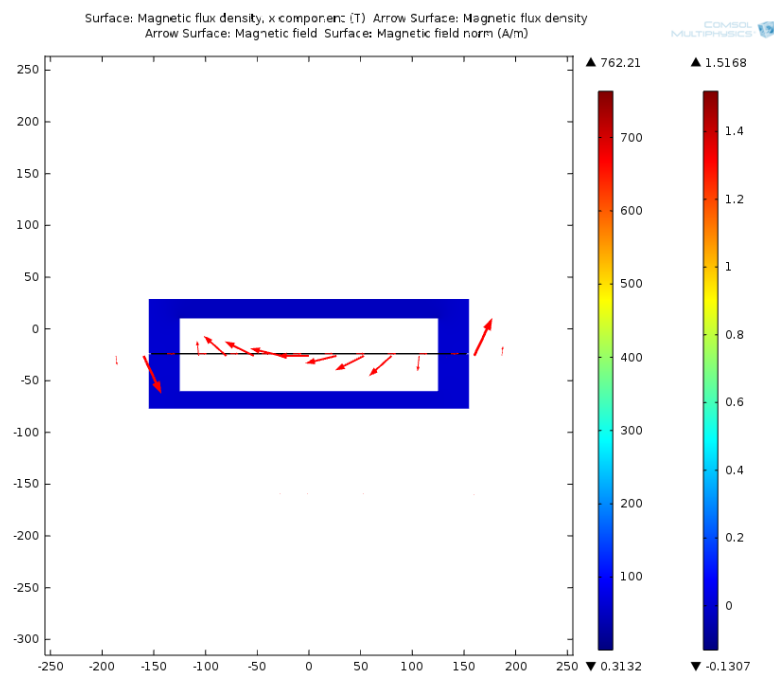
Fig 5-16 flux distribution, magnetic flux density and magnetic field intensity at 50 Hz

Table: 5-6 Eddy current power loss of an Epstein-size lamination at a peak flux density of 1.5 T obtained by extrapolation method, equation [5-4] and COMSOL modelling software.

Fig 5-16

Magnetising frequency Hz	Eddy current power loss(W/kg)by extrapolation method	Eddy current power loss (W/kg) by equation (5-4)	Eddy current power loss (W/kg) by COMSOL modelling
50 Hz	0.62	0. 59	0.57
100	2.48	2.37	2.33
200	9.92	9.48	8.57
400	39.68	37.9	35.8

Summary

There was remarkable agreement found between the eddy current power losses obtained from the conventional method and those of the extrapolation method at low frequencies, but slight discrepancies were observed at higher frequencies exceeding ≈400 Hz. This is a consequence of distorted flux penetration due to eddy current shielding, which must be taken into account when using the conventional formula for eddy current loss calculation, as well as domain wall activity, which is the main cause for the micro-eddy currents within the material at microstructural level. More generally, higher frequency and the increase of flux shielding caused by eddy currents in the magnetisation process tend to become highly inhomogeneous in the lamination cross section [5-33]. Therefore, it is difficult to make accurate loss estimations without fully studying the dynamic problem.

References

[5-1] M.Daniels, "power from designer domain," phys. world, pp33-36, 1988.

[5-2] A. J. Moses, "Electrical steels: past, present and future developments," in *IEE Proceedings A - Physical Science, Measurement and Instrumentation, Management and Education*, vol. 137, no. 5, pp. 233-245, Sept. 1990.

[5-3] S.Tumanski,"handbook of magnetic measurements." CRC Press, Boca Rton, FL: 2011.

[5-4] C. P. Steinmetz, "On the law of hysteresis: Part ii," *Trans. Ame. Inst. Elect. Engrs.*, vol. 9, pp. 621 – 724, 1892.

[5-5] C. P. Steinmetz, "On the Law of Hysteresis (Part II.) and Other Phenomena of the Magnetic Circuit," in *Transactions of the American Institute of Electrical Engineers*, vol. IX, no. 1, pp. 619-758, Jan. 1892.

[5-6] T L Mthombeni and P Pillay, "Physical basis for the variation of lamination core loss coefficients as a function of frequency and flux density" in Proc. IECON, Paris, Nov. 6–10, 2006, pp. 1381-1387

[5-7] Hysteresis in Magnetism, I. Mayergoyz, Ed. Academic Press, 1998.

[5-8] Space-time correlation properties of the magnetization process and eddy current losses: Theory," Journal of Applied Physics, vol. 54, no. 9, pp. 5293–5305, 1983

[5-9] P. Beckley (1999), "Modem steels for transformers and machines", IEE Power Engineering Journal, Vol. 13, No. 4, p. 190-200.

[5-10]3-2 D. Jiles (1998) "Introduction to magnetism and magnetic materials", 2nd Edition, Chapman and Hall, London, p. 328.

[5-11] G. Bertotti (1988), "General properties of power losses in soft ferromagnetic Materials", IEEE Trans. Magn. MAG-24, no. 1, pp. 621-630.

[5-12] W.Gilbert and pf. Mottelay, demagnete. New York: Dover publication, 1958, p368

[5-13] G. Bertotti, "General properties of power losses in soft ferromagnetic materials," *IEEE Trans. Magn.* Vol. 24, pp. 621-630, January1988

[5-14] Y. Zhang, M.-C Cheng, P. Pillay, "Magnetic Characteristics and Excess Eddy Current Losses," in proc. *IEEE Industry Applications Society Annual Meeting,* 2009. pp. 1-5.

[5-15] I. Mayergoyz and C. Serpico, "Nonlinear diffusion of electromagnetic fields and excess eddy current losses," *J. Appl. Phys.* 85, 4910 (1999).

[5-16] C. Serpico, C. Visone, I. Mayergoyz et al., "Eddy current losses in ferromagnetic laminations," *J. Appl. Phys.* 87, 6923 (2000).

[5-17] Y. Zhang, R. Guan, P. Pillay, and M.C Cheng, "General core loss models on a magnetic lamination," in proc. *IEEE Int. Electric Machines and Drives Conf.* , 3-6 May 2009, pp. 1529 – 1534,

[5-18] H. J. Williams, W. Shockley and C. Kittel (1950), "Studies of the propagation velocity of a ferromagnetic domain boundary", Phys. Rev., 80, pp. 1090-1094

[5-19] J. W. Shilling and G. L. Houze, Jr. (1974) "Magnetic pro perties and domain Structure in grain-oriented 3% Si-Fe", IEEE Trans. Magn. MAG-10, no. 2, pp. 195 **222**

[5-20] M. Balehosur (2012) Prediction *of No-Load Losses of Stacked 3-Phase, 3-Limb Transformer Cores.Ph.D.* Cardiff University: UK

[5-21] S. Somkun (2010) Magnetostriction and Magnetic Anisotropy in Non-oriented Electrical Steels and Stator Core Laminations. Ph.D. Cardiff University: UK

[5-22] T.L.Mthombeni,; , P.Pillay.; R. M W Strnat, , "New Epstein Frame for Lamination Core Loss Measurements Under High Frequencies and High Flux Densities," Energy Conversion, IEEE Transactions on , vol.22, no.3, pp.614,620, Sept. 2007

[5-23] BS EN 60404-2:1998 + A1:2008, "Magnetic Materials-Part 2: Method of Measurement of the Magnetic Properties of Electrical Steel Sheet and Strip by Means of an Epstein Frame," British Standard, 2009.

[5-24] Magnetic Materials Part-2: Method of Measurements of the Magnetic Properties of Electrical Steel Sheet and Strip by Means of an Epstein Frame, IEC Standard 60404-2, 1996.

[5-25] Magnetic Materials Part-3: Method of Measurements of the Magnetic Properties of Electrical Steel Sheet and Strip by Means of a Single Sheet Tester, IEC Standard 60404-3, 1992

[5-26] National Instruments, "DAQ NI 6115/6120 User Manual -Multifunction's devices for

PCI/PXI/Compact PCI bus computers," 2002.

[5-27] A. Boglietti, A. Cavagnino, "Iron Loss Prediction with PWM Supply: An Overview of Proposed Methods from an Engineering Application Point of View," in proc. IEEE Int. Industry Applications Society Annual Meeting, 2007, pp. 81 – 88.

[5-28] Y Chen and P Pillay, "An improved formula for lamination core loss calculations in machines operating with high frequency and high flu density excitation," IEEE 37th IAS Annual Meeting, Vol. 2, pp. 759–766, 13-18 Oct 2002 .

[5-29] M Ibrahim and P Pillay, "Advanced testing and modelling of magnetic materials including a new method of core loss separation for electrical machines "IEEE Transactions on Industry Applications, VOL. 48, NO. 5, Sep/Oct 2012, pp. 1507 - 1515

[5-30] D M Ionel, M Popescu, S J Dellinger, T J E Miller, R J Heideman and M I McGilp, "On The Variation With Flux And Frequency Of Core Loss Coefficients In Electrical Machine", IEEE Trans. Magn Vol. 42, No. 3, pp. 658-666, May/June 2006.

[5-31] B. D. Cullity and C. D. Graham, "Introduction to Magnetic Materials," 2nd ed. John Wiley & Sons, 2009.

[5-32]E. W. Lee, "Eddy-current losses in thin ferromagnetic sheets," in *Proceedings of the IEE - Part C: Monographs*, vol. 105, no. 8, pp. 337-342, September 1958

[5-33] V. Basso, G. Bertotti, 0. Botknscio, F. Fiorillo, M. Pasquale, "Power losses in magnetic laminations with hysteresis: Finite element modelling and experimental validation," J. Appl. Phys., vol. 81, no. 8, pp. 5606-5608, 1997

6.1. Concept of edge burrs as a source of short circuiting between core laminations

The cores of electrical machines are normally built from thin steel laminations to reduce eddy current losses for high-efficiency operations [6-1]. Each lamination is covered on both sides with an inorganic coating. This thin layer is 1 to 3μm thick is used to prevent direct electrical contact between them. Punching and cutting of electrical steel at low cost causes mechanical stress, which deforms the lamination and deteriorates its magnetic properties close to the cut edge [6-2]. In general, the cores of electrical machines are subjected to different processes which may have direct impacts on their properties. These include mechanical damage during assembly, rewind or re-wedge, foreign particles during assembly, vibration, arcing, heating and degradation of the insulation between the sheets [6-3], [6-4]. During the cutting process, however, mechanical deformations cause shearing burrs on the cutting edges [6-5]. These burrs tend to cause insulation breakdown between the sheets, resulting in electrical shorting between the stacked laminations. If this electrical shorting covers several laminations, high currents begin to circulate, leading to a significant increase in power loss and local overheating, which may cause burning or melting of the laminations. Thus, it causes the potential for complete machine failure [6-6], [6-7]. Fig 6-1(a and b) show an example of machine failure as a result of inter-laminar fault which has significantly damaged the core. The winding and stator core have to be replaced [6-8]. Statistical studies have shown an estimated cost for the manufacture was $17.1 million dollars and $270.1 million dollars of lost revenue for machine replacements [6-8]. Such huge figures have driven the researchers to investigate the causes of such defects and find the means to eliminate such faults in the future. Further inter-laminar shorts are induced by small insulation faults on the lamination surface inside the core at the middle of the sheet; however, the probability of such faults occurring is very low and stochastic [6-9].

An example of total machine failure was described by [6-10] in which a 187 MVA transformer failed during the first run. Another example is a machine stator core of 430 MW, 496 kVA rated generator with steel that melted as a result of short circuits between laminations [6-18]. Fig 6-1(a, b) illustrates damage in the stator core teeth. In this case, it is not possible to know the main cause of the fault, as it was either by inter-laminar fault or by coating failure [6-11].
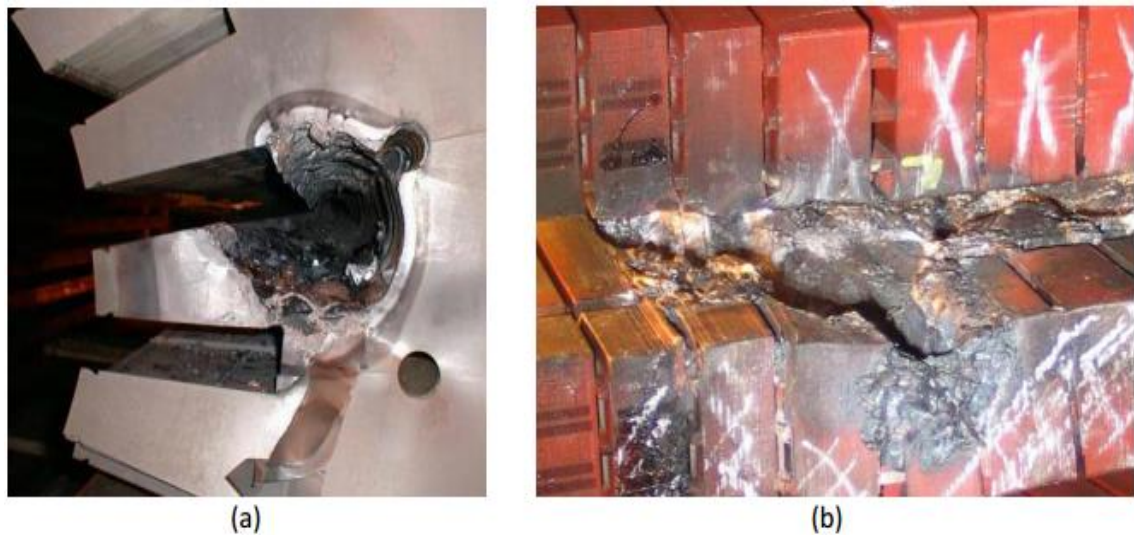
Fig 6-1 Stator core melting caused by inter-laminar insulation failure (a) core fault in tooth wall (b) core fault in tooth bottom [6-19]

Burrs are formed during the punching process of the sheets, which results in the interlayer short circuits as well as on the cut edges. Burr formation is also caused by shearing during the separation of the metal by two blades of the guillotine. The moving blade contacts the sheet which starts to roll over, and this causes an increase of the load, leading to fracture shear stress of the sheet [6-12]. At this stage of the cutting process, the load increases, causing a crack that leads to rapid breakthrough involving a ductile fracture and formation of burrs [6-13], Fig 6-2 illustrates the impact of the cutting process.
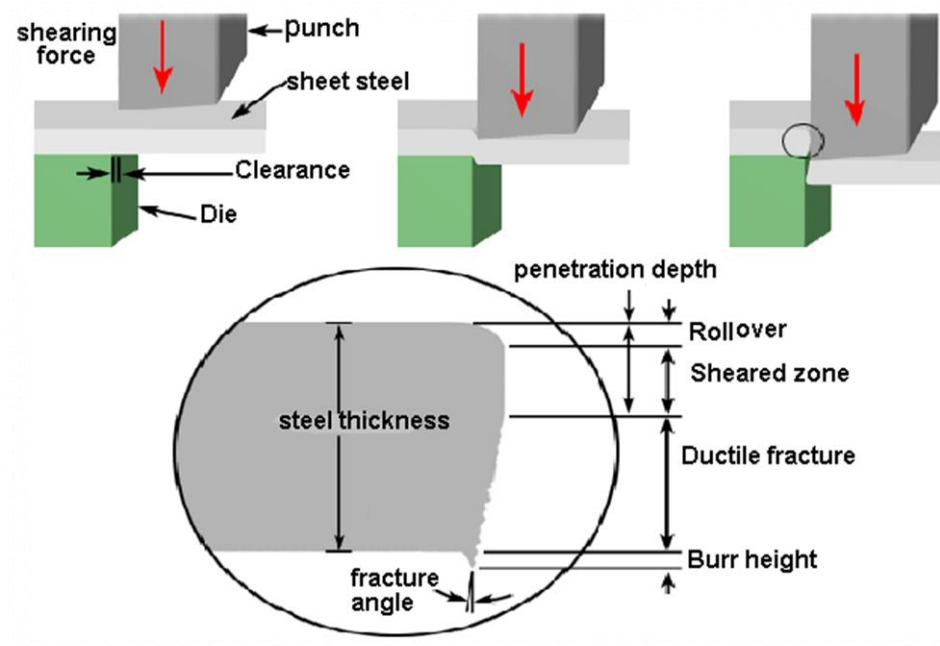
Fig 6-2 Cutting process of a lamination and created edge burr. Reproduced from [6-14].

6.2. The main causes of inter-laminar fault in electrical machine cores

All electrical machine cores are normally built from a stack of laminations of electrical steel material alloyed with silicon in order to minimise the impact of hysteresis and eddy current power losses [6-15]. These laminations, as mentioned before, are coated with inorganic material to prevent electrical conduction between them, which will cause restriction for eddy current circulation [6-16]. However, the coating is likely to degrade or deteriorate, causing electrical conduction between the laminations. This defect of insulation failure is due to different reasons which can be summarised by the following points [6-17] [6-18] [6-19].

> ➤ Mechanical damage during assembly, rewind or re-wedge
> ➤ Foreign particles introduced during assembly
> ➤ Vibration, arcing and heat
> ➤ Degradation of the insulation between the sheets
> ➤ Heat and chemical factors or mechanical forces when stripping windings during re-wind
> ➤ During assembly and operation of stator-rotor rubs
> ➤ Surface coating defects due to poor inter-laminar insulation coating
> ➤ Inadequate or damaged lamination coating

Inter-laminar faults caused by any of the above reasons lead to the circulation of eddy currents between the affected laminations that are larger than eddy currents caused by normal operation [6-18],[6-20]. These currents are normally called inter-laminar fault currents. In fact, these fault currents are formed as loops between the shorted lamination and the fault points, which are perpendicular to the direction of the flux density in the core [6-21].

6.3. Coating and winding failure

Electrical steel coating damage over a large surface allows electrical contact between the laminations, causing eddy currents to flow over the volume. A simulation for this phenomenon is shown in Fig 3-12(a), illustrating eddy currents associated with short circuited laminations.

6.4. Modelling of edge burrs as a source of short circuiting between core laminations

In previous studies on the impact of edge burr faults, various techniques have been implemented [6-22], [6-23]. For example, Moses and Aimoniotis simulated the short circuit by drilling 0.33 mm holes near the edges of the laminations for a single phase transformer core. The laminations were shorted by inserting a pin to the stacks under test. Mazurek et al. [6-24] used 8 μm thick copper tape. The length and height of the tape were cut according to the number of laminations under investigation, and then they were uniformly clamped on both sides of the core laminations. Lamprecht and Graf [6-25] simulated the short circuit by coating the edges of a ring core with galvanic nickel with a thickness of roughly 0.1 mm. In this project, packs of two and three 0.5 mm thick non-oriented steel 3% Si laminations were artificially short circuited by lead-free solder, which has similar properties of electrical steel.

They applied 10 mm long solder at three different points, and the thickness of the artificial burrs was chosen to be comparable with actual burr dimensions [6-26]. In fact, the burr size produced during the shearing process varies depending on the machining technique as well as the quality and wear of the cutting tool [6-27]. Fig 6-3 illustrates how the burr size in electrical steel can grow with blade wear. The burr height and the stress created by the cutting process are largely increased with increased blade usage. For example, 2,000 cuts have no visible impact on the steel sheet; there might be slight impact of cutting, but that impact is eradicated by the annealing process. However, after 20,000 or more cuts, the burr height and the stress increase dramatically and may cause harmful impacts in the burrs remains [6-27].

44 000 cuts   22 000 cuts   2 000 cuts
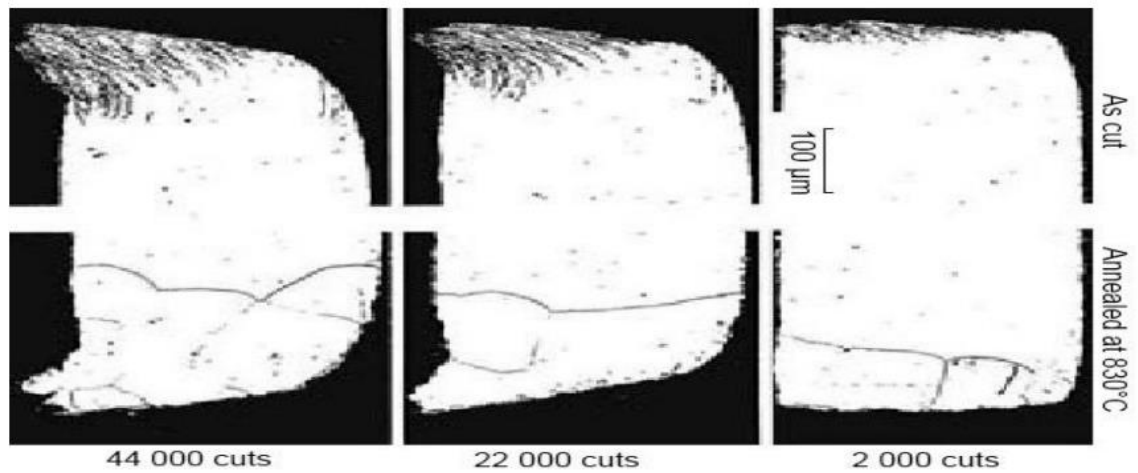
Fig 6-3 Sections through a cut edge of grain-oriented electrical steel showing variation of burr height with age of the cutting blade. Burrs as cut are shown in the top row and after annealing at the bottom (Figure taken from [6-27]).

6.5. Burr height

The height of the burrs in electrical steel lamination is defined by the British standard BS EN 10251:1997 [6-28] as the difference between the measured thickness at the cut edge of the lamination and at distance of 10 mm from this edge. This is illustrated in Fig 6-4, where h is burr height, which is calculated by subtracting h_2 at the edge and the lamination thickness h_1 measured 10 mm from the edge of the lamination.
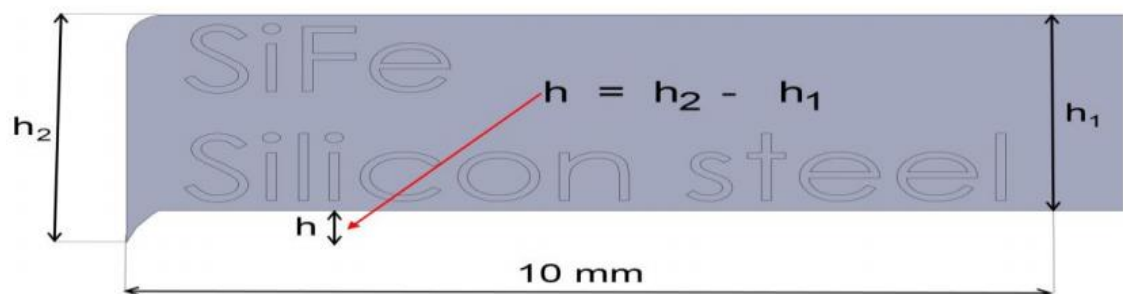
Fig 6-4 Burr height definition as per British Standard BS EN 10251:1997 [6-28].

The procedure for measuring edge burr height is fully described in British standard EN 10251:1997 [6-28]. Measurements are based on steel sheets required for use in specific application, and the measurements are applied for 1 m length samples with required specifications provided by the measurement standard listed below:

➤ Resolution of 1 μm

➤ Uncertainty of 2 μm

➤ Axial movement of the sliding anvil is obtained without rotation

➤ Force which is applied on the anvil is 4 N ±0.2 N

➤ The sliding dimensions of anvil are 16 mm × 8 mm

The measurement system, as depicted in Fig 6-5, is that the samples are placed on a flat support table, onto which the comparator is fixed to ensure 90-degree movement of the anvil in relation to the table surface. The latter guarantees that the anvil is parallel to the table surface. This can be achieved by using a three-point surface table construction, as shown in Fig [6-5] by the three bold triangles. The difference in the height of any point of the table's plane should not exceed 2 μm. The measurement includes finding the length h_1 & h_2, as presented in Fig 6-4.

In order to achieve accurate measurement, the measurements are repeated 20 times for every 50 mm along 1 m of length. Then the final results are obtained by averaging the 20 measurements.
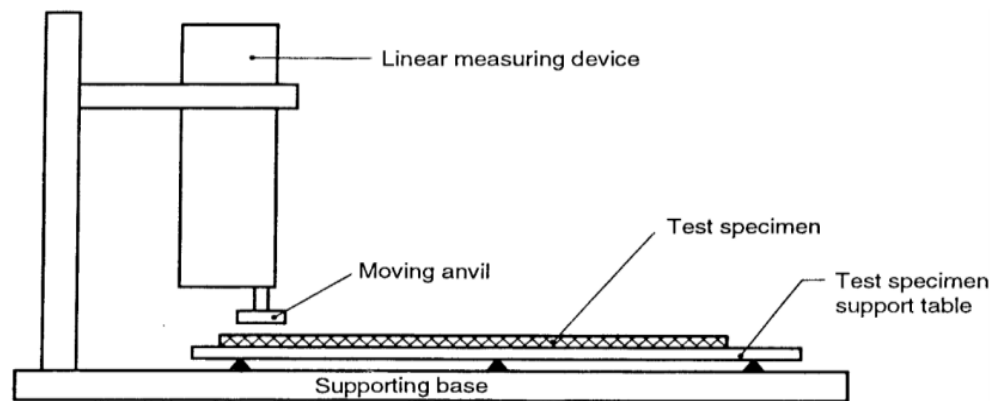
Fig 6-5 Burr height measurement rig reproduced from [6-28].

In fact, an edge burr height of 25 μm is allowed by the BS EN 10107:2005 [6-29], but this value is not enough to eliminate faults caused by edge burrs in electrical machine cores. Therefore, a height under 15 μm is set as the maximum value for edge burr height to significantly minimise the impact of edge burrs [6-30]. The coating thickness of electrical steel is around 0.5-2 μm [6-31]; therefore, the burr height should not be higher than that thickness, otherwise it will cause direct contact between the laminations. Achieving this value is not possible; however, 5 μm height is achievable [6-32].

6.6. Power loss measurement

The power losses for each stack were measured at peak flux densities of 1 T, 1.1 T, 1.3 T and 1.5 T and magnetising frequencies from 50 Hz up to 500 Hz with no fault applied, and then the power losses were measured at each set of short circuit positions. The purpose of this study was to show the impact of the number of shorts on the total power loss. Power loss measurements were performed three times with repeatability of 0.3%. The results presented here are the average values of the three measurements.

Table 6-1 Specific power loss for a stack of three laminations at different flux densities and different magnetising frequencies in the rolling direction.

Total measured power loss (W/kg)					
B_{pk} (T)	50 Hz	100 Hz	200 Hz	400 Hz	500 Hz
1	1	2.54	7.43	23.1	33.7
1.1	1.13	3.08	9.193	29.1	42.63
1.3	1.62	4.4	13.4	43.9	65.2
1.5	2.28	6.15	18.5	60.5	90.1
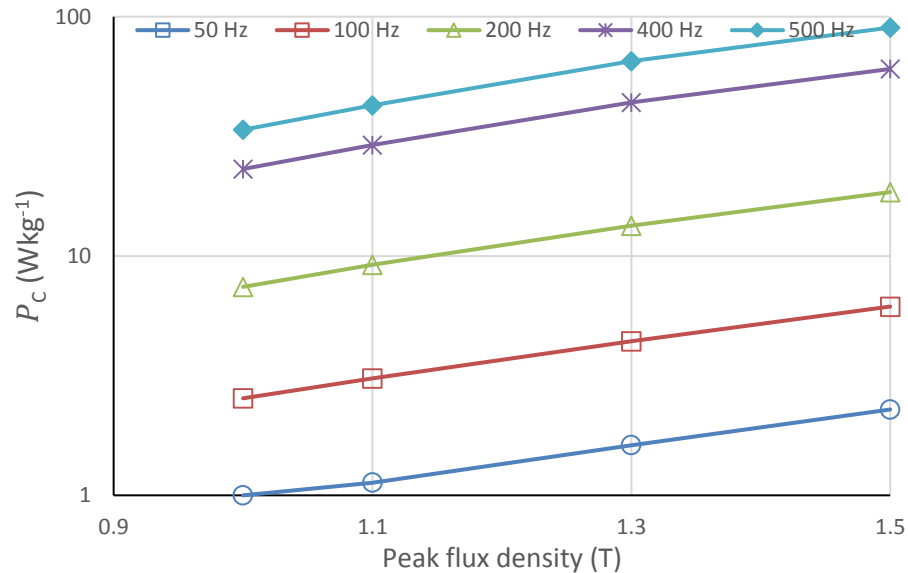
Fig 6-6 Measured power loss for a pack of three Epstein-size laminations of non-oriented steel in the rolling direction.

Table 6-2 Specific power loss for stack of three laminations at different flux densities and different magnetising frequencies in transverse direction.

Total measured power loss (W/kg)					
B_{pk} (T)	50 Hz	100 Hz	200 Hz	400 Hz	500 Hz
1	1.27	3.27	9.14	27.3	39.3
1.1	1.51	3.87	10.9	32.9	47.7
1.3	2.08	5.36	15.1	46.3	67.7
1.5	2.79	7.25	20.4	62.7	91.8
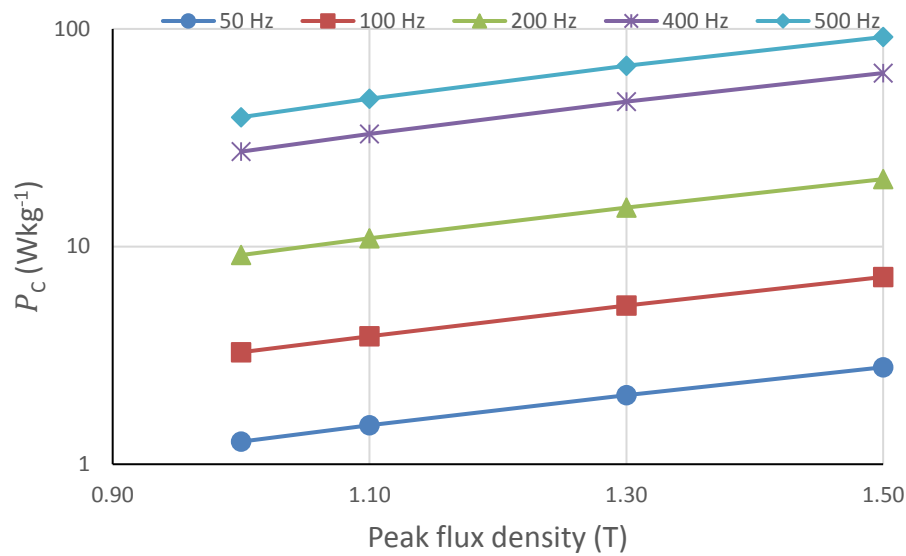
Fig 6-7 Measured power loss for a pack of three laminations in the transverse direction.

6.7. Studying the impact of multiple shorts on the total power loss

In this study, the effect of inter-laminar fault is conducted at set positions. The total power loss was first measured for the pack of three laminations in the rolling and transverse directions; then 10 mm wide artificial burrs were applied at three set positions and the power loss was measured in each case. Schematics of the side view are illustrated in Fig 6-8. Stacks with one, two and three short circuits are shown. Also schematics and a photograph of the top view of the stack with three short circuits are illustrated in Fig 6-9 and Fig 6-10, respectively. The purpose of this study is to investigate the impact of the number of shorts on the stack of laminations, and the obtained power losses versus the

number of applied short circuits at different magnetising frequency are shown in Fig 6-11 and Fig 6-12.
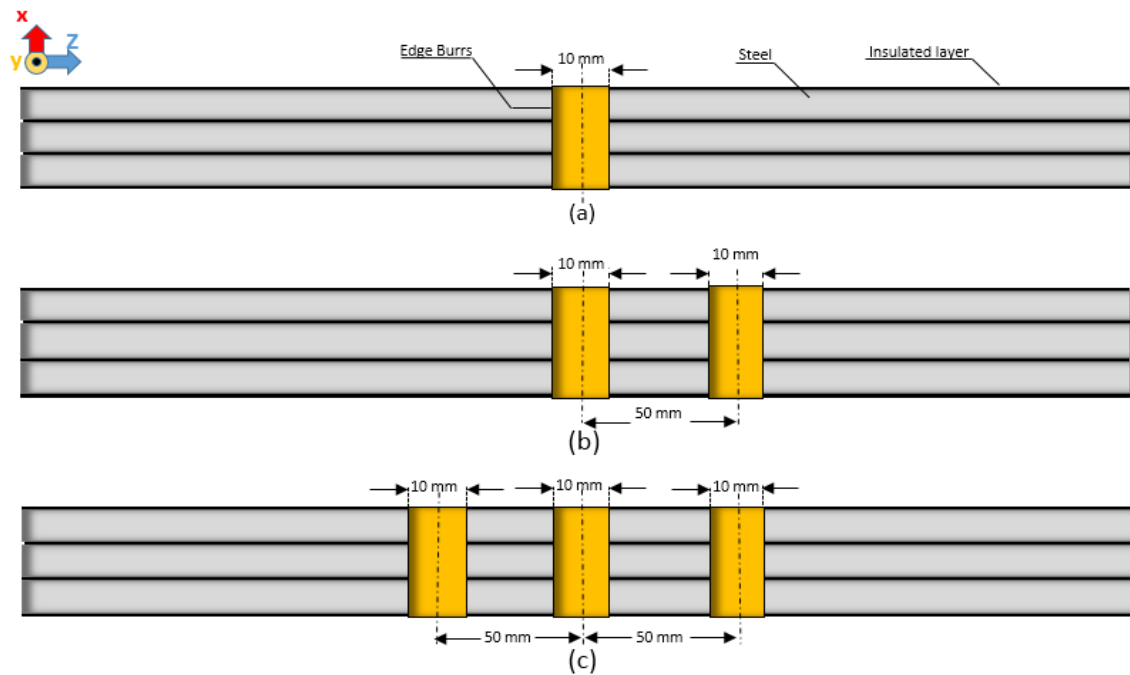
Fig 6-8 Side view for a stack of three laminations with edge burrs applied at (a) one set position (b) two set positions (c) three set positions.
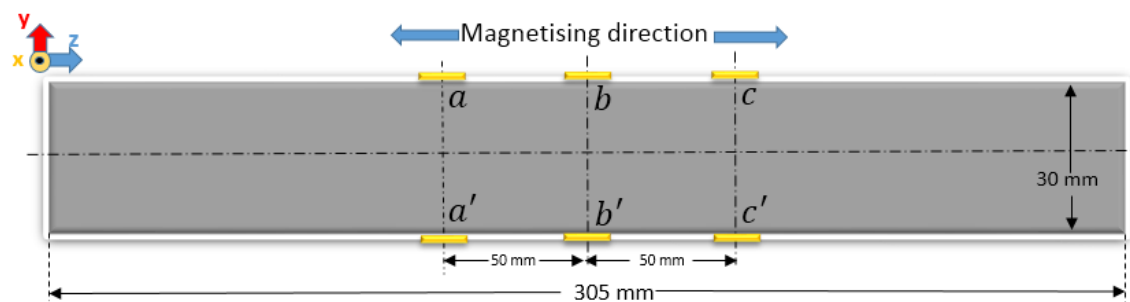
Fig 6-9 Top view for a stack of three laminations with artificial edge burrs applied at three different set-points. Short circuit applied at three set-points.
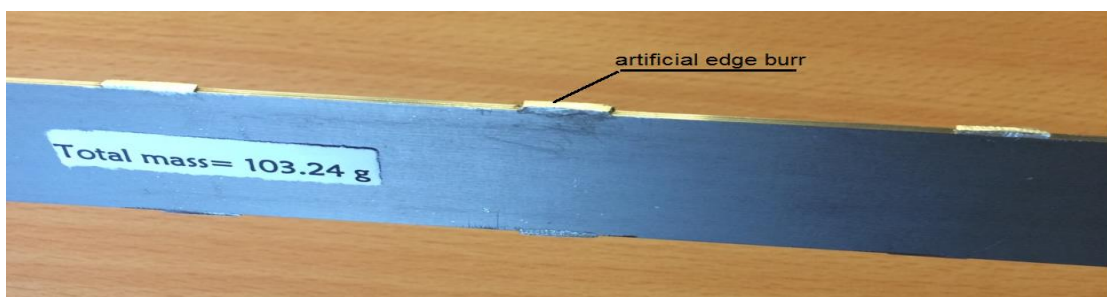
Fig 6-10 A photograph for stack of three laminations with short-circuit applies at three set points.
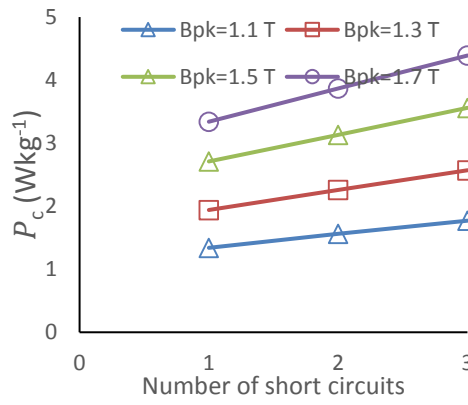
(a)
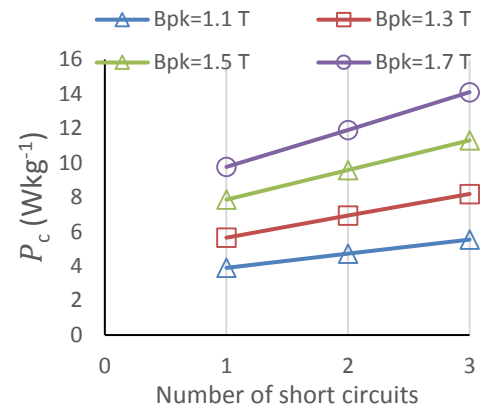
(b)
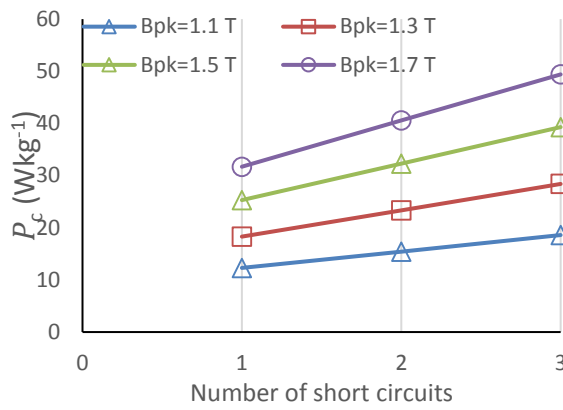
(c)
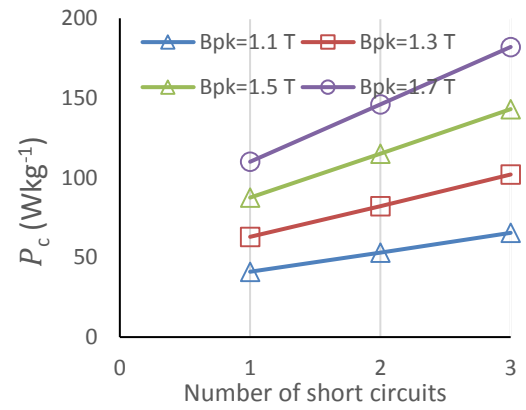
(d)
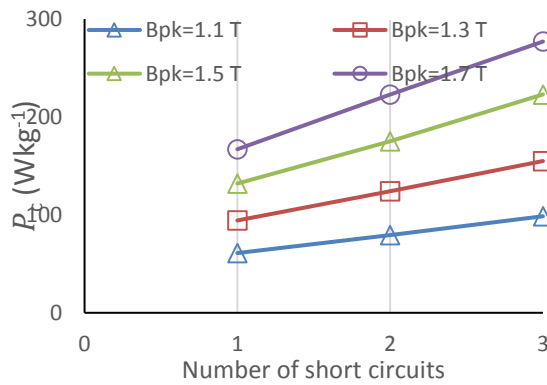
(e)

Fig 6-11 Measurement of power loss caused by artificial burrs at magnetising frequency of (a) 50 Hz (b) 100 Hz (c) 200 Hz (d) 400 Hz and (e) 500 Hz for the material B32L in the rolling direction

(a)

(b)

(c)

(d)
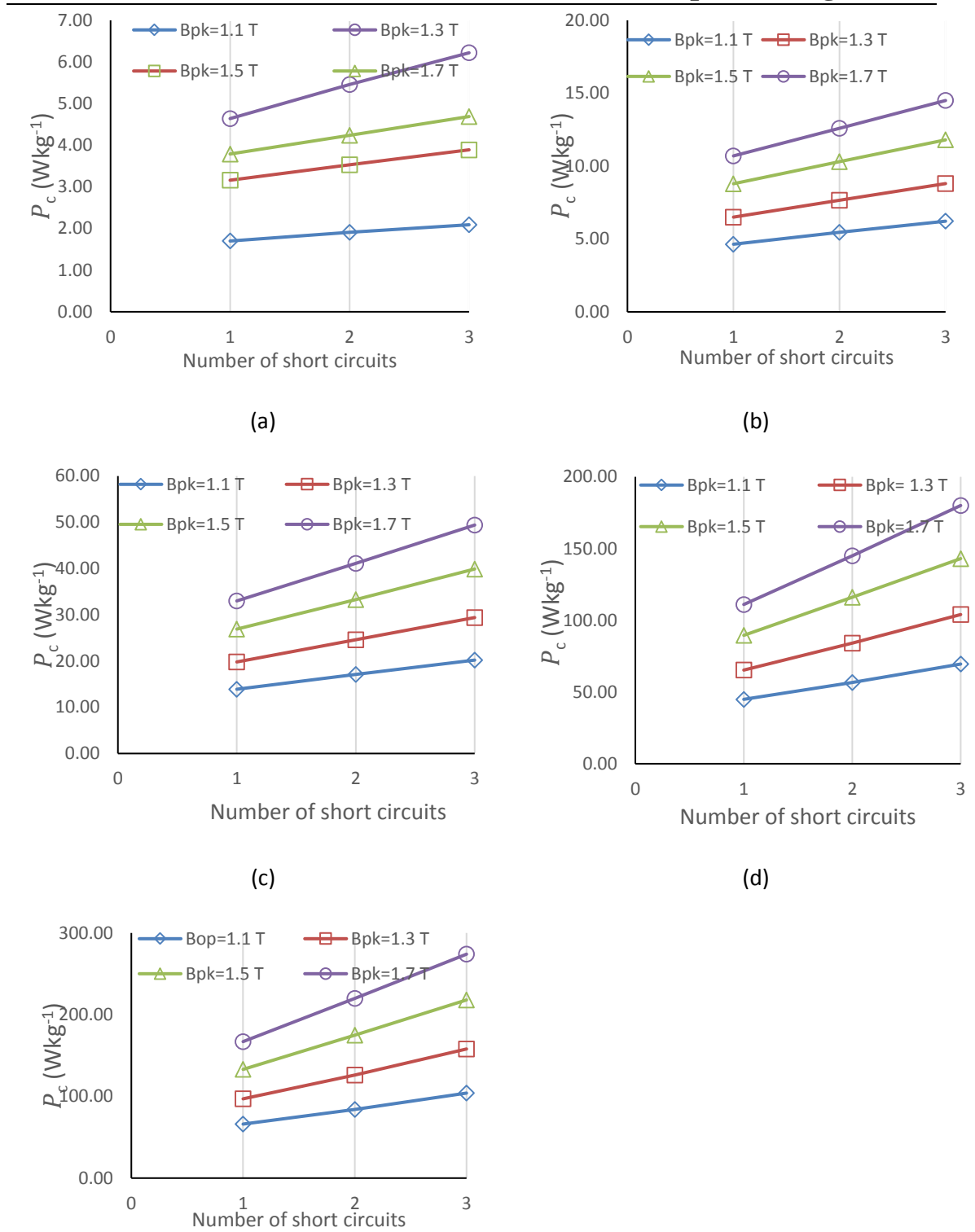
Fig 6-12 Measurement of power loss caused by artificial burrs at magnetising frequency of (a) 50 Hz (b) 100 Hz (c) 200 Hz (d) 400 Hz and (e) 500 Hz for the material B32L in the transverse direction.

6.8. The impact of edge burrs on total power loss of Epstein-size laminations

In the next part of the experiments, the effect of edge-burrs on total power loss was studied for Epstein size lamination, hence different techniques of shorts were applied to investigate the impact of this phenomena from different perspective, then this study was extended to include large size laminations.

6.9. Modelling the edge burr faults with axial off-set positions

This section focuses on the impact of edge burrs at set positions on total power loss. The power loss for stacks of two and three laminations was first measured with no burrs. Then artificial burrs of 10 mm width were applied at three different positions, and the power loss of the stacks were measured at each stage, see Fig 6-13.
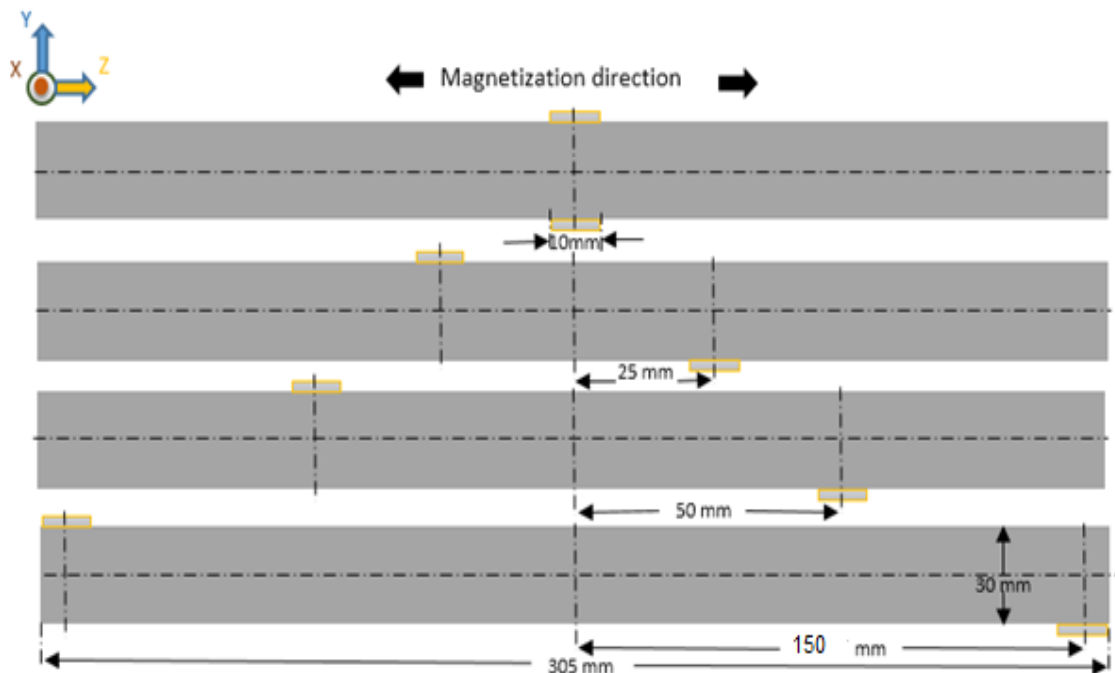
Fig 6-13 Stack of two and three laminations in the rolling and transverse directions with artificial burrs at different set points.

The power losses were measured at a peak flux density of 1.5 T, which is near the usual working flux density for electrical machines, and at magnetising frequencies of 25 Hz, 50 Hz, 100 Hz, 200 Hz, 400 Hz and 500 Hz by using a strip tester. The low magnetising frequencies were used to calculate the power loss separation for specific cases. These measurements were repeated while the artificial burrs were present. When the fault was

applied with zero separation (mid-point), higher power loss was observed. In this geometry, the electrical resistance between the faults will be the smallest, allowing high fault currents to circulate. In the second case, when the axial off-set between faults is increased by 25 mm, this caused an increase in the electrical resistance between the contact points, which allowed less inter-laminar fault current to flow. A higher reduction in power loss was observed with a 50 mm off-set between fault points. This was due to less electrical resistance between the faults which has allowed small fault currents to circulate. In the final case, the shorts were applied when the off-set point was made at the 150 mm of laminations. This made the power loss approach the nominal loss when no fault was applied. Results are depicted in Fig 6-14, Fig 6-16, Fig 6-18 and Fig 6-20, showing the specific power losses for two and three laminations in the rolling and transverse directions with and without fault. The percentage change between faulty and un-faulty conditions are depicted in Fig 6-15, Fig 6-17, Fig 6-19 and Fig 6-21.
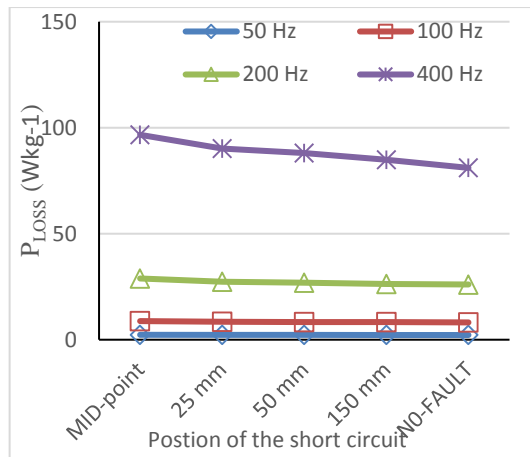
Fig. 6-14. Specific power loss for two laminations in the rolling direction (RD) at different set-points of short circuits.
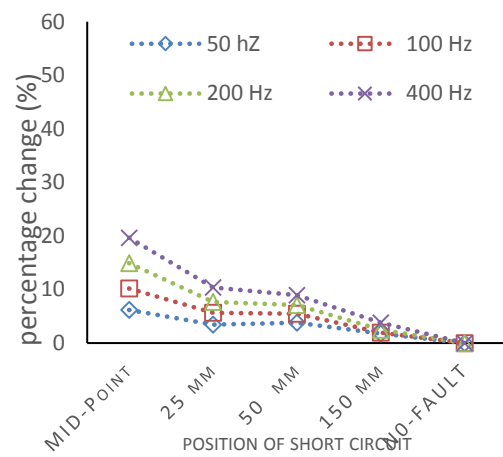
Fig. 6-15. Relative percentage of change between no fault and fault conditions for two laminations in the rolling direction (RD).
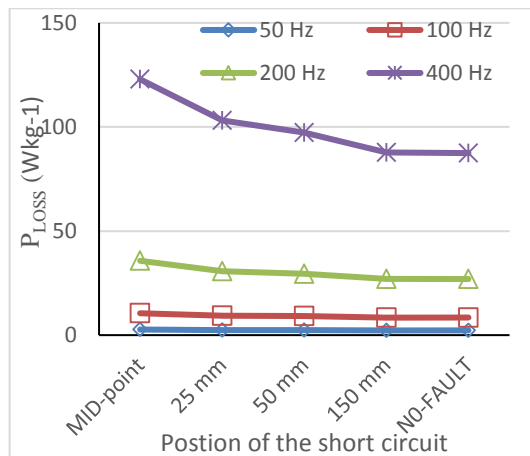
Fig. 6-16. Specific power loss for three laminations in the rolling direction (RD) at different set-points of short circuit.
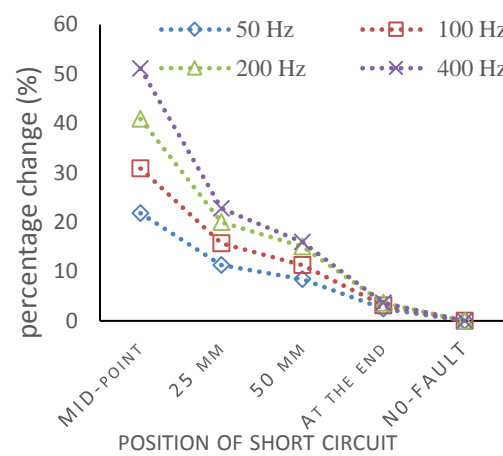
Fig 6-17. Relative percentage of change between no fault and fault conditions for three laminations in the rolling direction (RD).
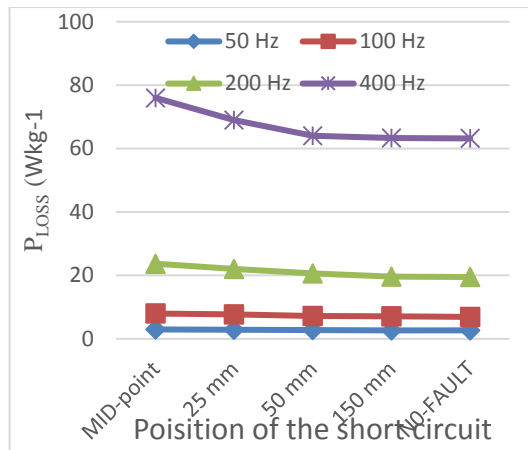
Fig. 6-18. Specific power loss for two laminations in the transverse direction (TD) at different set-points of short circuits.
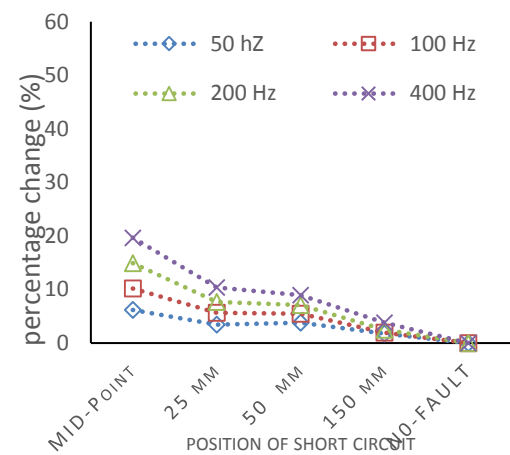
Fig. 6-19 Relative percentage of change between no fault and fault conditions for two laminations in the transverse direction (TD).
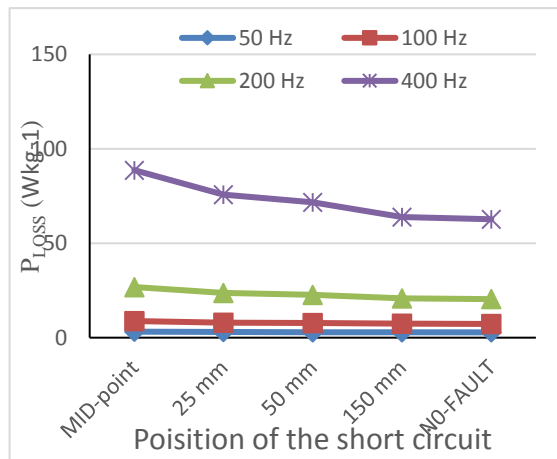
Fig. 6-20. Specific power loss for three laminations in the transverse direction (TD) at different set-points of short circuit.
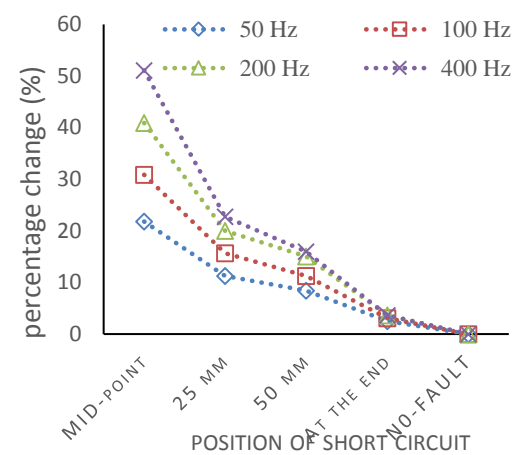
Fig. 6-21. Relative percentage of change between no fault and fault conditions for three laminations in the transverse direction (TD).

The obtained power losses for the stacks in the rolling and transvers directions were close; this is due to the almost isotropic nature of the material. This was always the case for the non-oriented electrical steel material under investigation. When the short circuit was present, an increase in the power loss was observed. This is attributed to the effect of the lamination thickness. This increase is based on the number of shorted laminations, which in turn raise the induced eddy currents. A single short circuit between two laminations may not be serious, but with several shorts in the adjacent layers, the induced eddy currents can be high enough to cause excessive heating. In order to have a more clear explanation of the impact of edge burrs on core lamination performance and their locations, the conductance for the samples was measured at different contact points, as

depicted in Fig. 6-22. These results show that higher conductance was observed when a short circuit was applied at mid-point, which provides low contact resistance. Therefore, high eddy currents will be induced. The value of conductance decreases with increasing axial offset, yielding higher contact resistance. In general, power losses in electrical steel materials consist of three components. To investigate which component has a significant role in the increase of power loss while edge burrs are present, an extrapolation method for power loss separation was applied. In all cases and based on the obtained results, the eddy current power loss, as depicted in Fig 6-24, was found to be the dominant factor, while the hysteresis and anomalous loss components did not show any large impact, which was expected for the material under investigation, as shown in Fig 6-26 and Fig 6-28. The increase in eddy currents varies from one case to another; it was lowest when no fault was applied (Fig 6-23). A significant increase in eddy currents was shown when the separation between contact points was zero, mainly at higher frequencies. This is also due to flux shielding caused by eddy currents, known as the skin effect, which caused the magnetic field to become highly inhomogeneous within the lamination. As a result, incomplete flux penetration occurred, which represents the dominant nature of losses due to the increased wall activity that causes a strong shield against magnetisation inside the lamination [6-33]. Most of the measurements were taken three times, and their average values are presented. The repeatability of these measurements is in the range of 0.0003 to 0.001%, which reflects the level of measurement accuracy.
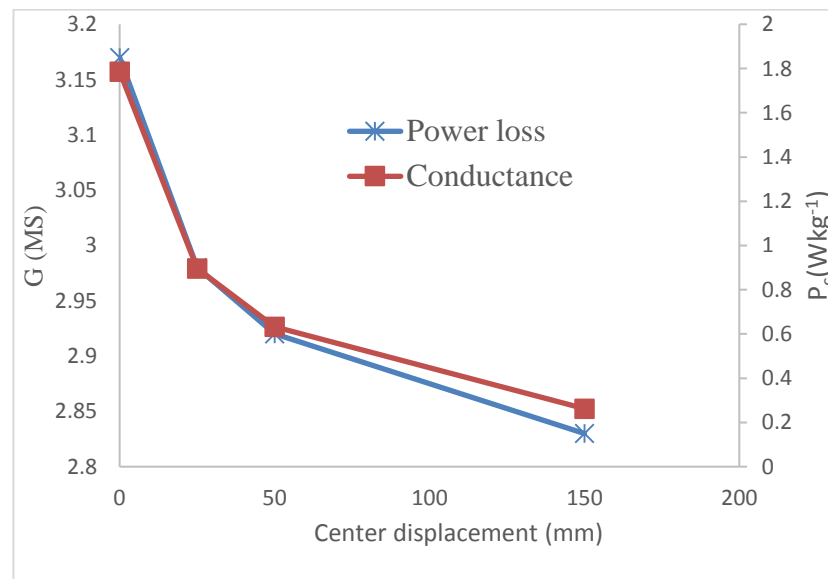
Fig. 6- 22. Measured conductance for a pack of three laminations in transverse directions at different contact points.
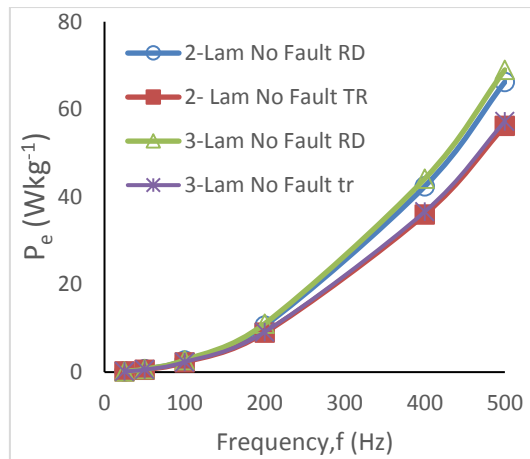
Fig. 6-23. Derived eddy current power loss for two and three laminations in the rolling and transverse directions for no fault condition.
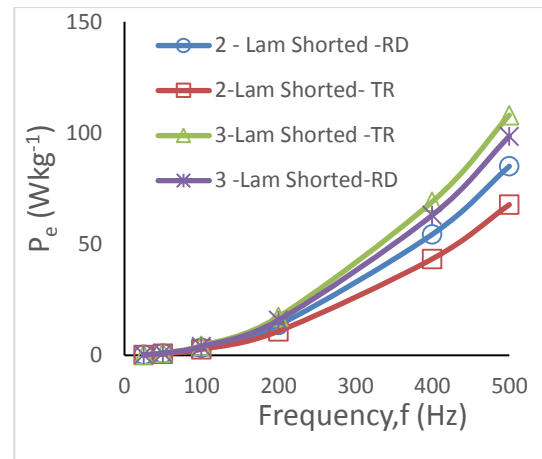
Fig. 6-24. Derived eddy current power loss for two and three laminations in the rolling and transverse directions with fault in mid-point position.
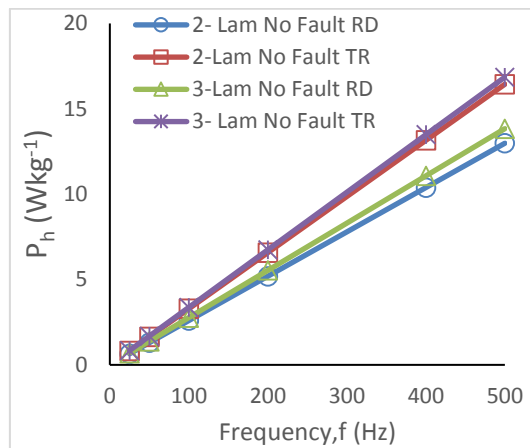
Fig. 6-25. Derived hysteresis loss for two and three laminations in the rolling and transverse directions with no fault.
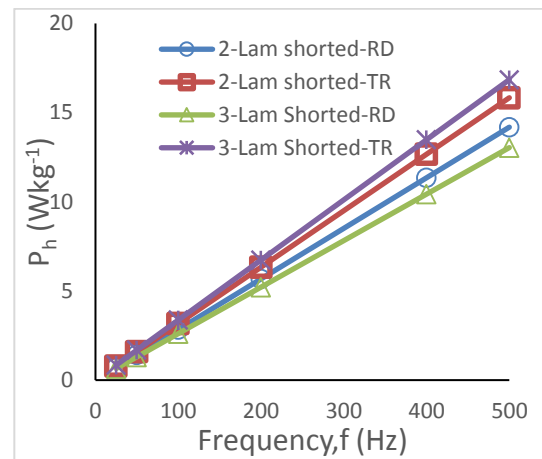
Fig. 6-26. Derived hysteresis loss for 2 and 3 laminations in the rolling and transverse directions with fault in mid- point position.
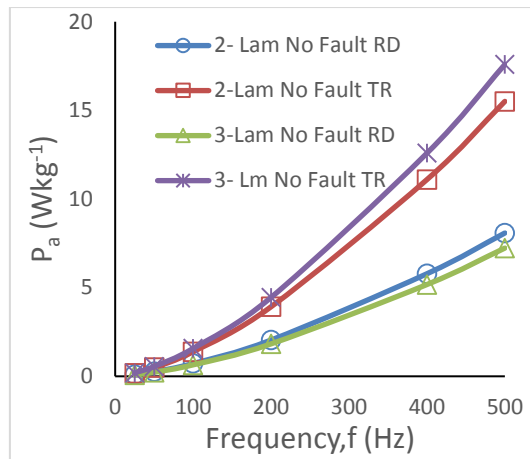
Fig. 6-27. Derived anomalous loss for two and three laminations in the rolling and transverse directions with no fault.

Fig. 6-28 Derived anomalous loss for two and three laminations in the rolling and transverse directions with fault in the mid-point position.

6.10. The impact of edge burrs on total power loss of large-scale machine laminations

In this section, the impact of edge burrs were simulated by using large-scale motor laminations and 0.5 mm thick non-oriented electrical steel, and the size of the laminations were 300 mm × 300 mm.
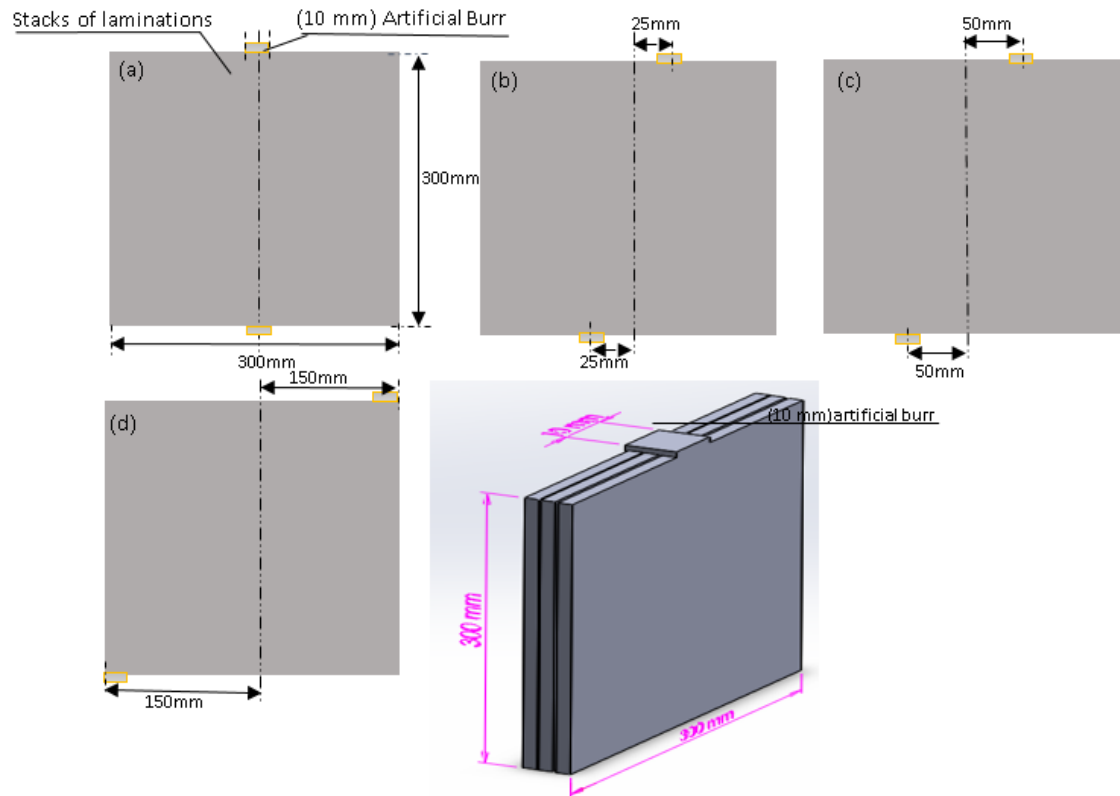
Fig 6-29. (a, b, c, d) Stacks of two and three laminations with artificial burrs at different set points. (e) Stacks of three laminations with artificial burrs at midpoint.

The power loss measurement of the test specimens was carried out by means of a large scale strip tester (300mm*300 mm). The system consists of a computer with the virtual instrumentation software LabVIEW and a data acquisition/generation card NI BNC-2110(DAQ). It generates a sinusoidal voltage signal which is fed into the power amplifier which provides the magnetising current for the strip tester. The power loss generated in the test specimen is measured by the system from the magnetising current and the induced secondary voltage in the strip tester. This method enables the system to measure the power loss in single lamination or packs of two or three laminations at a peak magnetic flux density of 1.5T and magnetising frequencies of 25 Hz, 50 Hz, 100 Hz, 200Hz and 400 Hz. Each measurement was repeated three times with an estimated uncertainty in the

determination of power loss of ± 1%. Importantly, an appropriate time delay was left between measurements in order for the test specimens to be fully demagnetised and to be stabilised thermally. The results of the measurements showed an increase in power loss when edge burrs were present in the test specimens compared to burr-free specimens. The power loss was highest when the artificial burrs were applied at the mid-point of the multi-layer test specimen. As the axial displacement between the contact points was increased, the power loss gradually reduced. The results are illustrated in Fig 6-30 and Fig 6-32, which show how the power loss for test specimen packs of two and three non-oriented electrical steel laminations changes with and without the applied faults. Fig 6-31 and Fig 6-33 illustrate the percentage changes between the fault and no-fault conditions.
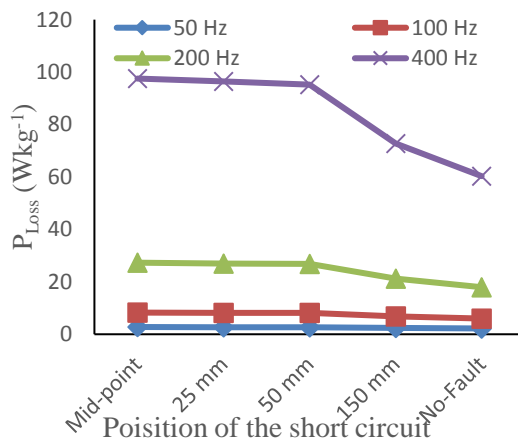
Fig. 6-30. Specific power loss for two laminations in the rolling direction (RD) at different set-points of short circuits.
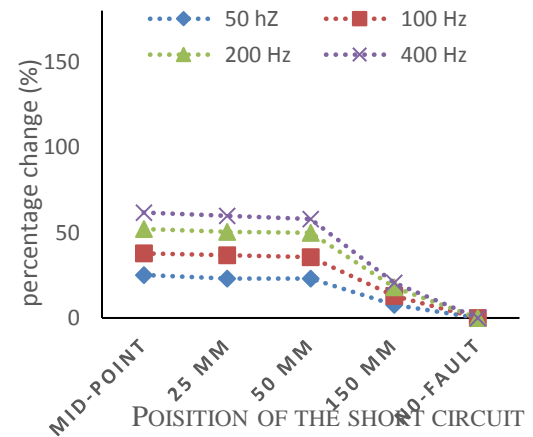
Fig. 6-31. Relative percentage of change between no fault and fault conditions for two laminations in the rolling direction.
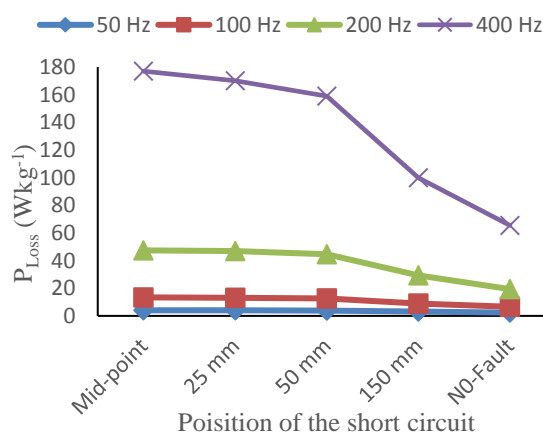
Fig. 6-32. Specific power loss for three laminations in the rolling direction (RD) at different set-points of short circuits.
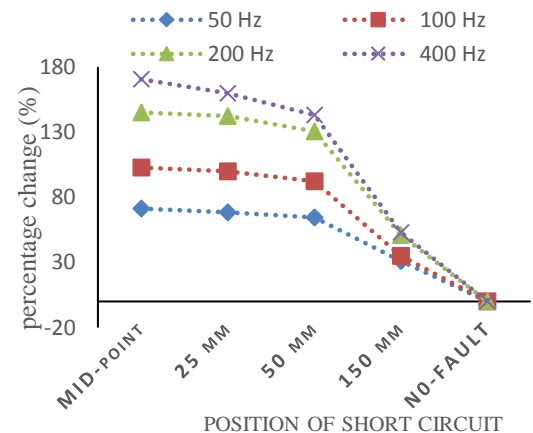
Fig. 6-33 Relative percentage of change between no fault and fault conditions for three laminations in the rolling direction.
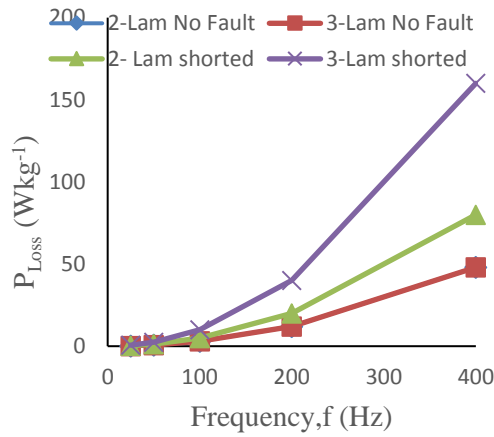
Fig. 6-34. Derived eddy current loss for two and three laminations in the rolling direction with no fault and fault.
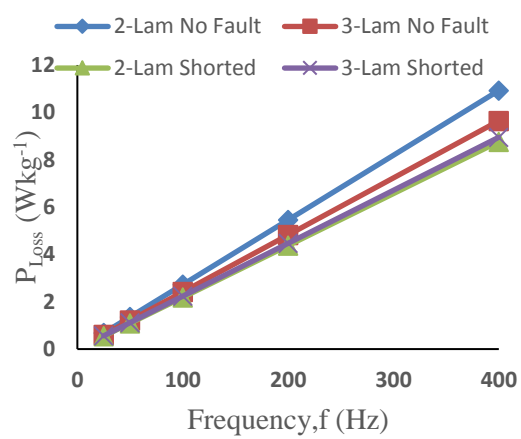
Fig. 6-35. Derived hysteresis loss for two and three laminations in the rolling direction with no fault and fault.

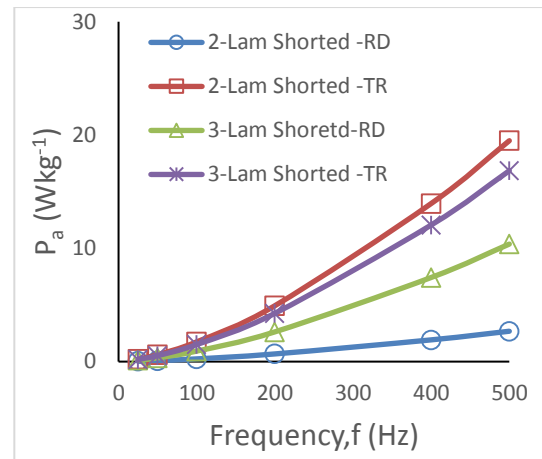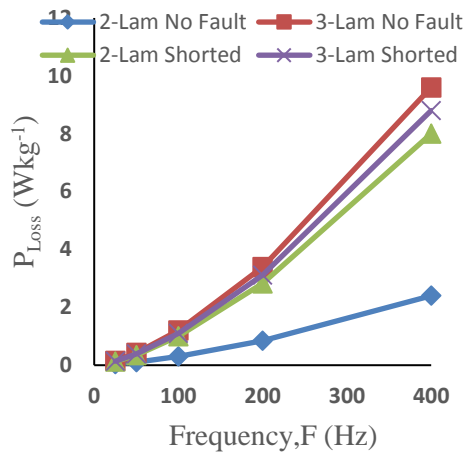**Fig.** 6-36. Derived anomalous loss for two and three laminations in the rolling direction with no fault and fault.
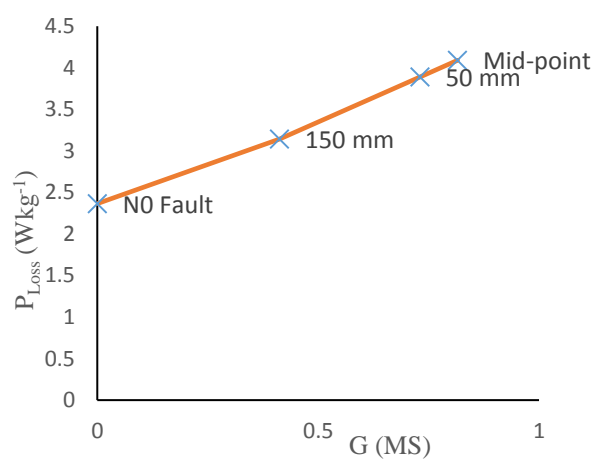
Fig. 6-37 Measured conductance for a pack of three laminations at different contact points.

The same procedure was applied for the laminations in the transverse direction.

This area shows the results in transverse direction.
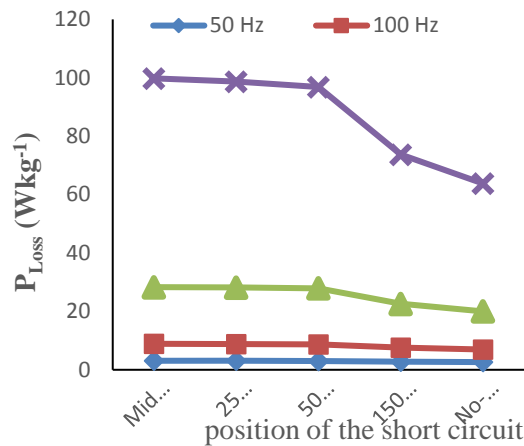
Fig 6-38 Specific power loss for two laminations in the transverse direction (TR) at different set-points of short circuits.
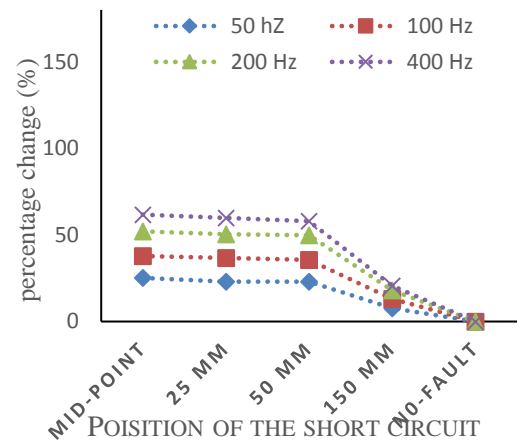
Fig. 6-39. Relative percentage of change between no fault and fault conditions for two laminations in the transverse direction.
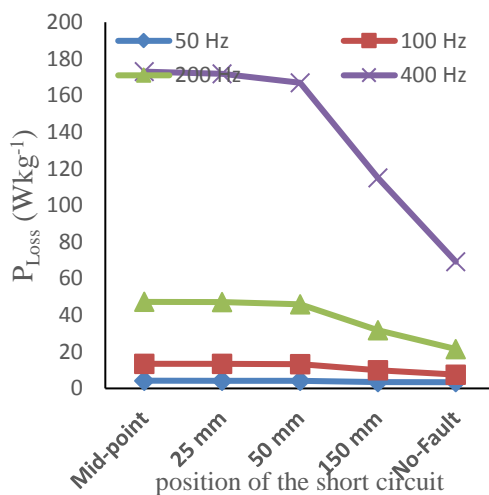
Fig. 6-40 Specific power loss for three laminations in the transverse direction (TR) at different set-points of short circuits.
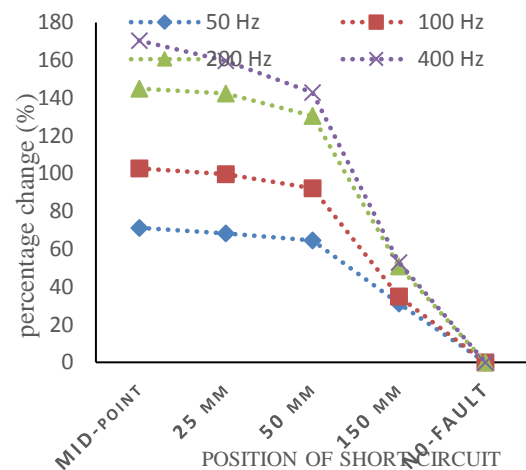
Fig. 6-41. Relative percentage of change between no fault and fault conditions for three laminations in the transverse direction.
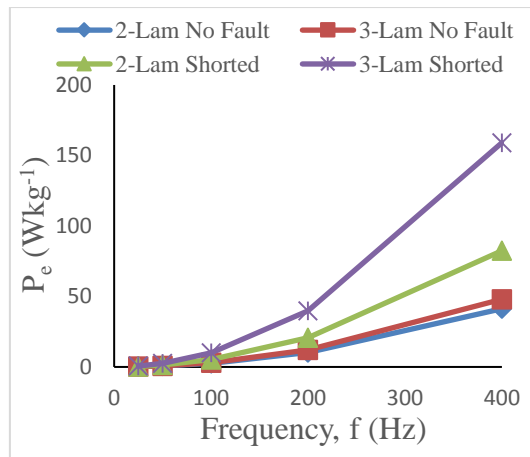
Fig 6-42. Derived eddy current loss for two and three laminations in the transverse direction with no fault and fault.
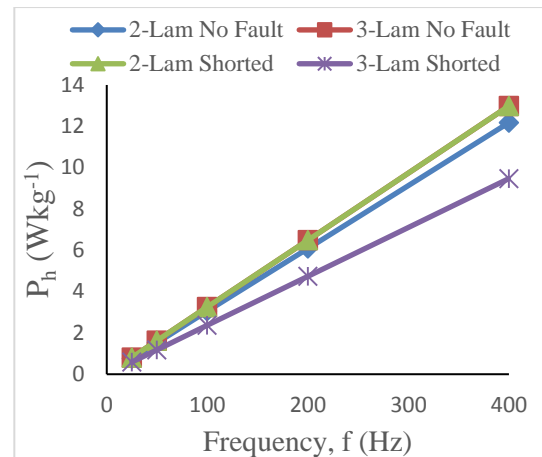
Fig 6-43 Derived hysteresis loss for two and three laminations in the transverse direction with no fault and fault.
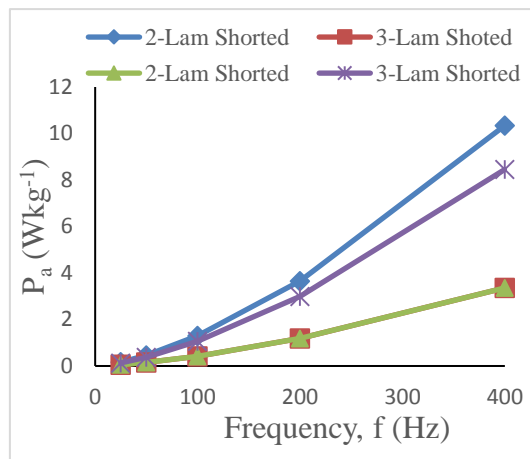
Fig 6-44. Derived anomalous loss for two and three laminations in the transverse direction with no fault and fault.

6.11. Edge burr length

Fig 6-45 shows the schematic of the artificial burrs applied to stacks of two and three laminations. Burr length from one side was set as 100 mm and kept constant throughout the measurement, while on the other side, burr lengths from 2 mm up to 30 mm were applied. The position of the burrs on the other side of the lamination was set on the mid-point.
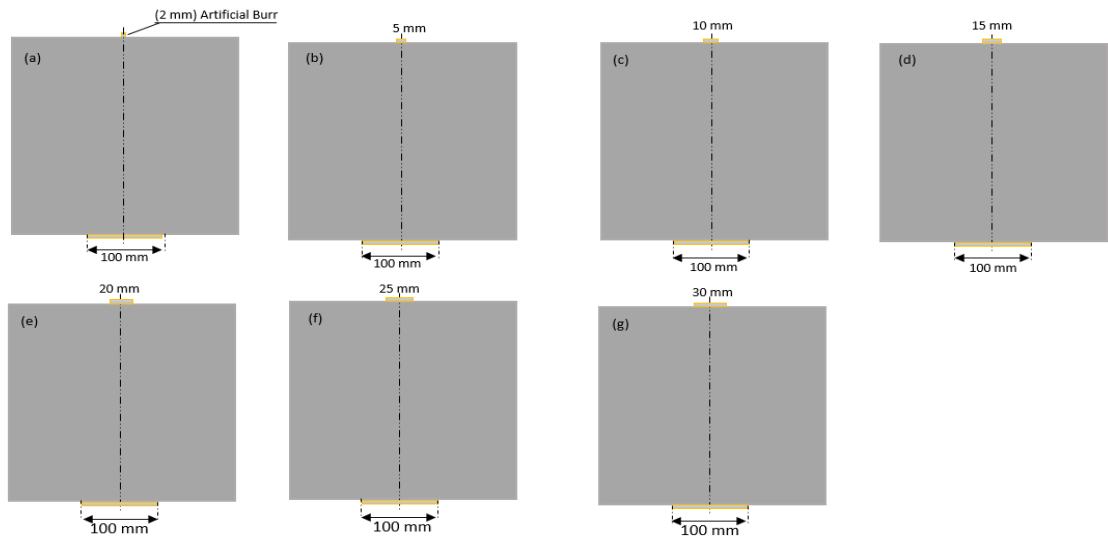
Fig 6-45 Schematic of placement of burrs of different length on stacks of two and three laminations
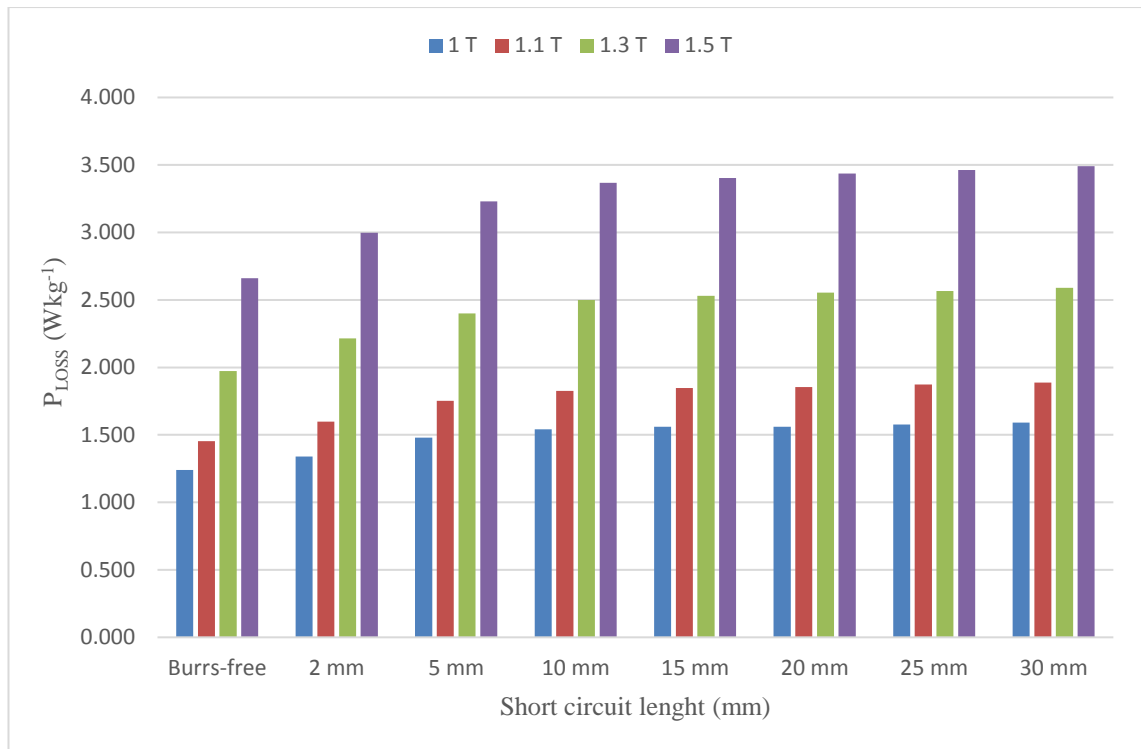
Fig 6-46 The effect of edge burr length on the total specific power loss for two laminations in the rolling direction.
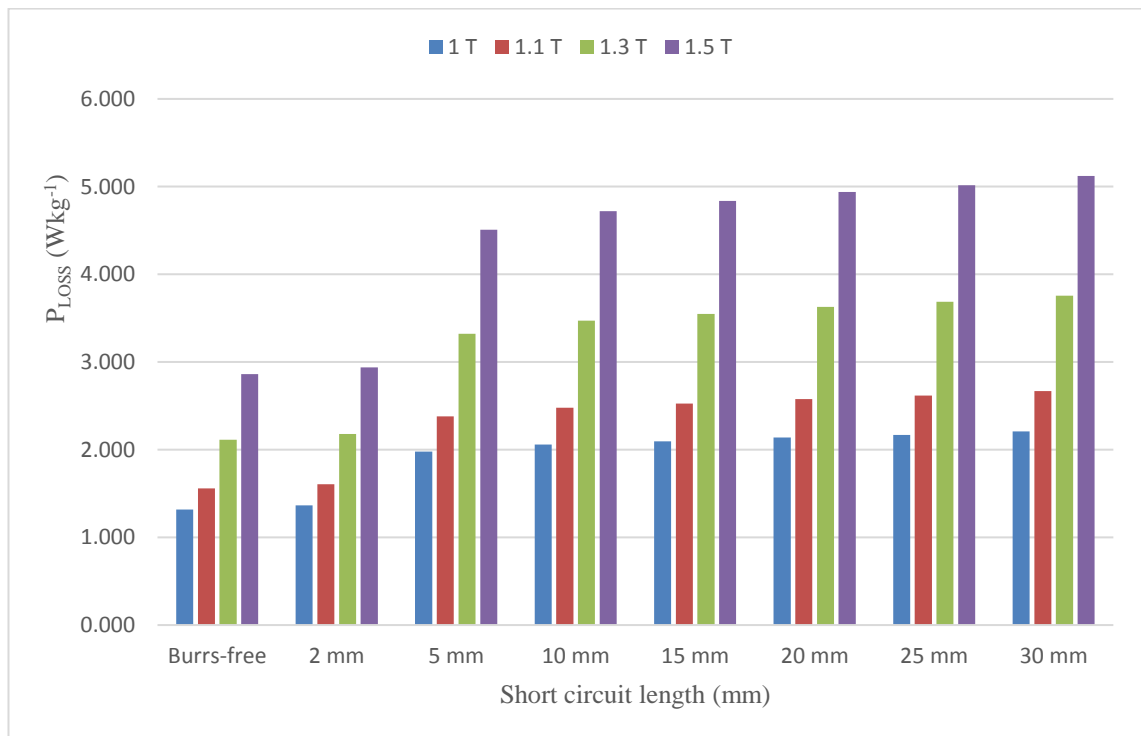
Fig 6-47 The effect of edge burr length on the total specific power loss for three laminations in the rolling direction.

6.12. Discussion of the results

The results of the power loss measurement for the material under investigation have shown the impact of short circuiting on the edges of the laminations. When a short circuit was present, an increase in power loss was observed due to the increased eddy current faults. It was also shown that the losses increased with an increasing number of shorted laminations, which raised the induced eddy current as a result of a larger fault loop for the number of shorted laminations. This study has specifically studied the impact of burrs and their influence on core lamination performance in the rolling and transverse directions. Single shorts were applied to the specimens at different set points. It has been observed that the impact of burr contact differs from one case to another, in contrast to the no-fault case. There was a 71% increase in power loss when shorts were applied at the mid-point, and a gradual decrease in power loss was observed by increasing the axial off-set between the contact points, e.g. 68.28% at 25 mm axial off-set, 64.48% at 50 mm axial off-set and 31.07% at 150 mm axial off-set. In order to investigate the impact of the position of the short circuit, an Agilent 34420A Micro Ohm Meter was used to measure the conductance between contact points for each fault position. The results showed larger conductance when a fault was applied at mid-point compared to the other three cases of axial off-sets. Hence, the conductance was found to be decreased with an increasing axial off-set, and it was found to be the lowest when the fault was applied at 150 mm axial off-set. The measured conductance between the contacts points supported the reason behind the variation of power loss based on burr position. The short circuit test was then extended to include the effect of short circuit length on total power loss. It was found that the loss increased gradually from 11.34% with a short circuit length of 2 mm at 1.5 T, 50 Hz magnetising frequency, to 43.18% at 30 mm length under the same condition for two laminations on the rolling direction. It was also found that the loss increased 12% to 78.8% for three laminations on the rolling direction under the same test procedure. Fig 6-46 and Fig 6-47 have full details regarding loss increase based on short circuit length. This work has theoretically studied the power loss separation using the extrapolation method for power loss separation. The purpose of this investigation was to investigate which component had a significant role in increasing the power loss while the edge burrs are present. Based on the results of this investigation, the eddy current power loss is found to be the dominant factor, due to the impact of the short circuit, while the hysteresis and

anomalous loss components did not show any large impact, which was expected for the material under investigation.

Summary

This chapter reviewed the concept of edge burrs, starting from the manufacturing process, and then went through the impact of this phenomenon on total power loss. Hence, different edge burr simulations were used in this study. All studies were conducted in the rolling and transverse directions for the material under investigation. The three power loss components were calculated in this study in order to see the variation on power loss components under the fault. This chapter also investigated the severity of edge burrs based on their locations, which was largely attributed to the conductance between the contact points. Finally, different lengths of edge burrs were used to see their impacts on total power loss.

References:-

[6-1] Sang Bin Lee; Kliman, G.B.; Shah, M.R.; Mall, W.T.; Nair, N.K.; Lusted, R.M., "An advanced technique for detecting inter-laminar stator core faults in large electric machines," Industry Applications, IEEE Transactions on , vol.41, no.5, pp.1185,1193, Sept.-Oct. 2005

[6-2] A. Kedous-Lebouc, B. Cornut, J. Perrier, P. Manfe and T. Chevalier, "Punching influence on magnetic properties of the stator teeth of an induction motor," Journal of Magnetism and Magnetic Materials, Vol. 254-255, pp. 124-126, 2003.

[6-3] R. M. Tallam, S. B. Lee, G. S. Stone, G. B. Kliman, J. Yoo, T. G. Habetler, and R. G. Harley, "A survey of methods for detection of stator related faults in induction machine," IEEE Trans. Ind. Appl., vol. 43, no. 4, pp. 920–928, Jul./Aug. 2007.

[6-4] C. Rickson, "Electrical machine core imperfection detection," Proc. Inst. Elect. Eng. B—Elect. Power Appl., vol. 33, no. 3, pp. 190–195, May 1986.

[6-5] Handgruber, P.; Stermecki, A.; Biro, O.; Ofnery, G., "Evaluation of inter-laminar eddy currents in induction machines," in Industrial Electronics Society, IECON 2013 – 39th Annual Conference of the IEEE , vol., no., pp.2792-2797, 10-13 Nov. 2013"

[6-6] P. Beckley, Electrical Steels for Rotating Machines. The Institution of Engineering and Technology, 2002.

[6-7] M B Aimoniotis and A J Moses, "Evaluation of Induced Eddy Currents in Transformer Sheets Due to Edge-Burrs, Employing Computer Aided Design Programs," in Athens Power Tech '93 Proc., 1993, vol. 2, pp. 847–849

[6-8] Pacificorp Hunter I Outage Filing. Public Service Commission of Utah. [Online] Available: http://www.commerce.state.ut.us/ccs/HunterIFiling.htm,Cunningham Testimony.pdf, Cunningham Exhibits.pdf

[6-9] Lamprecht, E.; Graf, R., "Fundamental investigations of eddy current losses in laminated stator cores created through the impact of manufacturing processes," in Electric Drives Production Conference (EDPC), 2011 1st International , vol., no., pp.29-35, 28-29 Sept. 2011

[6-10] A. Moses, "Transformer Fault Analysis Report," Wolfson Centre for Magnetics Technology.

[6-11] D. R. Bertenshaw, J. F. Lau, and D. J. Conley, "Evaluation of EL CID indications not associated with stator core interlaminar insulation faults," in Electrical Insulation Conference (EIC), 2011, 2011, pp.254-260.

[6-12]Mazurek, R.; Hamzehbahmani, H.; Moses, A.J.; Anderson, P.I.; Anayi, F.J.; Belgrand, T., "Effect of Artificial Burrs on Local Power Loss in a Three Phase Transformer Core," in Magnetics, IEEE Transactions on , vol.48, no.4, pp.1653-1656, April 2012

[6-13] M. C. Marion-Pera, A. Kedous-Lebouc, T. Waeckerle, and B. Comut, "Characterization of Si Fe Sheet Insulation," IEEE Trans. Magn., vol. 31, no. 4, pp. 2408–2415, 1995.

[6-14] S. L. Ko and A. D. Dornfeld, "A study on burr formation mechanism," Transaction of the ASME Journal of Engineering Material and Technology, vol. 113, no 1, pp. 75-87, 1991.

[6-15] K Lee, J Hong, K Lee, S B Lee and E J Wiedenbrug, "*A Stator Core Quality Assessment Technique for Inverter-fed Induction Machines*", IEEE Industry Applications Society Annual Meeting, Oct 2008, pp 1-8

[6-12] P. Baudouin, M. Wulf, L. Kestens and Y. Houbaert, "The effect of the guillotine clearance on the magnetic properties of electrical steels," Journal of Magnetism and Magnetic Materials, vol. 256, pp. 32-40, 2003.

[6-13] http://www.custompartnet.com/wu/sheet-metal-shearing

[6-14] T.L Mthombeni and P. Pillay, "Physical basis for the variation of lamination core loss coefficients as a function of frequency and flux density," in Proc. IECON, Paris, France, Nov. 6–10, 2006, pp. 1381–1387.

[6-15] G. Bertotti, "General properties of power losses in soft ferromagnetic materials," IEEE Trans. Magn., vol. 24, no. 1, pp. 621–630, Jan. 1988.

[6-16] J M Bourgeois and F Lalonde, "*Apparatus and Method for Evaluation a Condition of a Magnetic Circuit of an Electric Machine*," U.S. Patent 5 990 688, Nov. 23, 1999

[6-17] G B Kliman, S B Lee, M R Shah, R M Lusted, and N K Nair, "*A new method for synchronous Generator core quality evaluation*," IEEE Trans. Energy Convers., Vol. 19, NO. 3, Sep. 2004, pp. 576–582

[6-18] S B Lee, G B Kliman, M R Shah, W T Mall, N K Nair and R M Lusted "*An Advanced Technique for Detecting Inter-Laminar Stator Core Faults in Large Electric Machines*" IEEE Trans On Ind. App, Vol. 41, NO. 5, Sep/Oct 2005, pp. 1185–1193

[6-19] D R Bertenshaw, J F Lau and D J Conley, "*Evaluation of EL CID Indications not Associated with Stator Core Inter-laminar Insulation Faults*" IEEE Electrical Insulation Conference, June 2011, pp 254-260

[6-20] S B Lee, G Kliman, M Shah, D Kim, T Mall, K Nair and M Lusted, "*Experimental Study of Interlaminar Core Fault Detection Techniques based on Low Flux Core Excitation*" IEEE Trans On Energy Convers, Vol. 21, No. 1, March 2006, pp 85-94

[6-21] H Hamzehbahmani, P Anderson, J Hall, and D Fox, "*Eddy Current Loss Estimation of Edge Burr-Affected Magnetic Laminations Based on Equivalent Electrical Network—Part I: Fundamental Concepts and FEM Modelling*", IEEE TRANSACTIONS ON POWER DELIVERY, VOL.29, NO. 2, APRIL 2014, pp 642-650

[6-22] M B Aimoniotis and A J Moses, "*Evaluation of Induced Eddy Currents in Transformer Sheets Due to Edge-Burrs, Employing Computer Aided Design Programs*," in Athens Power Tech '93 Proc., 1993, vol. 2, pp. 847–849

[6-23] R Mazurek, P Marketos, A J Moses and J N Vincent "*Effect of Artificial Burrs on the Total Power Loss of a Three-Phase Transformer Core*", IEEE Trans. Magn., VOL. 46, NO. 2, 2010, pp.638 -641

[6-24] R Mazurek, H Hamzeh Bahmani, A J Moses, P I Anderson, F J Anayi and T Belgrand, "*Effect of Artificial Burrs on Local Power Loss in a Three-Phase Transformer Core*" IEEE Trans. Mag. VOL.48, NO. 4, April 2012, pp 1653-1656

[6-25] E Lamprecht, R Gräf, "*Fundamental Investigations of Eddy Current Losses in Laminated Stator Cores Created Through the Impact of Manufacturing Processes*" 1st International conference on Electric Drives Production (EDPC), Sept. 2011, pp. 29-35

[6-26] http://www.custompartnet.com/wu/sheet-metal-shearing

[6-27] P. Beckley, Electrical steels for rotating machines: Institution of Electrical Engineers, 2002.

[6-28] T. B. S. Institution, "Magnetic materials – Methods of determination of the geometrical characteristics of electrical steel sheet and strip," vol. BS EN 10251:1997, Ed: The British Standards Institution, 1997.

[6-29] T. B. S. Institution, "Grain-oriented electrical steel sheet and strip delivered in the fully processed state," in Technical requirements vol. EN 10107:2005 €, Ed, 2005.

[6-30] T. Belgrand, "client requirements regarding burr height in electrical steel," ed. Email, 2012.

[6-31] D. Snell and A. Coombs, "Novel coating technology for non-oriented electrical steels," Journal of Magnetism and Magnetic Materials, vol. 215– 216, pp. 133-135, 2000.

[6-32] M. Lindenmo, A. Coombs, and D. Snell, "Advantages, properties and types of coatings on non-oriented electrical steels," Journal of Magnetism and Magnetic Materials, vol. 215-216, pp. 79-82, 2000.

[6-33] Popescu, M.; Miller, T.; Ionel, D.M.; Dellinger, S.J.; Heidemann, R., "On the Physical Basis of Power Losses in Laminated Steel and Minimum-Effort Modelling in an Industrial Design Environment, "Industry Applications Conference, 2007. 42nd IAS Annual Meeting. Conference Record of the 2007 IEEE, vol., no., pp.60, 66, 23-27 Sept. 2007

7.1. Toroid cores

Toroid cores used for medium- and high-frequency applications are normally made from soft ferromagnetic materials, such as Si Fe, Ni Fe, Co Fe, and other materials such as amorphous or nanocrystalline alloys [7-1]. In laminated toroid cores, the flux is driven in the rolling direction since no corners or air gaps exist like in other cores. Moreover, proper annealing would eliminate the stress, and good core winding would provide a high stacking factor. These factors contribute to reducing power loss and enhancing the permeability of the toroid, which in turn reduces the noise and provides lower cost and requires less ampere-turn to transmit the flux from one layer to another. Based on these features, toroids have a large number of applications [7-2]. Though the geometry of toroidal cores is simple, these cores are subjected to various parameter limitations which have an influence on their performance, such as permeability and power loss [7-3].
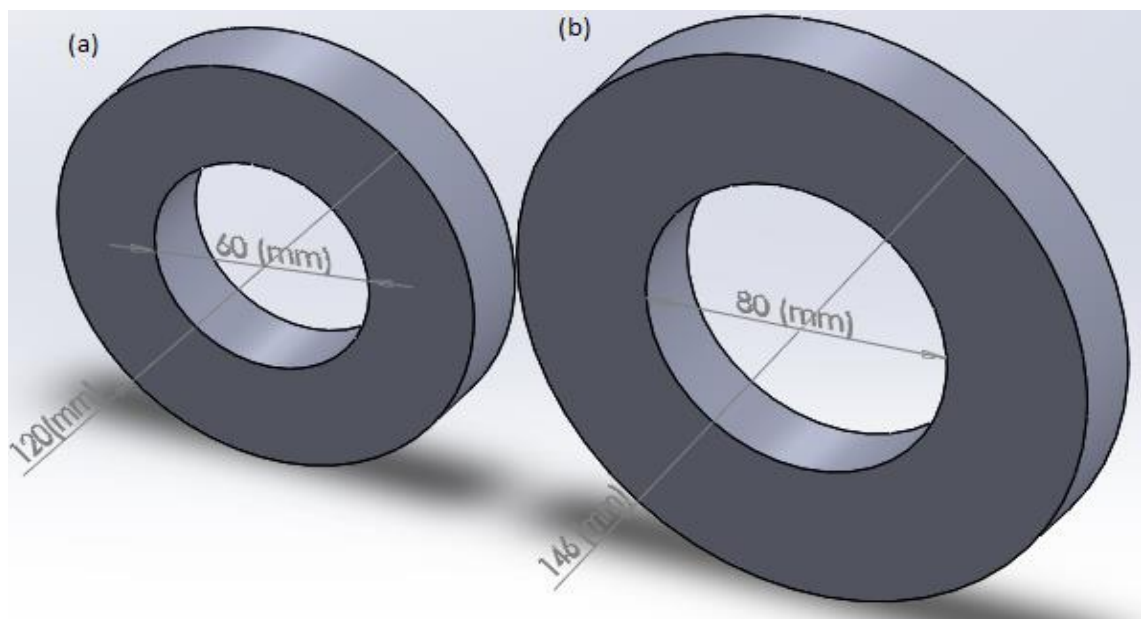
Fig 7-1 Dimensions of two toroids: toroid (a) (60 *120*20) mm and toroid (b) (80*146*20) mm

Factors such as strip slitting, core winding, effects of cutting edge and bonding are largely attributed to the manufacturing process. Moreover, the geometrical factors have a huge influence on the performance of the toroid; hence, the circumferential magnetic field varies in magnitude with radius and affects the localised flux density, which in turn influences power loss and the magnetising current [7-3].

This chapter presents power loss measurement results obtained using toroidal cores with different dimensions. This study is further extended to include artificial simulation of the impact of short circuits between laminations by means of edge burrs.
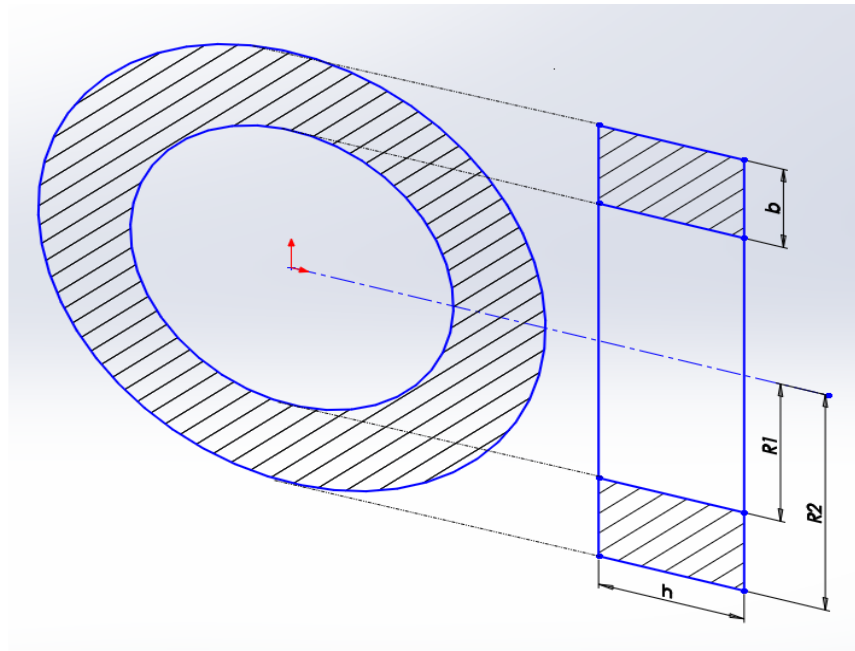
Fig 7-2 Cross-section for test specimen.

7.2. Test specimen

The two single-phase transformer toroid cores, indicated as core (a) and core (b), are shown in Fig 7-1 and were assembled from grain-oriented steel of 3% silicon content. The core material had a density of 7.65 g/cm^3, 0.3 mm thick with power losses of 0.732 W.kg^{-1} and 0.762 W.kg^{-1}, respectively, at 1.5 T 50 Hz. The aspect ratio and the winding ratio have been defined as AR=h/b and WR=R_1/h, where h is the strip width and b is the build-up of the toroid core (see Fig 7-2).

The cores had masses of 1.2575 kg and 1.7455 kg, respectively. Both cores were manually wound with 50 primary turns and 4 secondary turns. Fig 7-1 illustrates the two cores' dimensions with a height of 20 mm. In order to provide a flux, which was confined to the core, the current-carrying coil was uniformly wound across the core to result in higher relative permeability [7-3].

The power loss measurement on both cores was conducted using the system setup as described in [7-4]. This system, illustrated in Fig 7-3, consisted of a PC equipped with an NI BNC-2110(DAQ) data acquisition/generation card and LabVIEW virtual instrumentation software installed on it. Sinusoidal waveform voltage was generated by the PC and was fed into a power amplifier whose output current was used to magnetise

the specimen. An insulation transformer IT removed the DC component of the amplitude voltage. The alternating current injected into the primary winding induced a secondary voltage that provided information about the generated loss in the samples. By using this system, the cores were magnetised at peak flux densities of 1.5 T and different ranges of magnetising frequencies of 50 Hz, 100 Hz, 200 Hz, 400 Hz and 500 Hz. A flux density of 1.5 T was the most practical magnetisation level, as at this value relative permeability remains almost constant by reaching its highest value [7-4],[7-5].
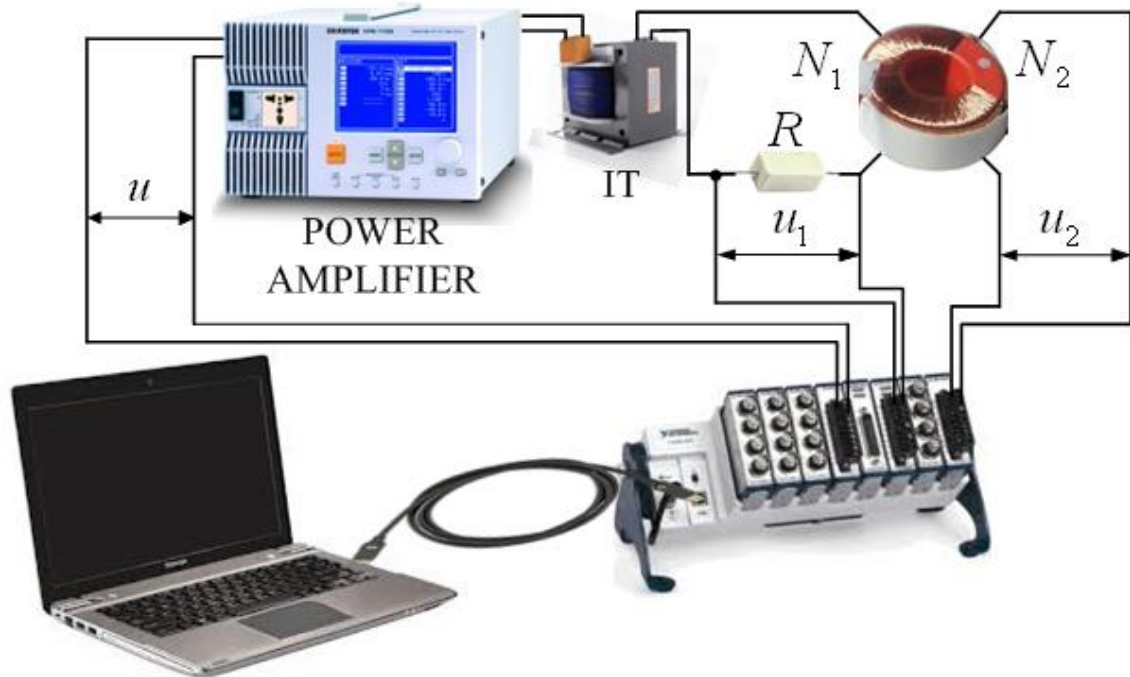
Fig 7-3 Block diagram for the measurement system.

7.3. Techniques used to apply edge burrs

Previously, there have been different techniques, which used to simulate edge burrs in machine cores, including soldering, conductive paint, drilling holes, metal wool and copper foil. However, these techniques did not provide promising results. For example, using soldering is not controllable to cover the planned number of laminations and has a significant impact on the property of the material and its coating; therefore, it was not possible to differentiate between losses caused by shorts and those by the change in material properties. [7-6] et al. used a conductive paint in order to simulate edge burrs on laminations, but this method did not maintain contact under magnetisation conditions and so was discarded as unreliable. Also, the paint was found to break when the core was vibrated. Another method used was drilling 0.3 mm holes close to the edges of the lamination and inserting a steel pin to short out the number of laminations being tested.

Though this method provided complete control of the burr positions, the pin suffered wear with each insertion, and this method did not provide repeatable results for a range of measurements.

The effect of the short circuit between the laminations in this chapter is introduced by clamping the laminations. This was done by a clamping mechanism, as illustrated in Fig 7-4. This clamping device offered a mechanical lock between the stacks and provided electrical connection. The electrical connection was made by conductive copper foil of approximately 8 micron thickness which was glued onto the wooden blocks located on both sides of the clamping device. Four bolts were used to gradually tighten the blocks over the area of the core being tested. In order to apply an equal pressure, a 4 Nm torque was applied on each bolt ensuring repeatable results. It should be noted that the impact of using the clamping device with 4 Nm on burr-free cores did not have an effect on the total power loss.

The dimensions of copper foil were proportional to the number of laminations under investigation, which offered an easy path for eddy current to flow through the connected laminations between the interlocked edges. The copper foil within the clamping device simulated the application of burrs of various sizes to the core. Shorts were applied on both sides of the core from 10 laminations up to 40 laminations. Generally, burrs occur in a random way, not at set points as in this experimental work. However, this method provided full control of burr positions.
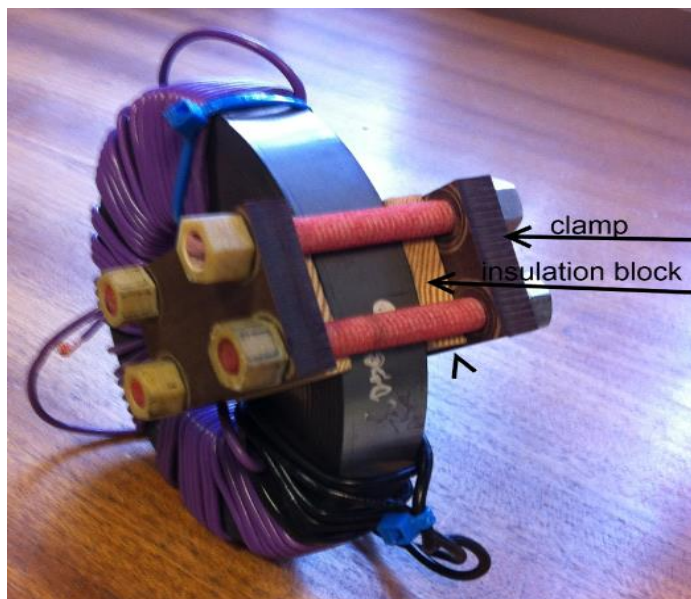
Fig 7-4 Test specimen with clamping device.

7.4. Results and discussion

It is evident from the obtained results in Fig 7-5 and Fig 7-7 that the core with the larger diameter had a lower power loss compared with the smaller diameter core. These results agree well with [7-2], the authors of which concluded that improved performance for toroidal cores may be achieved by increasing the diameters. Variation in the power loss in both cores is mainly related to individual effects such as microstructural change in material, variation in magnetic field strength and magnetic induction inside toroidal cores due to the difference between inner and outer diameter [7-5]. In general, toroidal cores should be designed using wide strips having larger internal diameter and low build-up. This in turn will minimise the impact of the normal flux, which contributes to the increase in power loss. For this reason, toroidal cores with small internal diameters should be avoided. It is also recommended that the ratio of the outer to inner diameters should not be greater than 1.4, and a value less than 1.25 is preferred [7-7]. The results obtained for both cores in Fig 7-5 and Fig 7-7 also show the impact of short circuits on total power loss generally. Fig 7-6 and Fig 7-8 show the percentage of change between no fault and faulty conditions for both cores, respectively. When the core laminations were well insulated from each other, the eddy current paths were restricted to flow in each individual lamination. This was due to the insulation coating on both surfaces of the lamination which prevent electrical connection between the adjacent laminations. When burrs were present, the configurations of the affected laminations change and approximate to a solid core.
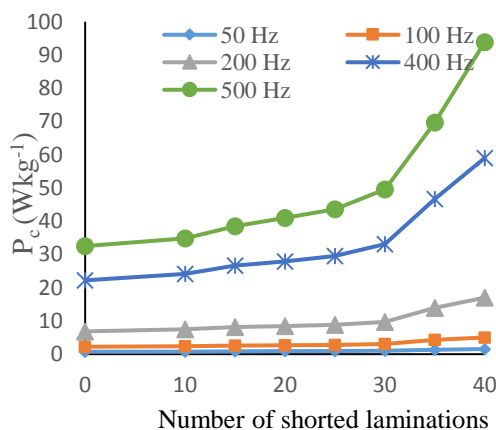
Fig 7-5 Specific power loss for the core with 60 mm internal diameter.
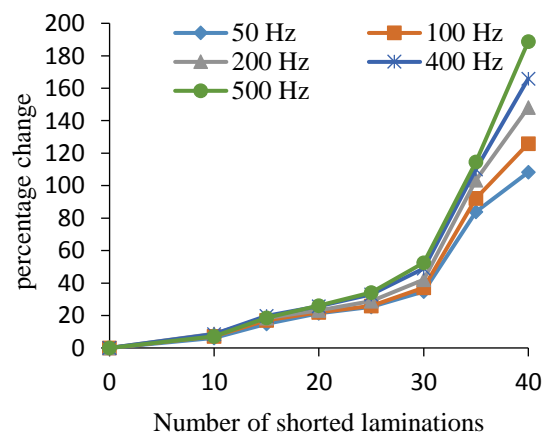
Fig 7-6 Relative percentage of change between no fault and fault conditions for core with 80 mm internal diameter.
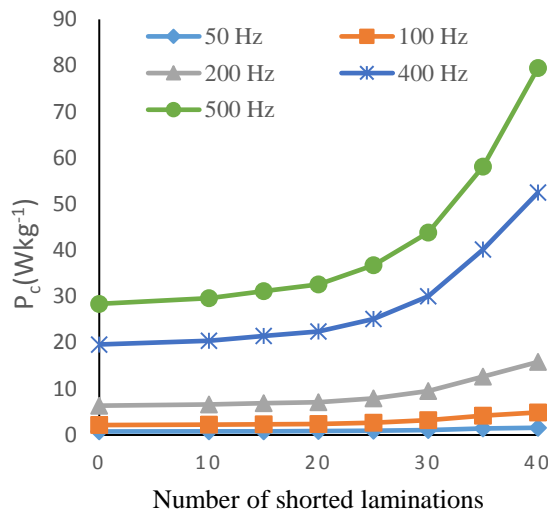
Fig 7-7 Specific power loss for the core (b) with 80 mm internal diameter.
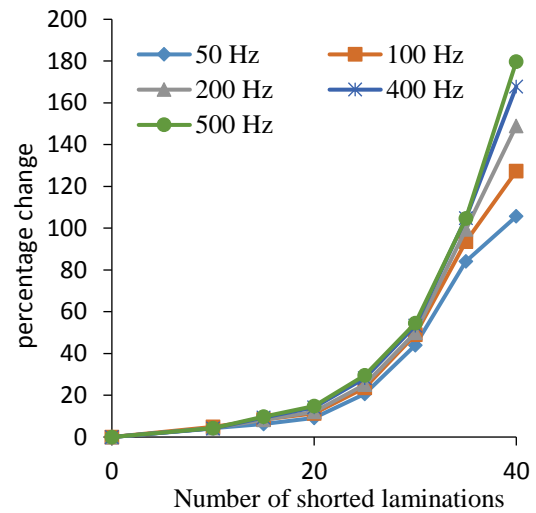
Fig 7-8 Relative percentage of change between no fault and fault conditions for core with 60 mm internal diameter.

An increase in power loss corresponding with increasing number of shorted laminations was observed. The percentage difference for both cores is mainly attributed to core geometries, i.e. the smaller core showed higher flux density concentration than the bigger core. This increase in power loss was due to the increase in surface magnetic flux density, which was confirmed by COMSOL software results and is shown in Fig 7-9, Fig 7-10, Fig7-11 and Fig 7-12. Computational results obtained by COMSOL show that there was an increase of 15% in the surface magnetic flux density at 50 Hz magnetisation when the core internal diameter had reduced from 80 mm to 60 mm. The increase in the surface magnetic flux density at 500 Hz magnetisation was 5% when the core internal diameter had reduced from 80 mm to 60 mm. The peak surface magnetic flux densities at 50 Hz were 0.1847 T and 0.1595 T for the 60mm and 80mm core internal diameters, respectively. The peak surface magnetic flux densities at 500 Hz were 0.5618 T and 0.534 T for the 60mm and 80mm core internal diameters, respectively. When burrs were present at both sides of the laminated toroid core, higher eddy currents were induced, and the value of these currents increased with the number of shorted laminations. Hence, the eddy current was proportional to the lamination thickness. A small number of shorted laminations may not be serious, but in the case of several shorts occurring in adjacent layers, the induced eddy currents can be large. Moreover, due to the frequency dependency of eddy current caused by the skin effect at higher frequencies, and as the magnetisation occurs by domain wall motion [7-8], this could provide more information

to justify loss increase due to increased domain wall activity, which tends to cause a strong shield against magnetisation inside the lamination.
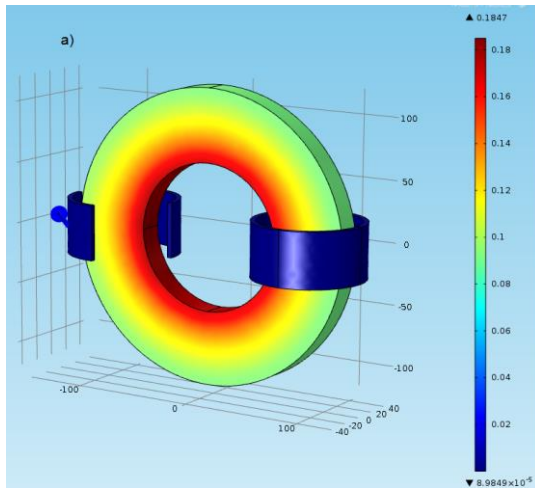
Fig 7- 9 Surface magnetic flux density at 50 Hz for the core of 60 mm internal diameter.
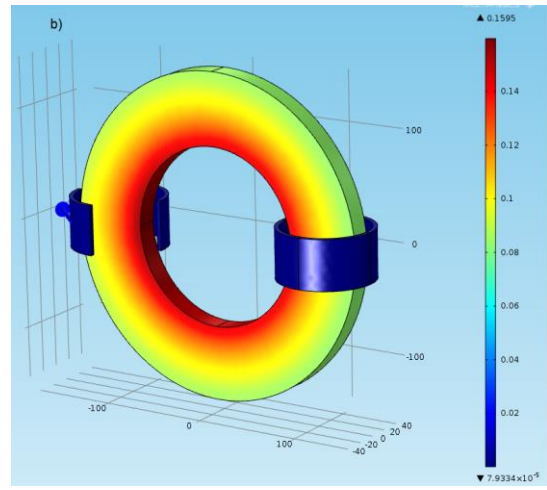
Fig 7-10 Surface magnetic flux density at 50 Hz for the core with 80 mm internal diameter.
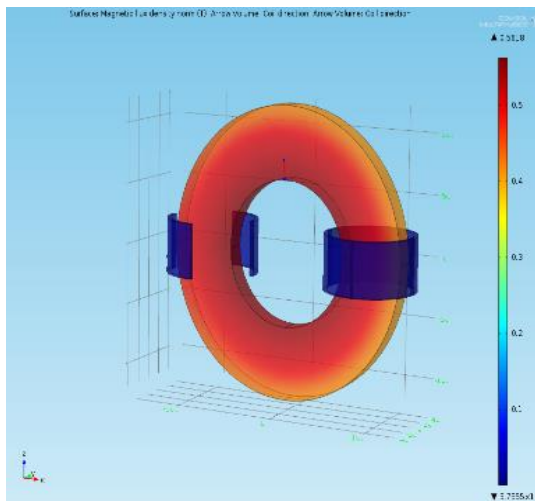
Fig 7-11 Surface magnetic flux density at 500 Hz for the core of 60 mm internal diameter.
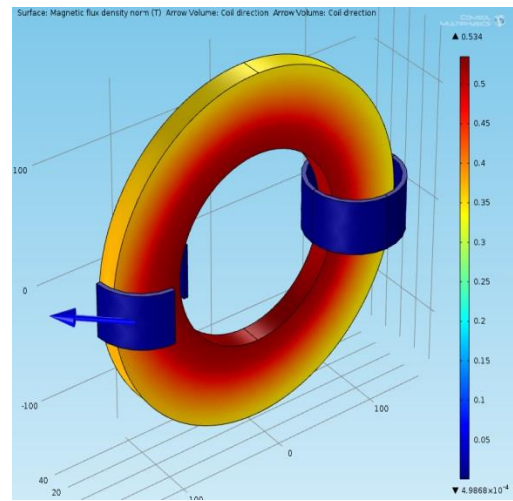
Fig 7-12 Surface magnetic flux density at 500 Hz for the core of 80 mm internal diameter.

Summary

This chapter demonstrates a study performed experimentally and analytically to show the impact of toroid core geometry on total power loss. Power loss measurements for two twin toroid cores with slight differences in geometry were taken to observe the impact of geometry on total power loss. FEM modelling was used as well to visualise the flux distribution and the surface flux density. This study also included the impact of edge burrs on toroid cores.

References:-

[7-1] A.Kamada,; T.Mochizuki,; K.Suzuki,; M.Torii, , "Optimum Ferrite core characteristics for a 500 kHz switching mode converter transformer," Magnetics, IEEE Transactions on, vol.21, no.5, pp.1726, 1728, Sep 1985

[7-2] W. Grimmond,; , A. J.Moses; P.C.Y. Ling, , "Geometrical factors affecting magnetic properties of wound toroidal cores," Magnetics, IEEE Transactions on, vol.25, no.3, pp.2686, 2693, May1989

[7-3] Derebasi, Nairn, and Eker Kucuk. "Prediction of MAGNETIC PROPERTIES OF STRIP WOUND TOROIDAL CORES UP TO 2 KHZ USING ARTIFICIAL NEURAL network." Mathematical & Computational Applications 8.2 (2003): 217-223.

[7-4] Methods of measurement of the magnetic properties of magnetically soft metallic and powder materials at frequencies in the range 20 Hz to 200 kHz by the use of ring specimens," IEC, 60404-6:2003

[7-5] V. Basso, G. Bertotti, O. Bottauscio, F. Fiorillo "Power losses in magnetic laminations with hysteresis: Finite element modelling and experimental validation." Journal of validation." Journal of applied physics 81.8 (1997): 5606-5608.

[7-6] A. J. Moses and M. Aimoniotis, "Effects of artificial edge burrs on the properties of a model transformer core," *Physica Scripta,* vol. 39, pp. 391-393, 1989.

[7-7] IEC 60404-6: Magnetic Materials – Part 6: Methods of Measurement of the Magnetic Properties of Magnetically Soft Metallic and Powder Materials at Frequencies in the Range 20 Hz to 200 kHz by the use of Ring Specimens, Geneva, Switzerland, June 2003.

[7-8]G. Bertotti, "General properties of power losses in soft ferromagnetic materials," IEEE Trans. Magn., vol. 24, no. 1, pp. 621–630, Jan. 1988.

8.1. Introduction

In order to gain insight into the properties of magnetic materials, it is essential to be able to study the magnetic domain structure of the material under investigation. The understanding of the structure and dynamics of magnetic domains is becoming increasingly important in various applications of magnetic material, such as those used to build the cores of electrical machines.

In this chapter, magnetic domain optical microscopy is briefly explained, showing the best way for achieving the best visibility of the magnetic domain structure in non-oriented electrical steel specimens.

Magnetic materials are normally composed of small-volume regions called magnetic domains. In the domain structure, spontaneous magnetisation takes different directions in different domains [7-1]. Inside each domain, the orientation of the magnetisation is uniform, but this differs from one domain to another. Magnetic domains normally have microscopic size.
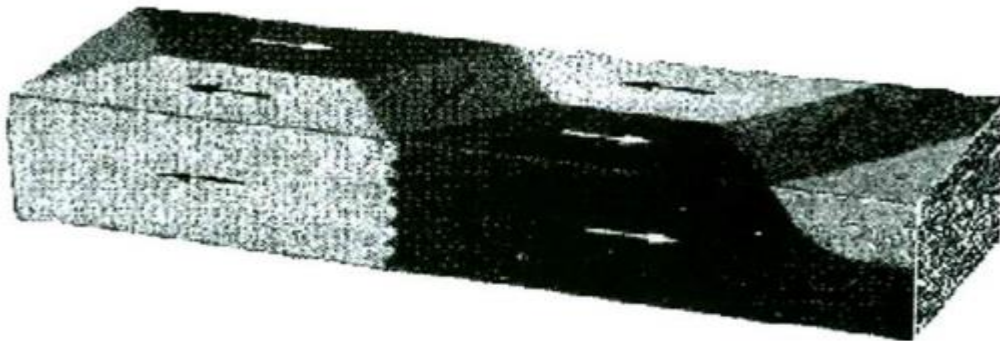
Fig 8-1 Domain observed from two sides of an iron whisker, combined in a computer to simulate a perspective view. Reproduced from [8-2].

The interface layer shown in Fig 8-1 separating one domain from the other is known as a domain wall. For the material under investigation, the domain wall is considered as a surface due to the size of the magnetic domain. In ideal material, the magnetic domains correspond very well to the applied field, and the domain walls move smoothly as the orientation of the domains in the direction of the field.

Domain walls are classified based on the magnetisation direction of magnetisation in the neighbouring domains separated by the wall. One has a 180-degrees domain wall when the wall separates domains of opposite magnetisation. In some other cases, they are called 90-degrees domain walls, even if the magnetisation does not necessarily rotate by 90

degrees when passing from one domain to the other. Those are briefly illustrated in Fig 8-2 (a, b, c).
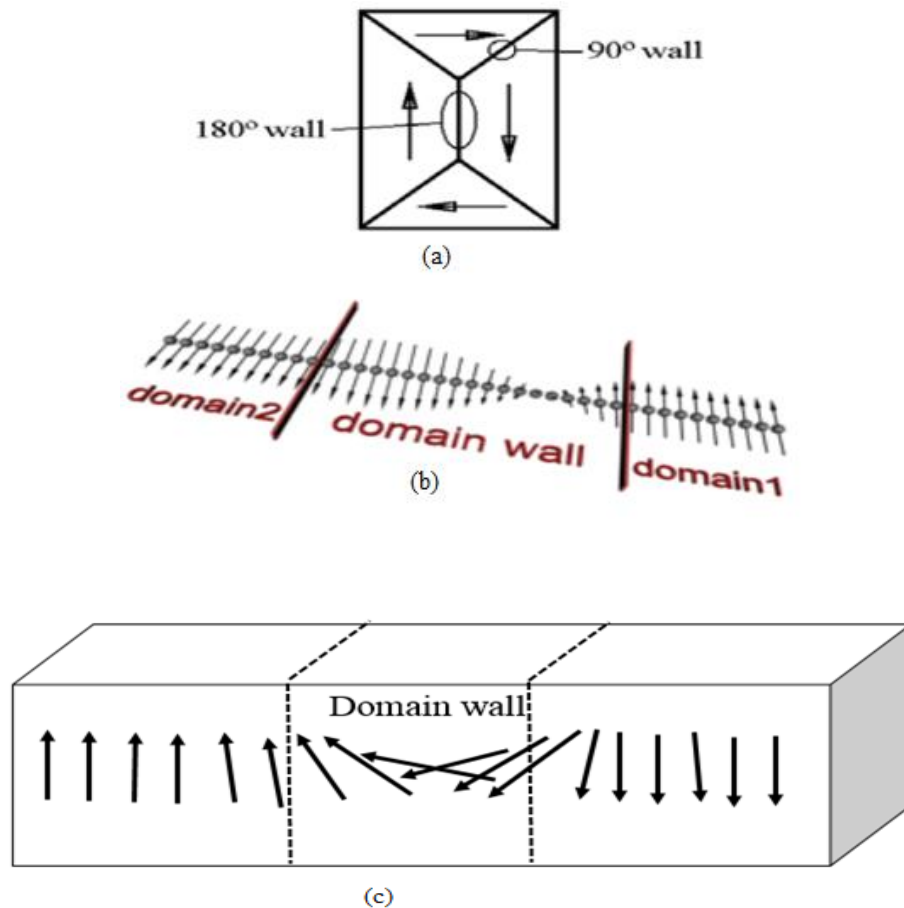
Fig 8-2 (a) Simple domain structure, (b) Structure of domain wall (c) 90-degree domain orientation across a domain wall. Reproduced from [8-3].

The most important character of the domain wall is its mobility, which is a measure of how likely the material is to be able to be magnetised. The displacement of domain wall is due to the external applied magnetic field. Therefore, the domain rotates parallel to the direction of the applied field, or the boundary between two domains moves, causing the entire magnetisation change to be localised at the domain boundary.

Different techniques are now used for observing the magnetic domains which provide more detailed information about the material properties and detailed information on the internal structure of domain walls. Each of these techniques has unique advantages and limitations, this chapter will only focus on using two available different techniques to observe magnetic domain structure.

8.2. Atomic force microscopy

A magnetic force microscopy, (MFM), has a high-resolution scanning probe which is utilised for viewing micro- and nano-sized structures for their materials. This technique was first used in 1986 based on the scanning tunnelling microscope concept [8-4]. Binning et al. developed the atomic force microscope, (AFM). The microscope in this technology provides surface topology of the material to be imaged through a non-conductive method [8-5]. This tool has been successfully used for the characterisation of the surface topography of a wide range of materials. The AFM has shown great advantages compared to scanning electron microscopy (SEM) by providing images in different environments with high resolution without any special sample treatment. It has also shown the ability to evaluate quantitatively selected surface features. This scanning tool (AFM) has a force-detective tip (Sharp Tip) a couple of microns long and a force-sensitive cantilever which is used to detect near-surface atomic forces. The cantilever deflects as the tip moves across the scanning surface. A laser beam is used for sensing the deflection angle and photo detector together for plotting the topographic image.

8.3. Magnetic force microscopy

In 1988, Saenz [8-6] and Martin [8-7] developed the MFM microscope for domain image observation based on the success of the AFM. In this new method, an MFM tip is used to obtain the magnetic images. Whereby the tip is made from an AFM tip that is coated with a thin ferromagnetic material layer.

In fact, MFM is a near-surface raster scanning microscope, and so a moderate sample preparation is necessary. The sample needs to have smooth surface to avoid tip damaging the tip by crashing it into the sample. Additionally, a smooth surface improves the signal-to-noise ratio. This technique of domain imaging offers a typical scanning area of up to $100\ \mu m \times 100\ \mu m$.

During the scanning process, the MFM tip interacts with the leakage field above the surface of the magnetic material to produce an image showing the stray field profile over the scanned surface area. The highest spatial resolution provided by MFM technology is reported at less than 10 nm [8-8]. This provides detailed information on Micro- and Nano scale structures.

The images obtained by MFM contains information about the topography and the magnetic properties of the surface. If the magnetic tip is close to the specimen surface in the region where standard non-contact AFM operates, this will provide topographic image

of the specimen, as shown in Fig 8-3 (a). By increasing the distance between the tip and the sample surface, the magnetic effect will become apparent until the magnetic images are separated from the topographic effect (Fig 8-3 b).

In fact, the most important factor affecting the image resolution is the lift scan height, since smaller lift scan heights provide better resolution. Conversely, magnetic features smaller than the lift scan height may not be resolved. The closer the tip to the sample surface, the more improved are the signal-to-noise ratios. This work has resolutions of 50 nm and 100 nm.
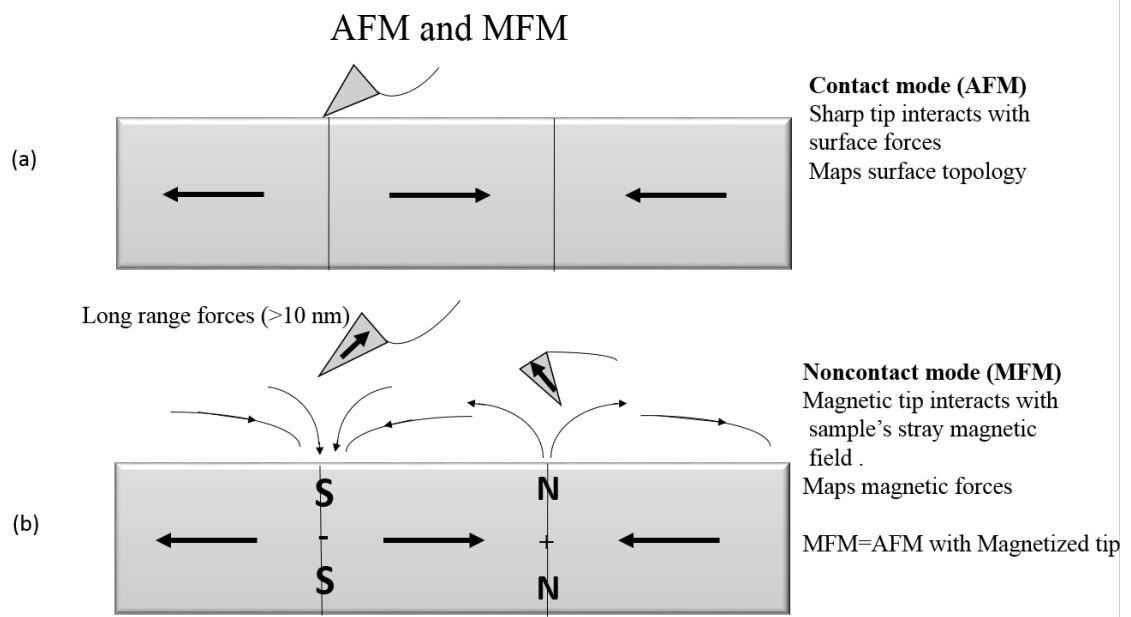
Fig 8-3 (a) Atomic force microscopy (AFM) and (b) Magnetic force microscopy (MFM).

The MFM cantilever and the tip are usually made of Si or $Si_3 N_4$. The Tip is coated with magnetic thin film, such as CoCr, and has an end radii of ~20-40 nm (Fig 8-4 and Fig 8-5). The resolution of MFM is limited by the size of the magnetic volume at the tip apex end radii.
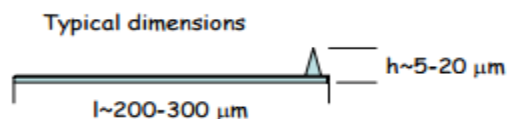
Fig 8-4 Magnetic tip, typical dimensions.
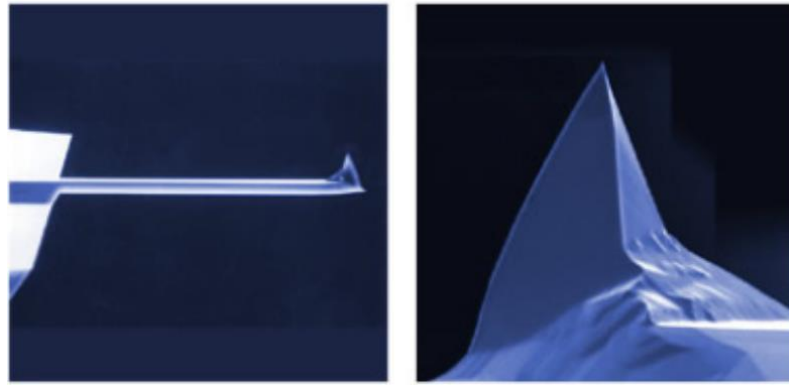
Fig 8-5 Scanning electron image of a typical AFM probes. MFM probes are coated with a magnetic thin film to allow them to deflect in a magnetic field.

In this experimental work, the effect of polishing the surfaces is investigated in order to determine the best conditions for MFM sample imaging. Two experiments have been conducted where first a smooth-coated material was scanned followed by measurement of the same material through long procedures of coating removal and polishing

Fig 8-6 (a) and (b) show the output of an AFM scan for a non-oriented steel specimen. The surface topology is shown in Fig 8-6 (a) while Fig 8-6 (b) shows the magnetic force gradient (phase) image obtained. The scanned area was 50 μm*50 μm, and it was performed at a resolution of 4000 nm (lift scan height).
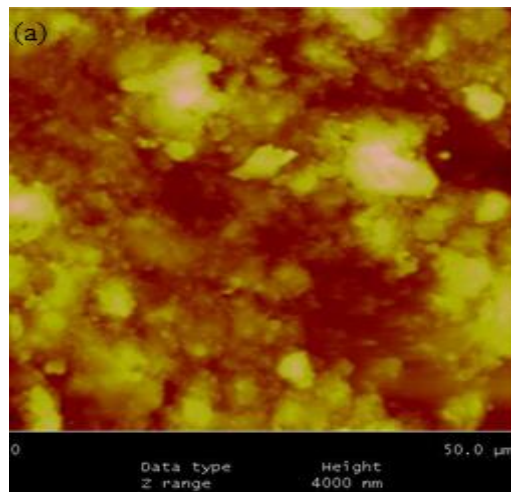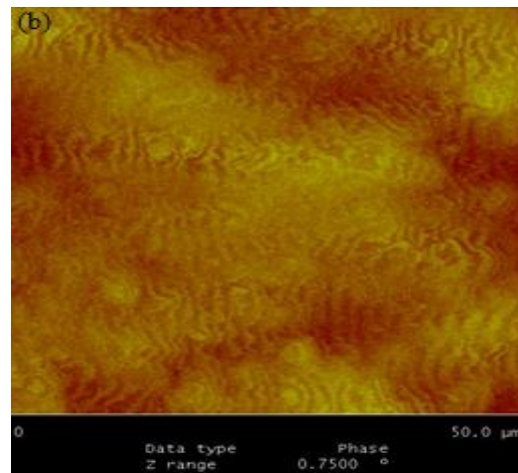
Fig: 8-6 The output of an MFM scan of non-oriented steel material.

Fig (a) Surface topology of the sample 2-D.
Fig (b) The (phase) magnetic field activities at the surface of the material 2-D.
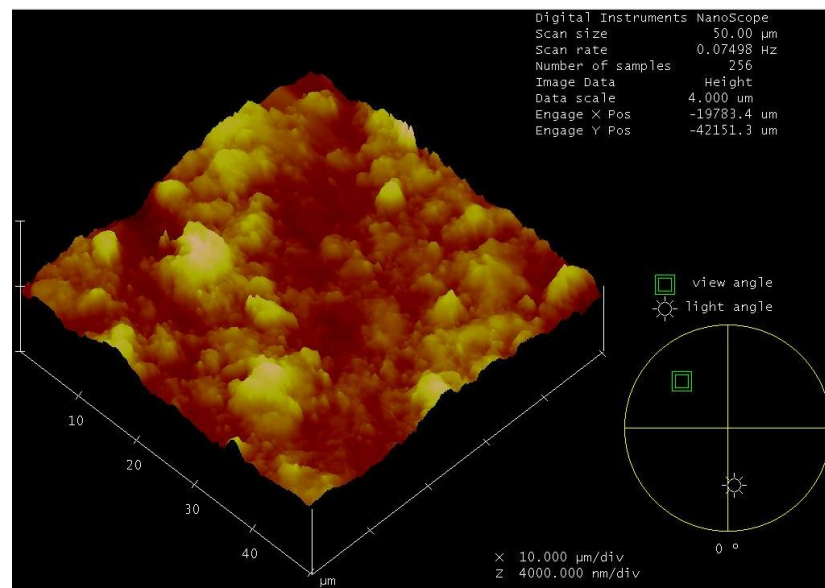
Fig 8-7 Topographic image of the magnetic surface activities. 3-D image.
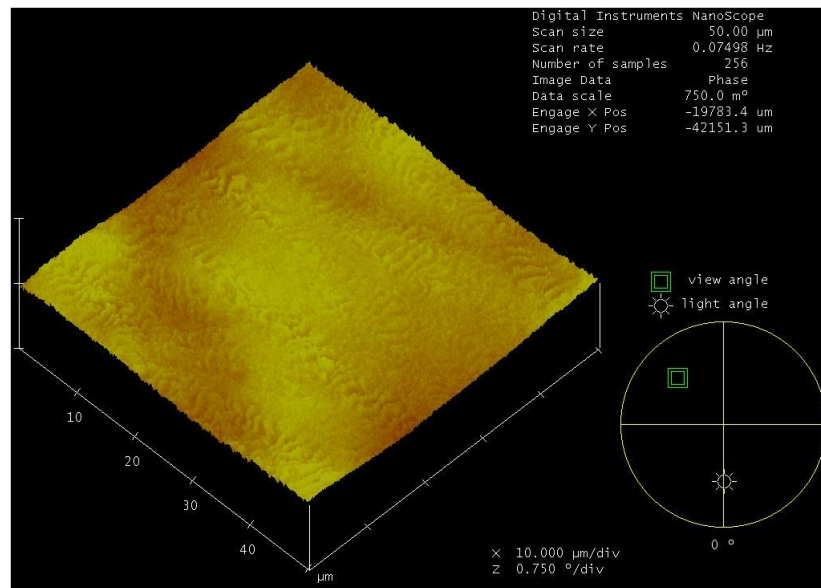
Fig 8-8 Magnetic phase image. 3-D.

8.4. Specimen selection and preparation

Sample preparation plays a major role in successful observation of the domain structures for some specific techniques used to investigate the microstructure of the materials.

The main purpose of sample preparation is to reveal the structure of a sample, whether it is metal, ferrite, ceramic or any other material.

The material under investigation for local magnetic properties is non-oriented electrical steel, which was provided by Cogent in Surahamar. Epstein-size samples of 305 mm * 30 mm were cut into small square sheets of 30 mm* 30 mm using a mechanical guillotine. This material had undergone different procedures before the test.

8.5. Preparation of the test specimen

The results obtained using AFM and MFM showed that there was no specific sample preparation on smooth surface was required, in the second part, the specimen had undergone long procedures for the preparation, this is required mainly for Kerr effect, hence the sample was prepared to a mirror finish surface, thus this test requires clean surface for the specimen. To achieve this, the sample had undergone further procedures including grinding and polishing, which was carried out by using the Struers magnetic disc (MD) machine.

The sharp edges at the sample corners were removed by silicon carbide paper prior to metallurgical preparation to protect the discs from scratches. The specimen was then attached onto a sample holder using high-strength, double-sided tape.

8.5.1. Coating removal

Before testing the material, it should have the coating insulation removed. This was done by soaking the specimen in an HCL bath of 38% concentration for approximately half an hour. During this procedure, constant inspection during the chemical reaction was necessary to avoid etching the test specimen. Once the coating was properly removed, the test specimen was soaked in an acetone bath of 99% concentration to wash away the remaining acid. Then the specimen was rinsed with Kemet cleaning fluid Co42 and then dried using a clean paper towel to prevent any further oxidation.

8.5.2. Sample mounting

The 30 mm *30 mm non-oriented steel specimen was mounted on a Tufnol block by means of double-sided adhesive tape. The purpose of the mounting was for appropriate handling of the material in the polishing machine and to preserve the microstructure of the specimen from mechanical and heating injuries [8-9], [8-10].

8.5.3. Grinding

As the first step of mechanical preparation for the sample, proper grinding will lead to removing the damage from the material's surface while introducing only a limited amount of new deformation. The grinding process was carried out by using the Struers Rotopol135 machine with automatic control of applied pressure, rotation speed, cooling and time procedure. Abrasive silicon carbide of 200, 600 and 1,200 grades were used until the sample surface became plane and smooth.

8.5.4. Polishing

Polishing was performed by using the same grinding machine but with an automatic multi-doser added. A diamond disk MD-Largo, cloth disk MD-Mol and MD-Nap were used with appropriate abrasives. The final polish was with a 0.25 μm diamond abrasive. Then the specimen had a mirror finish Fig 8-9.

Fig 8-9 Polished electrical steel sample.

8.5.6. Structure

Despite the long procedures for sample preparation, it was difficult to achieve perfect results. Therefore, for most examinations, a few scratches do not matter as long as the material surface is good enough. This is called an acceptable preparation result.

Some other issues follow the sample preparation, such as the induced stress on the specimen surface during mechanical preparation. These stresses affect the magnetic microstructure of the material, causing a distortion of the magnetic anisotropy. During this mechanical process, there were steps taken to avoid the stress. For example, no more than 50N force per (30*30) mm sample was used, and special care were taken with lubrication fluid and cooling of the sample. The residual strains were relieved during annealing in a vacuum furnace.

8.5.7. Annealing process

The non-oriented electrical steel sample was annealed for half an hour at 800˚C in a vacuum tube furnace. The whole procedure took at least eight hours to be finished. First, the sample was allowed to cool to room temperature while still under vacuum before removal from the furnace. The vacuum is very important to prevent any oxidation of the polished surface. The gradual heating and cooling procedure rate was adjusted to 1 ˚C/min to ensure a uniform temperature.

8.5.8. Chemical etching

The polishing process for the soft magnetic material may cause surface flow. In some cases, it causes a deterioration of the magnetic microstructure. Etching of metal surfaces after polishing is often performed during metallographic preparation.

Etching is the process whereby a very thin layer of the metal surface is dissolved or removed chemically. This is done by applying Nital solution (2 % HNO3) on the sample

surface for two minutes, and then the surface is cleaned by a soft cloth soaked in acetone (see Fig 8-10).
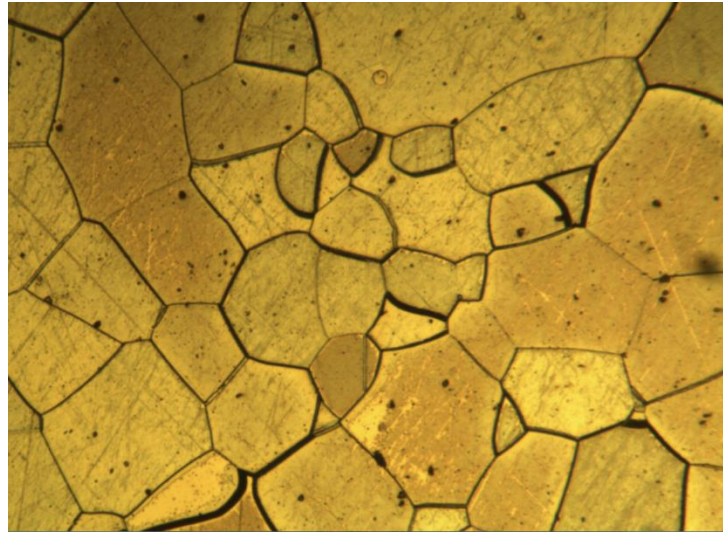
Fig 8-10 Etched electrical steel sample showing the grains.
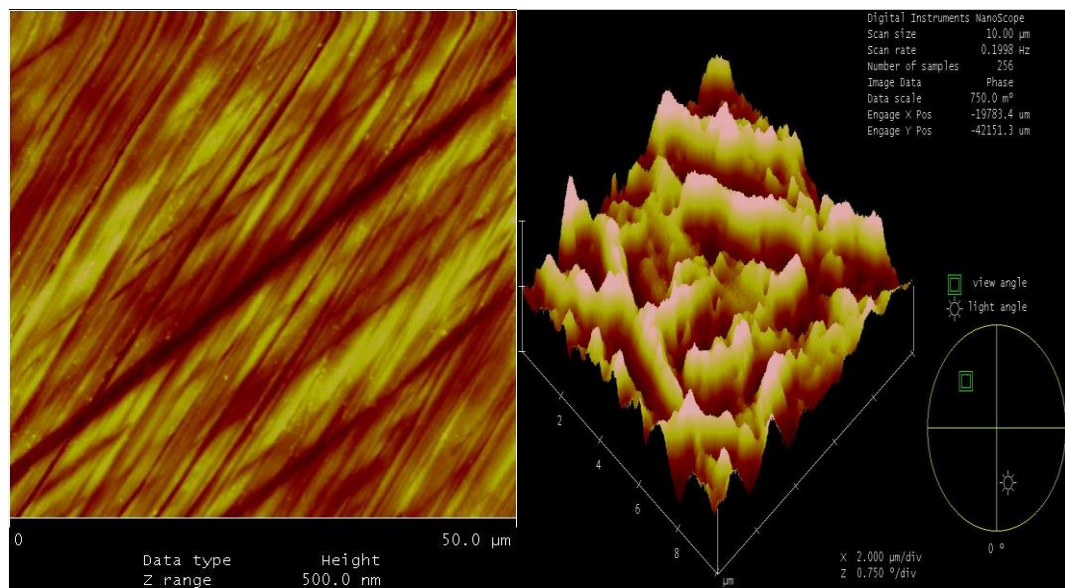
Fig 8-11 (a) Topographic image for polished sample (AFM) 2-D.

Fig 8-11 (b) Magnetic surface activities for polished sample in 3-D (AFM).
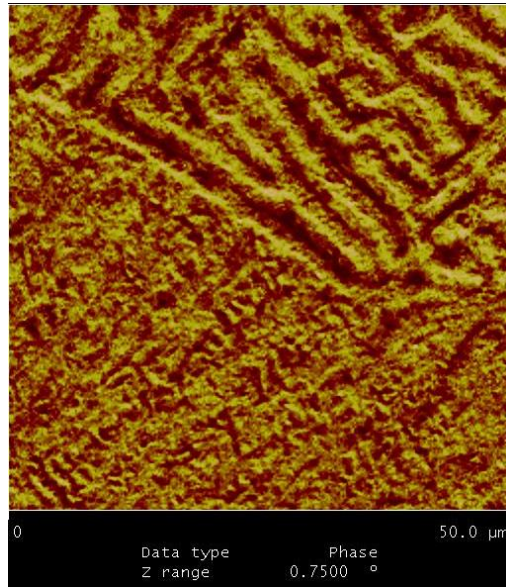
Fig 8-12 (a) The (phase) magnetic field activities at the surface of the material (MFM) 2-D.
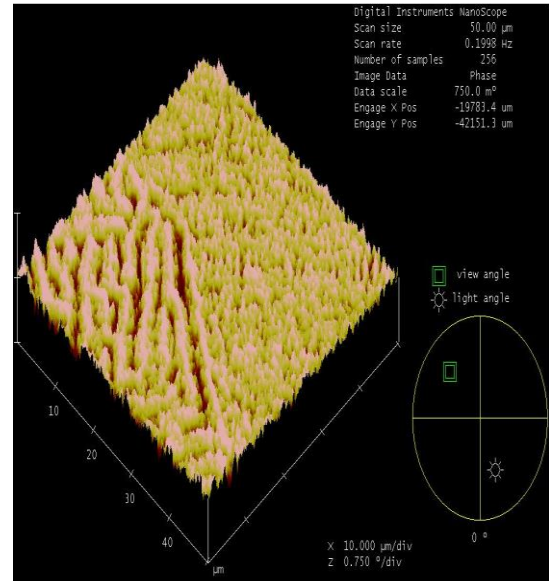
Fig 8-12 (b) Magnetic force gradient for 3-D for polished sample (MFM).

The surface topography of the material is shown in Fig 8-11 (a) while Fig 8-11 (b) illustrates the magnetic force gradient 'phase' image obtained. The scanned area for both cases was 50 μm*50 μm. This was performed at an optimal height of 100 nm (lift scan height) for better resolution, while Fig 8-12 (a) and (b) show the magnetic force gradient in 2-D and 3-D. It can be seen that greater magnitude of the magnetic field took place in some regions of the lighter areas than the darker areas. These certain regions (brighter spots) indicate higher magnetic field activity while the others show lower or negative activity [8-11].

Figure 8-6(b), for the non-polished sample, shows a high resolution of MFM. There are some irregularities of the domain. Some spots of contrast can be clearly seen in the figure, which correspond to the phase shift of the oscillating cantilever caused by the magnetic tip sample interaction (AC MFM). This gives a clear indication of magnetic activity present in the sample that caused the remarkable contrast. This is because of the variation in the magnetisation orientation along the sub-micrometre structure. In fact, the distribution is attributed to the second derivative of the sample's magnetic stray field.

8.6. Advantages and disadvantages of magnetic force microscopy

The MFM method has some advantages which are summarised in the following:

This method has spatial resolution (higher than 50 nm), it operates under ambient conditions and it measures bulk samples at low temperature measurements. The disadvantage of this method is that the magnetic tip can influence the sample. For better sensitivity, the cantilever was vibrated near its resonant frequency. Change in the magnetic force on the tip produces changes in the resonance frequency, amplitude and phase of cantilever oscillation. Typical amplitude variation of 10-30 nm and frequency shifts of 1-100 Hz.

8.7. Kerr Microscopy

The observation principle of Kerr microscopy is based on the Kerr effect [8.12], which was discovered by John Kerr in 1877 following the discovery of Faraday's effect.

The Kerr effect can be applied to any metallic or other light-absorbing magnetic material with a sufficiently smooth surface to avoid light from scattering. By using this technique, the magnetisation is oriented perpendicularly to the specimen surface. Then a linearly polarised light beam induces electrons to oscillate parallel to its plane of polarisation, the plane of electric field $\mathbf{E}$ of the light. Reflected light is then polarised in the same plane as the incident light.

To observe the domain pattern by using a Kerr microscope, the concept of Lorentz force is applied. An example is shown in Fig 8-13 and Fig 8-14. When the sample is subjected to a polarised light, a secondary light wave is induced by the Lorentz moment VLor, as illustrated in Huygen's principle [7-2]. This secondary light is polarised perpendicularly to the normal reflected light rotated by an angle of θk or −θk, an image contrast showing the direction of the magnetisation for that specific area Fig 8-13.
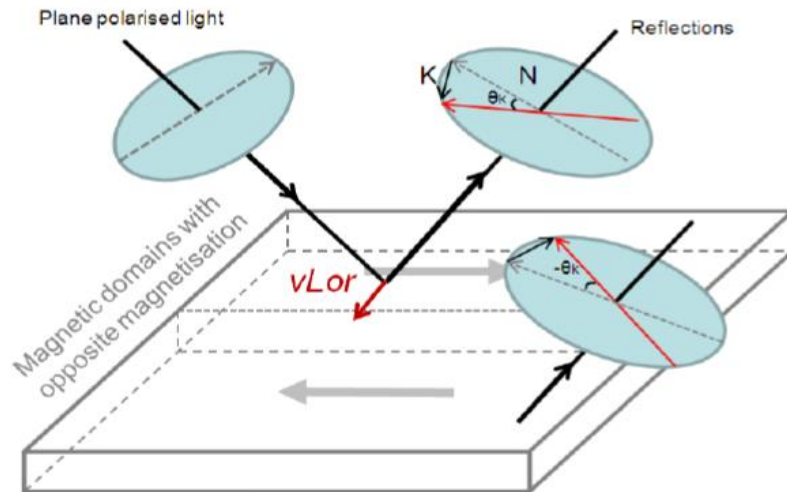
Fig 8-13 illustration of the longitudinal Kerr effect.

Kerr effect microscopy is an optical apparatus. The resolution of this technique is limited by the wavelength of the light (~200 nm). Takezawa [7.13] has shown that high resolution is achievable by utilising an ultra violet (UV) light source in the Kerr microscope.

8.8. Large view bright-field microscope

This system, used for imaging the magnetic domains by the Kerr effect at low magnification with a viewing field of up to several centimetres, is achieved by using a setup, which consists of an inclined microscope, and a separate symmetrical illuminating system [8-14].This system is used for imaging thin film samples with varying interlayer coupling [8-15] [8-16]. Modern systems for magnetic domain imaging demonstrate constant magnification imaging by direct wild field.

Schematic and real systems are shown in Fig 8-14 and Fig 8-15, respectively. This system consists of a collimated high-power emitting diode (HP LED) illuminator. Such a diode offers high stability of light intensity compared to conventionally used high-pressure lamps. Optical polarisation elements like rotatable polarisers and analysers, as well as a retarder plate, are integrated into the light path.
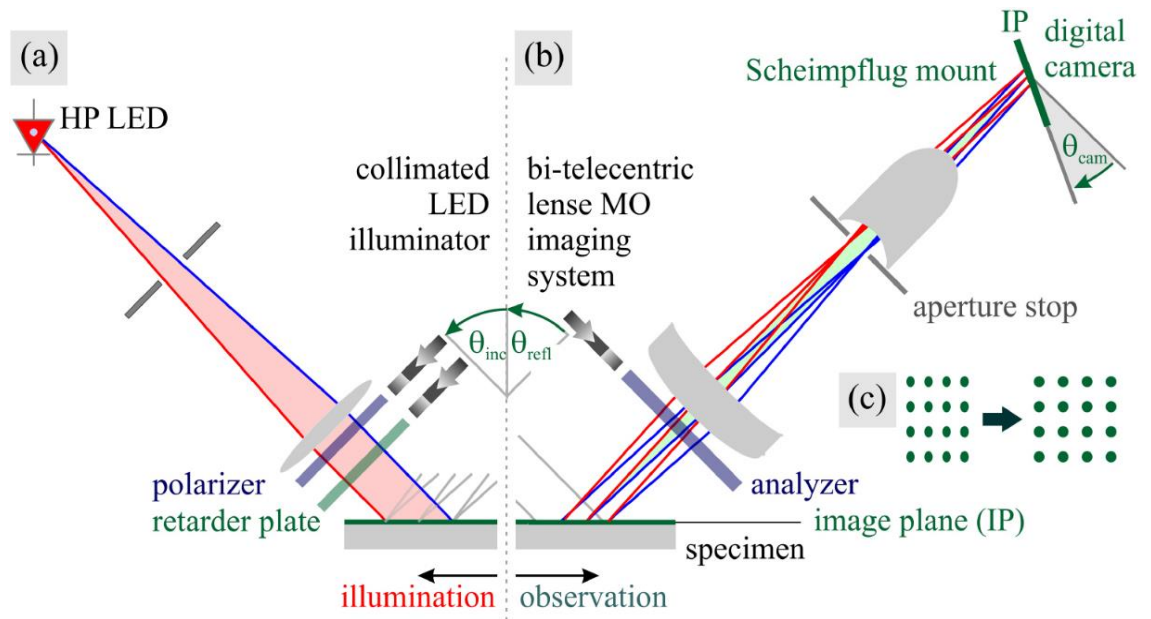
Fig 8-14 Schematic of magnetic domain observation device.

(a) Optical path of illumination
(b) Path of bi-centric observation
(c) Sketch of the linear operation to obtain an equalised image map.

Fig 8-15 High magnification in-plane/polar magnetic domain observation device.

Having polarisation optics in between imaging lenses eliminates the sensitivity to Faraday's effect in the imaging lenses with the application of a high external field. Polar and in-plane magnetic domain sensitivity relative to the plane of incidence can be achieved with proper adjustment of the optical polarisation component. Imaging of in-plane polarisation distribution at or close to the optimum angle with the highest magnetic domain sensitivity is possible independent of the magnetisation.

As discussed before, the main aspect of this system is the projection of the plane image onto the camera system without distortion by using bi-telecentric objective lenses in combination with a rotatable Scheimpflug mount.

The main drawback of this technique involves time-consuming metallurgical sample preparation (see section 8.5.) so that its surface has a high degree of optical flatness, which will reflect light uniformly and efficiently. This is followed by a stress relief anneal to remove the residual stress added to the sample during preparation.
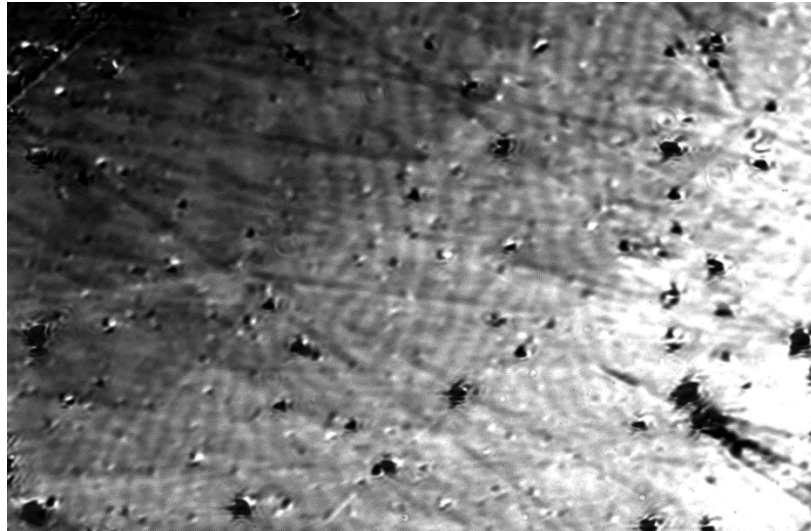
Fig 8-16 Magnetic domain image obtained by Kerr microscopy.

Figure 8-16 shows the image obtained by Kerr effect microscopy. Though different techniques were utilised to obtained a clear image of magnetic domains by this method, it was difficult to get a clear image for non-oriented steel due to the size of the domain and also because the quality of a Kerr image depends on how well the plane of incident and reflected light are aligned with the direction of domain magnetisation.

Table 8-1 Advantages and disadvantages of magnetic domain viewing techniques.

	Kerr	MFM
Sample size	Bigger sample	Smaller sample
Speed	Fast	Durable
Sample preparation	Required	Not required
Measurement and field condition	Yes	No

Summary:-

In summary, AFM and MFM are useful techniques for imaging the magnetic pattern with high resolution and minimal sample preparation. The AFM tip can be used effectively as a near field probe in near field microscopy. The MFM technique is an offspring of AFM, the only difference between the two techniques being the distance with the sharp magnetic tip is placed and interacts with the stray magnetic field emanating from the sample. The image is produced by the scanning tip with respect to the sample surface and measuring the force gradient as a function of position. The interaction strength is then determined by monitoring the motion of the cantilever using a sensor.

MFM and the other tools for scanning are powerful tools for studying the microstructure and magnetic properties of electrical steel specimens.

When the laminations are magnetised at power frequencies like those in electrical machine cores, magnetic loss takes place during domain wall motion. This loss contributes up to 10% of all the power losses in machines. Therefore, deep investigation is required in order to quantify metallurgical and processing parameters which control the losses. The magnetic domain motion, which can be physically measured, is associated with the loss process.

Kerr microscopy of a perfectly flat, defect-free, smooth surface will reflect incident light uniformly and efficiently by means of high reflectivity. Unpolished samples may have scratch lines that cause the incident light to reflect in different directions and cause the surface to appear to be less reflective. The whole process in this test followed the correct procedures, but the system was not able to view the magnetic domains of the sample, which was attributed to the small size of the magnetic domains.

References

[7-1] Ros, Tanya, et al. "Magnetic domain observation by atomic force microscopy." Revista Remetallica 13 (2014).

[7-2] A. Hubert, R. Schafer; magnetic domains", Oxford University Press, Sixth edition, 1998

[7-3] S. Somkun, "Magnetostriction and magnetic anisotropy in non-oriented electrical steels and stator core laminations", Ph.D. thesis, Cardiff University, (2010).

[7-4] P. W. Epperlein, H. Seifert and R. P. Huebener, "Two-dimensional imaging of the current-density distribution in superconducting tunnel junctions", Physics Letters A, vol. 92, pp. 146 – 150, (1982).

[7-5] G. Binning and C. F. Quate, "Atomic Force Microscope", Physical Review Letters, vol. 56, pp. 930 – 933, (1986).

[7-6] J. J. Sáenz, N. Garcia, P. Grutter and E. Meyer, "Observation of magnetic forces by the atomic force microscope", Journal of Applied Physics, vol. 62, pp. 4293 – 4295, (1987).

[7-7] Y. Martin and H. K. Wickramasinghe, "Magnetic imaging by "force microscopy" with 1000 Å resolution", Applied Physics Letters, vol. 50, pp. 1455 – 1457, (1987).

[7-8] M. Ohtake, K. Soneta and M. Futamoto, "Influence of magnetic material composition of Fe 100-xB x coated tip on the spatial resolution of magnetic force microscopy", Journal of Applied Physics, vol. 111, pp. 07E339-1 – 07E339-3, (2012).

[7-9] T.Lyman, Metals Handbook vol.8, Metals Park, Ohio (1973).

[7-10] Folks L, Street R, Warburton G. and Woodward R.C., A sphere forming and polishing machine, Meas. Sci. Technol. 5 (1994).

[7-11] V. Strom and K. V. Rao (2000), "A novel method for magnetic imaging: determination of local in-plane susceptibility at a surface", J. Mag. Mag. Mat., 215-216, p723.

[7-12] J. Kerr, "On rotation of the plane of polarization by reflection from the pole of a magnet", Philosophical Magazine, Vol. 3, p. 321, (1877).

[7-13] M. Takezawa, "Magnetic domain observation of Nd-Fe-B magnets with submicron-sized grains by high-resolution Kerr microscopy", Journal of Applied Physics, vol. 109, pp. 07A709-1 – 07A709-3, (2011).

[7-14] Williams H J, Foster F G and Wood E A 1951 Observation of magnetic domains by the Kerr effect Phys. Rev. 82 119–20

[7-15] Mccord J, Hubert A, Schäfer R, Fuss A and Grünberg P 1993 Domain analysis in epitaxial iron–aluminium and iron– gold sandwiches with oscillatory exchange IEEE Trans. Magn. 29 2735–7

[7-16] McCord J, Brendel H, Hubert A and Parkin S S P 1995 Hysteresis and domains in magnetic multilayers J. Magn. Magn. Mater. 148 244–6

Chapter 9 Conclusions and Recommendations for Future Work

9.1 Conclusions

A combination of theoretical and experimental results have been utilised to find the three components of power loss. This was done by obtaining the power loss coefficients by applying the curve fitting to Microsoft Excel. By using this method, a remarkable agreement was found between the eddy current power loss obtained by the conventional method (Maxwell equation) and the extrapolation method. The slight difference between the two methods is due to the eddy current shielding known as skin effect. There is a small contribution of magnetic domain dynamics leading to micro-eddy currents and hysteresis loss.

Inter-laminar short circuits were simulated to model their impact on the performance of electrical machines. The impact of the number of shorts on stacks of two and three laminations on the rolling and transvers directions was studied. It was observed that the number of shorted laminations is the most important factor in increasing the core losses. Even at low magnetising frequency, the effect becomes more significant at higher frequency.

It has been observed that the fault position has an impact on the total power loss, since the loss was high when the short was applied at mid- point and was least and close to nominal when the fault was applied at the far edges. This was justified by measuring the conductance between the set-points. This is related to short circuit resistance, which increases with increased axial off-set between the points.

The measured power loss with or without fault in the rolling and transvers directions was similar. This is due to the isotropic nature of the material.

An investigation was carried out by using the power loss separation formula when the short circuit was applied at the mid-point of the laminations, which generated the highest power loss. It was found that the eddy current component was consistently dominant.

The impact of edge burrs was simulated by using large-scale motor laminations for the same material used in this investigation. The edge burrs were applied at different set-points, and the same outcome of test was obtained. The increase of the power loss was dependent on the short-circuit position and the number of shorts applied to the material.

An experimental work presents results for specific power loss in grain-oriented electrical steel. A number of measurements were performed with two toroids of different dimensions, this study have shown the impact of geometry on total power loss which

Chapter 9 Conclusions and Recommendations for Future Work

correlate very well with previous research; hence, toroid cores should be designed with larger internal diameters and low build-up. Toroids with smaller inner and outer diameters have a higher power loss. This work was extended to study the effect of short circuits between the laminations.

3-D (FE) modelling was performed to study the effect of toroid core geometry on the flux density distribution. This modelling was an attempt to investigate why toroids with small internal diameters have a larger power loss than those with larger internal diameters.

MFM, the magnetic microscopy system, has successfully shown the internal microstructure for non-oriented electrical steel samples through the stray field at the sample surface. However, it has been rather difficult to quantify because of the magnetic tip and magnetic sample interaction and the non-linearity of the magnetic tip.

9.1.1 Recommendation for future work

This study's results indicate a need for an effective means of detecting edge burr faults in core lamination. There are already methods used to detect these faults, such as the Flux Injection Probe, but this method has shown some disadvantages. Today, frequency response analysis is used to detect various defects in electrical machines, such as axial movement of winding in transformers and hoop buckling. This method could be used as well to detect core faults because of its simplicity and sensitivity to the fault.

In addition, 3-D FE modelling of eddy current loss and distribution within the area affected by edge burrs will provide more understanding of the phenomenon.

Future research regarding investigating magnetic domains for non-oriented steel should include magnetic domain observation at low frequency. Further research should be done with real-time dynamic domain patterns capturing using the Kerr microscope.